

High order harmonic generation from preformed laser plasma plumes

By

Himanshu Singhal

Laser Plasma Division

Raja Ramanna Centre for Advanced Technology

Indore 452 013, M.P.

A thesis submitted to the

Board of Studies in Physical Sciences

In partial fulfilment of requirements

for the Degree of

DOCTOR OF PHILOSOPHY

of

HOMI BHABHA NATIONAL INSTITUTE



April 2011

Homi Bhabha National Institute

Recommendations of the Viva Voce Board

As members of the Viva Voce Board, we certify that we have read the dissertation prepared by Himanshu Singhal entitled "High order harmonic generation from preformed laser plasma plumes" and recommend that it may be accepted as fulfilling the dissertation requirement for the Degree of Doctor of Philosophy.


.....
Chairman – Dr. S. M. Oak Date: 19/10/2011


.....
Guide - Dr. P. D. Gupta Date: 19-10-11


.....
Co-Guide / Convener – Dr. P. A. Naik Date: 17/10/11


.....
Member – Dr. N. K. Gupta (BARC) Date: 19-10-11


.....
External Examiner – Prof. D. Narayana Rao Date: 19/10/2011

Final approval and acceptance of this dissertation is contingent upon the candidate's submission of the final copies of the dissertation to HBNI.

We hereby certify that we have read this dissertation prepared under our direction and recommend that it may be accepted as fulfilling the dissertation requirement.

Date: 19/10/2011

Place: Indore.


(Signature of the Co-guide)
Dr. Prasad A. Naik
Scientific Officer H &
Head, Laser Plasma Division


(Signature of the Guide) 19/10/11
Dr. P. D. Gupta
Distinguished Scientist
Director, RRCAT, Indore

STATEMENT BY AUTHOR

This dissertation has been submitted in partial fulfilment of requirements for an advanced degree at Homi Bhabha National Institute (HBNI) and is deposited in the Library to be made available to borrowers under rules of the HBNI.

Brief quotations from this dissertation are allowable without special permission, provided that accurate acknowledgement of source is made. Requests for permission for extended quotation from or reproduction of this manuscript in whole or in part may be granted by the Competent Authority of HBNI when in his or her judgment the proposed use of the material is in the interests of scholarship. In all other instances, however, permission must be obtained from the author.



Himanshu Singhal

DECLARATION

I, hereby, declare that the investigation presented in the thesis has been carried out by me. The work is original and has not been submitted earlier as a whole or in part for a degree / diploma at this or any other Institution / University.



Himanshu Singhal

Certificate of the Guide

This is to certify that the work entitled “*High order harmonic generation from preformed laser plasma plumes*” is a piece of research work done by *Shri Himanshu Singhal* under our joint supervision, for the degree of *Doctor of Philosophy (Science)* of Homi Bhabha National Institute, at RRCAT, Indore, a Constituent Institution of HBNI.

To the best of our knowledge and belief, the thesis :

1. embodies the work of candidate himself,
2. the work has been duly completed to our satisfaction,
3. fulfils the requirements of the Ph.D. degree of HBNI, and
4. is up to the international standard, both, in respect of contents and language, for being referred to the examiner.



(Signature of the Co-guide)

Dr. P. A. Naik



(Signature of the Guide)

Dr. P.D. Gupta

DEDICATION

The flower of this unassuming research work is offered at the feet of my dear motherland to whom I owe what I have. To be finally dedicated in the service of her daughters and sons, on whom she showers her beneficence in all the four directions.

Infinite striving to be the best is man's duty. It is its own reward. Everything else is in God's hands. Mahatma Gandhi

Acknowledgements

First of all, I thank the Almighty for His grace and blessings on me to provide me sufficient energy and strength to undertake and complete the present research work.

I am extremely thankful to my thesis guide *Dr. P. D. Gupta* for his valuable guidance, constant support, encouragement, and motivation throughout the course of this work. I am highly obliged to him that despite being extremely busy as Director, RRCAT, he took time out to go through thoroughly my thesis and made constructive criticism and gave valuable suggestions, which helped me to present the scientific results in an efficient and effective manner in the thesis.

I am highly thankful to my thesis co-guide *Dr. P. A. Naik* for his continuous guidance and support in carrying out the various experiments, discussing the results on daily basis during the experiments, in documenting the results and in thesis writing.

I take this opportunity to thank our collaborator *Dr. R. A. Ganeev*, who is among the pioneers of the research on high order harmonic generation from laser ablated plasma plumes. Only after getting the experience of working with him on high order harmonic generation experiments, I was able to make independent studies.

I am also thankful to *Dr. J. A. Chakera* for his support in planning and carrying out various experiments in the laboratory.

I am thankful to *Shri Vipul Arora*, who was first to introduce me to the exciting world of laser plasma experiments, and thereafter remained with me as a co-worker and my close friend.

I thank *Shri S. R. Kumbhare* for providing me all the support that I needed in setting up the experiments in the laboratory, *Shri S. Sebastin* and *Shri R. P. Kushwaha* for making quick modifications required while changing the experimental setups.

I thank *Shri R. A. Khan*, *Shri R. A. Joshi*, and *Shri R. K. Bhat* for the operation of the Ti:sapphire laser and staying late to make it available after office hours and on holidays.

The present research work could not have been completed without the help of my co-workers. I am thankful to all my co-workers *Shri B. S. Rao*, *Shri U. Chakravarty*, *Shri M. Tayyab*, *Shri M. Kumar*, and *Dr. S. Bagchi* for their time to time support during the experiments.

I am thankful to my wife *Mrs. Sheelu* for her unconditional support, care, and to the great pains she took to keep me in perfect health, without which it would have been impossible to complete the work.

Last but not the least, I would like to express my sincere gratitude to my *mother* and *father* for their never-ending love, and affection to me.

Himanshu Singhal

CONTENTS

SYNOPSIS	xi
LIST OF FIGURES	xxv
LIST OF TABLES	xxix
THESIS CHAPTERS	
Chapter 1 High order harmonic generation : An overview	1
1.1. Introduction	1
1.2. Theoretical background	3
1.2.1. Semiclassical model for HHG in gases	4
1.2.2. Propagation effects	8
1.2.3. Harmonic generation from solid surfaces	9
1.3. Overview of experimental studies	11
1.3.1. Harmonic generation in gases	12
1.3.1.1. Harmonic generation from gas jets	12
1.3.1.2. Quasi phase matched harmonic generation in hollow core fibres	14
1.3.1.3. Harmonic generation from gas cells	15
1.3.2. Harmonic generation from plasma plumes	17
1.3.2.1. Laser ablated plasma plumes	17
1.3.2.2. Resonance enhancement of harmonics	18
1.3.3. Harmonics from solid surfaces	20
Bibliography	22
Chapter 2 Experimental setup and diagnostic system	27
2.1. Ti:sapphire laser system	27
2.2. Characterization of the laser pulse	30
2.2.1. Laser spectrum	30
2.2.2. Pulse duration measurement	31
2.2.3. Beam divergence measurement	34
2.3. Experimental setup	35
2.4. XUV spectrograph for harmonic detection	38
Bibliography	40

Chapter 3	Parametric optimization of harmonic generation in laser ablated plasma plumes	42
3.1.	Characterization of generated harmonics	43
3.2.	Intensity optimization of harmonics with respect to various laser and plasma parameters	47
	Bibliography	51
Chapter 4	Resonance intensity enhancement of harmonics and wavelength tuning	54
4.1.	Occurrence of strongly enhanced single harmonic orders	55
4.2.	Wavelength tuning of harmonics with laser chirp	57
4.3.	Resonance intensity enhancement of specific harmonics through wavelength tuning	60
	Bibliography	63
Chapter 5	Phase matching considerations in HHG	66
5.1.	Effect of laser intensity and focussing conditions	68
5.2.	Dependence of harmonic intensity on length of plasma plume	75
5.3.	Estimation of the effect of various phase mismatch factors	77
	Bibliography	83
Chapter 6	Improvement in stability of HHG and extension of cut-off order	86
6.1.	Stable harmonic generation in plasma plumes	87
6.2.	Study of harmonic cut-off order in plasma plumes of different targets and its extension through second plateau generation	88
	Bibliography	93
Chapter 7	HHG from nanoparticles-containing plasmas	94
7.1.	Preparation of nanoparticles-containing plasma plumes	95
7.2.	HHG from plasma plume containing nanoparticles / fullerenes	100
7.2.1.	HHG from plasma plumes of nanoparticle targets	100

7.2.2.	HHG from plasma plumes of fullerene targets	103
7.2.3.	HHG stability from nanostructured targets	104
7.2.4.	Physical understanding of experimental results	105
7.3.	HHG from silver nanoparticles produced <i>in situ</i> during laser-matter interaction	107
	Bibliography	110
Chapter 8	Spectral broadening of the harmonic radiation	114
8.1.	HHG using self-phase modulated laser pulse	115
8.2.	Harmonic generation from plasma plumes containing nanoparticles	118
	Bibliography	122
Chapter 9	HHG using two-colour laser pulses	124
9.1.	Even and odd harmonic generation through symmetry breaking	125
9.2.	Experimental description	127
9.3.	HHG using weak two-colour pulses	129
9.3.1.	HHG from plasma plumes of bulk materials	129
9.3.2.	Occurrence of new resonances	132
9.3.3.	Harmonic intensity enhancement in plasma plumes of nanostructured targets	133
9.4.	HHG using strong two-colour pulses	134
	Bibliography	135
Chapter 10	Conclusion	137
10.1.	Summary of the important results	137
10.2.	Suggestions for further research work	139

SYNOPSIS

Coherent sources of short wavelength radiation are much sought after in view of their applications in a variety of fields such as microlithography, spectroscopic studies etc. Generation of optical harmonics of intense laser pulses using nonlinear crystals is an established method of generating coherent radiation at shorter wavelengths. However, this technique does not enable one to generate radiation at wavelengths < 200 nm due to strong absorption of the radiation inside the crystals. The interaction of intense fs laser pulses with under-dense gaseous media enables generation of harmonics of the laser into soft x-ray region. Nonlinear interaction of the laser with the gaseous medium results in the emission of odd multiples of the laser frequency to very high orders. The phenomenon is known as high order harmonic generation (HHG). No even harmonics are generated in this case because of the inversion symmetry of the process. The HHG has been understood in terms of a three-step model. The model explains HHG from tunnelling of electron from atom, its acceleration under the action of laser field, and its recombination with parent atom. The model correctly predicts the shape and cut-off of the emitted harmonic radiation. The intensity and the cut-off of the emitted harmonic orders depend on the density and the ionization potential of the gaseous medium, and also on the laser parameters such as intensity and pulse duration. Through the optimization of various laser/gas parameters, the cut-off for high order harmonics can be extended to the so called 'water window' region (2.3 – 4.4 nm). However, the conversion efficiency of the HHG process remains rather low ($\sim 10^{-6}$).

There are several interesting applications of HHG such as measurement of ultrafast photo-recombination cross sections, probing of rotational dynamics of molecules, detection of molecular structure, strong field fast alignment of molecules, achievement of ultrahigh focussed intensities etc. Many of these have been demonstrated,

however for practical utilization of these applications, it is desirable to have higher intensity of the harmonics. Hence, in order to increase the practical applicability of harmonic radiation, it is necessary to increase the conversion efficiency of HHG. Many efforts are being made to increase the conversion efficiency of HHG. It was observed that the conversion efficiency of the HHG process depends greatly on the properties of the nonlinear medium used. However, the number of gases available for this purpose (usually noble gases are used) is rather small, which restricts research investigations to only a few elements. To overcome this limitation, we have generated high order harmonics using low excited under-dense plasma plumes ablated from solid materials through their interaction with low intensity laser pulses. These plasma plumes mainly consist of neutrals, singly charged ions, and in some cases doubly charged ions. The interaction of fs laser with these plumes is similar to that with gases. The use of low-excited plasma plumes enables one to explore the nonlinear properties of HHG in wide variety of materials. This also provides increased possibility of matching atomic/ionic transitions in the medium used with one or more harmonic orders. This may result in resonant intensity enhancement of a particular harmonic order several times compared to the neighbouring ones. Efforts are also made to use novel media to improve on conversion efficiency and cut-off order of harmonics.

In the present research work, we have experimentally studied the HHG from the interaction of intense femtoseconds ($\tau = 45$ fs) laser pulses with low excited plasma plumes of various target materials. The target materials used may be broadly categorized as bulk solids such as: Ag, In, Cr, Mn, C etc. and nanostructured targets such as: fullerenes (C_{60}) and nanoparticles of various metals. The plasma plumes were generated by the interaction of low intensity laser pulse (hereafter referred to as ‘pre-pulse’) with the target surface. The pre-pulse was obtained by reflecting part of the uncompressed

chirped laser pulse before the grating compressor stage in the laser system. The high order harmonics were generated by the interaction of the compressed femtosecond laser pulse (hereafter referred to as main pulse) with the preformed plasma plume. The HHG was optimized for intensity and cut-off of the harmonic orders. The enhancement of the intensity of particular harmonic orders due to various atomic/ionic resonances in different plasma plumes was also observed. It was found that nanostructured materials generate high order harmonics with larger conversion efficiency whereas the harmonics generated in bulk materials have a higher cut-off. Various properties of HHG such as the dependence of harmonic intensity on the laser intensity and focussing conditions, length of plasma plume, etc. were studied. Spectral characterization of HHG from bulk and nanostructured targets was carried out and the effect of laser spectral broadening through self-phase modulation of laser pulse on the spectral characteristics of harmonic radiation was studied. The effect of symmetry breaking of HHG process through the use of two-colour laser radiation was also studied. A chapter wise summary of these studies is given below.

Chapter 1 gives a brief introduction to the theoretical background of HHG process and to the status of the various investigations in HHG. The Chapter starts with a discussion on the basic theoretical aspects, followed by a brief review of experimental results with HHG from gaseous media. This is followed by a brief description of the earlier experimental work on various optimization techniques utilized to increase the yield of HHG from gas jet plasmas.

Chapter 2 describes the experimental arrangement used in present research work. Characterization of the parameters of the driving laser namely: pulse duration, spectral profile etc. were carried out. A chirp pulse amplification based 10 TW Ti:sapphire laser of 45 fs pulse duration was used in this experiment. The harmonics were produced by the

interaction of this ultrashort laser pulse with a low-excited preformed plasma plume. The plasma plumes were created by the interaction of low intensity laser pre-pulse (energy ~ 30 mJ and pulse duration ~ 200 ps). The pre-pulse was generated by reflecting a part of the amplified uncompressed chirped Ti:sapphire laser pulse before the grating compressor. The extreme ultra-violet (XUV) harmonic radiation was detected by an in-house developed XUV spectrograph based on grazing incidence variable line spacing flat-field grating. The harmonic radiation was dispersed by the grating in the horizontal plane and detected on a microchannel plate (MCP) - charge couple device (CCD) assembly. In the later parts of the experimental study, the sensitivity of the XUV spectrograph was increased by a factor of ~ 10 by focussing harmonic radiation in vertical plane using a grazing incidence gold coated cylindrical mirror placed before the grating.

Plasma plumes of various targets were used for the generation of high order harmonics. Mainly silver, indium, chromium, manganese, GaAs, carbon, silicon were used for HHG. **Chapter 3** describes the HHG from these targets. Optimization of various parameters such as laser intensity, chirp, delay between the two laser pulses (pre-pulse and main pulse), etc. was carried out in order to maximize the yield and cut-off of the HHG process. A brief account of these optimizations is given in this chapter. Next, the tuning of the harmonic frequencies through the variation of laser chirp was studied. It was observed that the harmonic wavelengths shift toward red (blue) with the introduction of positive (negative) chirp in the main laser pulse.

Increasing the conversion efficiency of high order harmonics generation is an important aspect of this research. Recently, it was observed that the conversion efficiency of the harmonics could be increased through various atomic/ionic resonances with particular harmonic orders. In our study it was observed that in certain plasma

plumes the intensity of particular harmonic orders was much higher compared to that of their neighbouring harmonics, resulting in highly efficient harmonic generation. For instance, the intensity of 13th H (~61 nm) generated in indium plasma plume was ~200× higher, and the intensity of the 29th H (~27.5 nm) in chromium plasma plume was ~20× higher compared to the respective neighbouring harmonic orders. This is ascribed to the resonance enhancement of a particular harmonic order. In **Chapter 4**, we discuss important findings related to the resonance enhancement of the harmonic orders in various plasma plumes. It was demonstrated that the tuning of the harmonic radiation with chirp can move a resonantly enhanced harmonic order out of resonance, and also bring a normal harmonic order into resonance.

In order to understand the effect of laser and plasma conditions on the propagation of harmonics through the medium, a detailed knowledge of various phase-matching factors on the intensity of high order harmonics is required. In **Chapter 5**, we address the influence of these phase matching factors on HHG. For instance, the propagation of the high order harmonics in elongated silver plasma plume was studied. Since HHG is a coherent process, under perfect phase matching conditions, the intensity of high order harmonics (I_H) is expected to increase with medium length (L) as $I_H \propto L^2$. It was observed that the scaling exponent (p) of harmonic intensity on medium length ($I_H \propto L^p$, $p \sim 0.7-0.9$) was much smaller than the predicted value of $p = 2$ under perfect phase matching conditions. The smaller value of ' p ' occurs due to deviation from perfect phase-matching between the laser and the harmonic radiation, and the reabsorption of the harmonic radiation inside the plasma plume through its photo-ionization. The dispersive elements responsible for the phase mismatch are : atomic dispersion, plasma dispersion, Gouy phase shift, and intensity dependent dynamical phase shift. The phase-mismatch factors for these are calculated and included in the propagation equation along with re-

absorption factor. The intensity scaling laws with length for HHG are then calculated taking standard density and ionization conditions. A comparison of these scaling laws with the observed intensity scalings of various harmonic orders brings out the relative roles of various phase-mismatch factors on HHG.

Improvement in the stability and the cut-off of the HHG is important for their use as a coherent x-ray source for practical applications. These improvements through the optimization of laser and plasma parameters are discussed in **Chapter 6**. It was observed that after various optimizations of laser and plasma conditions, one can continuously generate high order harmonics for about 5 minutes from plasma plumes produced from silver target, without much change in their intensity and spectrum. During the experiment, the laser operated at 10 Hz repetition rate and pre-pulse irradiated the same spot on the target surface. Next, a second plateau of harmonics was observed in Mn plasma plumes. It was seen that HHG spectrum from Mn plasma consists of a plateau, followed by a sharp cut-off at $\sim 29^{\text{th}}$ order. The spectrum again starts at 33^{rd} harmonic and the intensity of the higher orders falls rapidly. Next, it was experimentally observed that if one increases the excitation of the pre-plasma, and optimizes the intensity of fs pulse, the harmonic orders below 33^{rd} order are suppressed, and the HHG cut-off extends to 73^{rd} H order. The spectrum looks as if the HHG plateau starts from 33^{rd} harmonic order. Details of observation of second plateau and physical understanding of its occurrence are presented in this chapter.

In order to increase the conversion efficiency of HHG process, we have tried out novel targets to explore the effect of the enhanced non-linear optical properties on the harmonic conversion. For instance, the nanoparticles, due to their small size exhibit increased optical nonlinearity and high absorption at surface plasmon resonance. It was anticipated that they would also generate high order harmonics with greater efficiency. In

Chapter 7 we present our study of HHG from plasma plumes of nano-structured targets. Nano-structured targets such as fullerene and metal nano-particles of Ag, Au, etc. were used. These targets were made from the dried mixture of nanoparticles of various materials with organic matrix or with simple glue. It was observed that the intensity of the lower order harmonics generated from these targets is much enhanced compared to that of the corresponding harmonics from bulk materials. For example, the intensity of the 9th harmonic from the plume of silver nano-particles is ~200 times higher compared to that from plasma plume of bulk silver. Apart from laser and plasma conditions, the intensity of harmonics from nano-structured targets also depends on the target preparation technique. This aspect is also discussed in this chapter. The HHG from nano-particles is not as stable as that from the bulk materials. This is primarily due to the fact that unlike in the bulk materials, only a thin layer of nano-structured material is available as target. Hence, the stability of the HHG from such targets is limited by the depletion of the target. The stability of HHG from these targets can be increased by increasing the target thickness and also by optimizing plasma formation conditions. It was observed that if one uses lower intensity of laser pre-pulse to produce plasma plumes, the harmonic generation could continue without appreciable loss of intensity for up-to ~200 laser shots fired at the same spot.

Spectral characterization of harmonic radiation is important especially for the matching of harmonic wavelengths with resonance transitions for the generation of high efficiency harmonic radiation. In this regard, the generation of broadband harmonics can be helpful for easier matching of harmonic wavelengths with atomic/ionic resonances. Spectrally broadened harmonics are also useful in various spectroscopic applications for the same reason. **Chapter 8** describes our study on broadband HHG. The spectrally broadened harmonics were observed when spectrally broadened fs laser was used. The

latter was accomplished by passing the fs laser pulse through a 5 mm thick glass plate while it was being focussed by the lens. The intensity of the laser at glass surface was kept low enough to avoid filamentation and white light generation. The self-phase modulation of the laser pulse inside the glass medium results in spectral broadening of the laser pulse. The bandwidth of the laser pulse was increased for ~ 18 nm to ~ 32 nm. It was observed that the bandwidth of the lower harmonic orders gets increased. For example, the bandwidth of the 17th harmonic generated from plasma plumes of Ag increased from ~ 0.5 nm to ~ 0.9 nm. Since the laser pulse, after passing through the glass plate, has inherent positive chirp, the harmonic orders are also shifted towards red side. It was also observed that the bandwidth of the high order harmonics generated from nanostructured targets can be increased by increasing the intensity of fs laser pulse inside the plasma plume. For example, the bandwidth of the 11th harmonic generated from plasma plumes containing Ag nanoparticles increased from ~ 1.4 nm to ~ 5 nm when the intensity of laser was increased from 1.8×10^{15} W cm⁻² to 3.5×10^{15} W cm⁻². In this case, the spectral broadening of harmonics was only towards the blue side. This phenomenon is similar to that observed in our previous study on the spectral blue broadening of picosecond laser pulses towards blue side during their interaction with rare gas clusters. A theoretical model was earlier proposed to explain the observed blue broadening of the spectrum of the scattered laser pulse ($\tau \sim 27$ ps) due to its interaction with rare gas clusters. The model explains that the interaction of intense laser pulse with expanding clusters results in blue broadening of the laser pulse through self-phase modulation (SPM). This SPM is prominent when the cluster is passing through its resonance phase at $3n_{cr}$, where n_{cr} is the critical density of the plasma. The same mechanism results in the blue broadening of the laser spectrum during its interaction with metal nanoparticles. The harmonics generated by this blue broadened laser pulse are also blue broadened. Salient

features of this model are described in this chapter for the understanding of underlying process.

The interaction of the femtosecond laser pulses with the plasma plume resulted in the generation of only odd harmonic orders. No even harmonic order was observed due to the inversion symmetry of the process. However, this inversion symmetry of the process could be broken by the introduction of small amount of second harmonic radiation in the main pulse. This led to the generation of both even and odd harmonics with similar conversion efficiency and thereby increasing the conversion efficiency by factor of ~ 2 . **Chapter 9** presents our experimental study on HHG from two-colour excitation. The Ti:sapphire laser pulse with its second harmonic was used for HHG. The second harmonic of the Ti:sapphire laser pulse was generated by passing the laser beam through a KDP crystal. The conversion efficiency of the second harmonic was kept low to $\sim 2.5\%$. When HHG was carried out using the fundamental laser radiation together with this small intensity second harmonic radiation, the harmonic spectrum showed both even and odd harmonic orders with comparable intensities. These observations indicated that although the relative intensity of the second harmonic pulse was very small, it was sufficient for symmetry breaking of the HHG process. It was observed that if one increases the intensity of the fs pulse inside the plasma plume, the cut-off for odd harmonic orders increases, whereas the cut-off for even harmonics decreases. The fundamental and second harmonic pulses got partially separated in time due to dispersion in SHG crystal, the separation depends on the thickness of the crystal. The observed reduction of cut-off order of even harmonics with increasing intensity is explained by HHG from leading edge of fundamental pulse. The HHG comes from the leading edge where intensity remains below saturation intensity. With increasing focussing, the HHG comes from progressively earlier part of the leading edge thereby reducing the overlap

between fundamental and second harmonic pulse resulting in disappearance of even harmonic orders.

Finally, the thesis concludes in **Chapter 10** with a summary of the results, and a brief discussion on possible future work.

List of publications constituting the Ph.D. thesis

A. Papers in Journals

1. **H. Singhal**, R. A. Ganeev, P. A. Naik, J. A. Chakera, U. Chakravarty, H. S. Vora, A. K. Srivastava, C. Mukherjee, C. P. Navathe, S. K. Deb, and P.D. Gupta,
“High order harmonic generation in plasma plume of in-situ laser produced silver nanoparticles”,
Phys. Rev. A **82**, 043821 (2010)
2. **H. Singhal**, R A Ganeev, P A Naik, A K Srivastava, A Singh, R Chari, R A Khan, J A Chakera and P D Gupta
“Study of high-order harmonic generation from nanoparticles”
J. Phys. B **43**, 025603 (2010)
3. R. A. Ganeev, **H. Singhal**, P. A. Naik, I. A. Kulagin, P. V. Redkin, J. A. Chakera, M. Tayyab, R. A. Khan, and P. D. Gupta
“Enhancement of high-order harmonic generation using a two-colour pump in plasma plumes”
Phys. Rev. A **80**, 033845 (2009)
4. **H. Singhal**, V. Arora, B. S. Rao, P. A. Naik, U. Chakravarty, R. A. Khan, and P. D. Gupta,
“Dependence of high-order harmonic intensity on the length of preformed plasma plumes”
Phys. Rev. A **79**, 023807 (2009)
5. R. A. Ganeev, **H. Singhal**, P. A. Naik, J. A. Chakera, A. K. Srivastava, T. S. Dhami, M. P. Joshi, and P. D. Gupta
“Influence of C₆₀ morphology on high-order harmonic generation enhancement in fullerene-containing plasma”
J. App. Phys. **106**, 103103 (2009)
6. **H. Singhal**, R. A. Ganeev, P. A. Naik, V. Arora, U. Chakravarty, and P. D. Gupta
“Dependence of high order harmonics intensity on laser focal spot position in preformed plasma plumes”
J. App. Phys. **103**, 013107 (2008)
7. R. A. Ganeev, **H. Singhal**, P. A. Naik, U. Chakravarty, V. Arora, J. A. Chakera, R. A. Khan, M. Raghuramaiah, S. R. Kumbhare, R. P. Kushwaha, and P. D. Gupta

“Optimization of the high-order harmonics generated from silver plasma”

Appl. Phys. B **87**, 243 (2007)

8. R. A. Ganeev, **H. Singhal**, P. A. Naik, V. Arora, U. Chakravarty, J. A. Chakera, R. A. Khan, I. A. Kulagin, P. V. Redkin, M. Raghuramaiah, and P. D. Gupta

“Harmonic generation from indium-rich plasmas”

Phys. Rev. A **74**, 063824 (2006)

B. Presentations in Conferences/symposia

1. **H. Singhal**, R. A. Ganeev, P. A. Naik, J. A. Chakera, U. Chakravarty, H. S. Vora, A. K. Srivastava, C. Mukherjee, C. P. Navathe, S. K. Deb, and P.D. Gupta

“High order harmonic generation in plasma plume of in-situ laser produced silver nanoparticles“

25th National Symposium on Plasma Science & Technology, held at IASST, Guwahati, December 8-11, 2010.

2. **H. Singhal**, R. A. Ganeev, P. A. Naik, J. A. Chakera, M. Kumar, M. P. Joshi, A. K. Srivastava and P. D. Gupta

“Study of high order harmonic generation from plasma plumes containing carbon nanotubes“

19th National Laser Symposium held at Raja Ramanna Centre for Advanced Technology Indore, December 1-4, 2010

3. **H. Singhal**, R. A. Ganeev, P. A. Naik, J. A. Chakera, M. Tayyab, R.A. Khan, and P. D. Gupta

“High-order harmonic generation from two-colour laser pulses”

9th DAE-BRNS National Laser Symposium, held at Bhabha Atomic Research Centre, Mumbai, January 13–16, 2010.

4. **H. Singhal**, R. A. Ganeev, P. A. Naik, J. A. Chakera, M. Tayyab, R. A. Khan, and P. D. Gupta

“Broadband high-order harmonic generation from spectrally broadened laser pulses generated from self-phase modulation effects”

9th DAE-BRNS National Laser Symposium, held at Bhabha Atomic Research Centre, Mumbai, January 13–16, 2010.

5. **H. Singhal**, R. A. Ganeev, P. A. Naik, J. A. Chakera, A. K. Srivastava, J. Jayabalan, A. Singh, R. Chari, S. R. Kumbhare, and P. D. Gupta
 “Enhanced high-order harmonic generation from nanoparticle targets”
9th DAE-BRNS National Laser Symposium, held at Bhabha Atomic Research Centre, Mumbai, January 13–16, 2010.
6. **H. Singhal**, R. A. Ganeev, P. A. Naik, J. A. Chakera, A. K. Srivastava, T. S. Dhami, M. P. Joshi, and P. D. Gupta
 “Enhanced harmonic generation in C₆₀-containing plasmas”
24th National Symposium On Plasma Science & Technology held at National Institute Of Technology Hamirpur (Himachal Pradesh), December 8–11, 2009.
7. J. A. Chakera, **H. Singhal**, R. A. Ganeev, P. A. Naik, A. K. Srivastava, A. Singh, R. Chari, R. A. Khan, and P. D. Gupta
 “Higher harmonic generation using nanostructured target plumes”
International Conference on Light at Extreme Intensities, held at AULA Brasov (Romania), October 16–21, 2009.
8. **H. Singhal**, V. Arora, B. S. Rao, U. Chakravarty, P. A. Naik, R. A. Khan, and P. D. Gupta
 “Dependence of high order harmonic intensity on the medium length in laser produced plasma plumes”
23rd National Symposium on Plasma Science & Technology held at Bhabha Atomic Research Centre Mumbai, December 10–13, 2008.
9. **H. Singhal**, V. Arora, B. S. Rao, U. Chakravarty, P. A. Naik, and P. D. Gupta
 “Generation of coherent XUV radiation by interaction of ultrashort laser pulses with preformed plasma plumes”
2nd IFCPAR/CEFIPRA Workshop on Lasers, quantum optics , ultrafast processes, and biophysics, held at Centre National de la Recherche Scientifique (National Centre for Scientific Research) Gif-sur-Yvette (France), October 29 –November 3, 2007.
10. **H. Singhal**, V. Arora, P. A. Naik, U. Chakravarty, J. A. Chakera, M. Raghuramaiah, R. A. Khan, S. R. Kumbhare, P. D. Gupta and R. A. Ganeev
 “On the use of ionization induced self-defocusing for efficient harmonic generation from plasma plumes”

21st National Symposium on Plasma Science and Technology, held at Malaviya National Institute of Technology Jaipur, December 19–22, 2006.

11. **H. Singhal**, V. Arora, P. A. Naik, U. Chakravarty, J. A. Chakera, M. Raghuramaiah, S. R. Kumbhare, R. A. Khan, P. D. Gupta and R. A. Ganeev

“Enhancement and extinction of single harmonic intensity of high order harmonics”

21st National Symposium on Plasma Science and Technology, held at Malaviya National Institute of Technology Jaipur, December 19–22, 2006.

12. **H. Singhal**, P. A. Naik, U. Chakravarty, V. Arora, J. A. Chakera, R. A. Khan, M. Raghuramaiah, S. R. Kumbhare, P. D. Gupta and R. A. Ganeev

“High order harmonic generation from plasma plumes: Tuning of the harmonic wavelengths by varying the chirp of the laser pulse”

6th DAE–BRNS National Laser Symposium, held at Raja Ramanna Centre for Advanced Technology Indore, December 5–8, 2006.

List of figures

Figure 1.1:	Three-step model of high order harmonic generation	4
Figure 1.2:	Electron recombination energy vs. laser phase	5
Figure 1.3:	Addition of the harmonic field with propagation results in generation of only odd harmonics	6
Figure 1.4:	Periodic modulation of solid surface by incident laser pulse resulting in emission of high order harmonics in the direction of reflected laser light	10
Figure 1.5:	Fig.-of eight orbit of an electron for: (a) p-polarized light, (b) s-polarized light.	11
Figure 1.6 :	Schematic of high order harmonic generation experiment from gas jets	12
Figure 1.7:	High order harmonic spectrum for different values of laser pulse duration	13
Figure 1.8:	HHG from modulated hollow core fibre	14
Figure 1.9:	Harmonic generation using variable length gas cells	15
Figure 1.10:	Harmonic intensity with gas pressure	16
Figure 1.11:	Harmonic intensity variation with medium length	17
Figure 1.12:	Schematic of high order harmonic generation from laser ablated plasma plumes	18
Figure 1.13	High-order harmonic spectra from (1) indium and (2) silver plumes	19
Figure 1.14:	Reduction in resonance enhancement with the change in driving laser wavelength	19
Figure 1.15:	Schematic of HHG from solid surfaces by using double plasma mirrors to reduce pre-pulse	22
Figure 2.1	Block diagram of the Ti:sapphire laser system	28
Figure 2.2 :	A typical wavelength spectrum of the Ti:sapphire laser pulse	31
Figure 2.3	A schematic of second order autocorrelator	32
Figure 2.4	Generation of autocorrelator trace in SHG crystal	32
Figure 2.5	(a) Autocorrelator signal, and (b) its trace using “Promise” software	33
Figure 2.6	Schematic of experimental setup for beam divergence measurement	34
Figure 2.7	a) Magnified image of laser focal spot on CCD, b) intensity profile of the laser spot closely matching the Gaussian fit.	35
Figure 2.8	Schematic of the experimental setup	35
Figure 2.9	A Schematic of XUV spectrograph	38
Figure 2.10:	Typical spectrum from the XUV spectrograph	39
Figure 2.11	A schematic of the improved XUV spectrograph	39

Figure 2.12:	Typical spectrum from the improved XUV spectrograph	39
Figure 3.1	Harmonic spectrum from silver plasma plume in the range of 13 to 38 nm. (a) A typical image of the harmonics and (b) its intensity scan across a horizontal line	44
Figure 3.2	Intense 13 th harmonic order generated in indium plasma plume at ($\lambda=61$ nm)	45
Figure 3.3	Optical spectrum from indium plasma plume: 1) shows the strong excitation conditions, 2) shows weak excitation conditions	46
Figure 3.4	Temporal characteristics of optical emission from low and high excited plasma plumes	47
Figure 3.5	Variation of the intensity of the 35 th harmonic with the pre-pulse laser intensity. The dashed curve is to guide the eye.	48
Figure 3.6	Variation of the intensity of the 13 th harmonic from indium plasma plume with respect to the time delay between the pre-pulse and the driving laser pulse. The dashed curve is to guide the eye.	49
Figure 3.7	Variation of the 21 st harmonic intensity as a function of the distance between the target surface and the axis of the main laser beam	50
Figure 3.8	Dependence of the 21 st harmonic intensity on the focal position of the driving laser radiation.	50
Figure 4.1	High harmonic spectrum as recorded on the CCD camera for (a) indium plasma, (b) InSb plasma (c) Cr plasma	55
Figure 4.2	Comparison of resonance enhancement of particular harmonic order, from GaAs, As and GaP plume, shows the role of target element on resonance enhancement.	56
Figure 4.3	Variation of the 47 th harmonic wavelength for different chirp conditions of the driving radiation. Each curve is shifted vertically to avoid overlap for visual clarity	59
Figure 4.4	Variation of the harmonic spectrum from indium plume with the pulse chirp and pulse width: (a) chirp-free 45-fs pulses, (b) negatively chirped 95-fs pulses, and (c) negatively chirped 250-fs pulses. Each curve is shifted vertically to avoid overlap for visual clarity.	61
Figure 4.5	Harmonic distribution of the Cr plume at different chirps of the driving pulse: (a) chirp-free 45 fs pulse, (b) and (c) negatively chirped 85 fs and 160 fs pulses.	62
Figure 4.6	Harmonic spectra from the GaAs plume as a function of pulse chirp and width. Each curve is shifted vertically to avoid overlap for visual clarity.	63
Figure 5.1	Ray diagram showing the focusing geometry and effect of defocusing on the beam propagation under different focussing conditions.	69
Figure 5.2	Variation of the 23 rd harmonic intensity with the change in focus position of the femtosecond laser w. r. to the centre of the plasma plume. The solid line is to guide the eye.	69

Figure 5.3	Variation of intensity of 41 st harmonic with the change in focus position of femtosecond laser w. r. to the centre of the plasma plume. The solid line is to guide the eye.	70
Figure 5.4:	The laser propagation geometry inside the plasma plume	76
Figure 5.5	Variation of the harmonic intensity with plume length	76
Figure 5.6	Variation of harmonic intensity with harmonic order at two different medium lengths	77
Figure 6.1	HHG spectra recorded for different number of laser shots fired on the same spot	88
Figure 6.2	Observation of second plateau in HHG from Mn plume (a) HHG before optimization (b) HHG after optimization	89
Figure 7.1	TEM images of (a) commercially purchased Ag nanoparticles, (b) commercially purchased Au nanoparticles, (c) chemically prepared Ag triangle platelets. The size of black lines on the images is 50 nm	97
Figure 7.2	TEM images of (a) deposited Ag nanoparticles obtained at low intensity of pre-pulse ($\sim 10^9$ W/cm ²) and (b) deposited disintegrated Ag nanoparticles obtained at high intensity of pre-pulse ($\geq 1 \times 10^{10}$ W/cm ²). The size of black lines on the images is 50 nm	98
Figure 7.3	(a) TEM image of C ₆₀ powder agglomerate before the deposition; (b) TEM image of deposited debris of C ₆₀ after strong excitation ($I = 1 \times 10^{10}$ W/cm ²) of fullerene-containing target. The scale lengths on the images correspond to 2 nm. In the insets, the Fourier transform patterns of the C ₆₀ crystalline nano-powder and debris are shown.	99
Figure 7.4	Typical HHG spectra from silver nanoparticles (solid line) and bulk silver target (dashed line). The intensity of HHG spectrum from bulk Ag target is 10× multiplied for better visibility.	101
Figure 7.5	Comparison of HHG yield from silver nanoparticles prepared in (a) PVA and dried naturally, (b) PVA and dried in oven, and (c) prepared by mixing nanoparticles with glue. The harmonic intensity from the nanoparticle target prepared in PVA and dried in oven is maximum. The spectra (b, c) are shifted up for visual clarity.	102
Figure 7.6	Comparison of relative intensities of harmonics for (a) bulk Ag, (b) Ag nanoparticles, (c) SrTiO ₃ nanoparticles, (d) Au nanoparticles, and (e) bulk In. The intensity of bulk Ag harmonics is multiplied by 10 for better visibility. The intensity of harmonics from nanoparticles is of the order of the enhanced 13 th harmonic from indium plasma. The spectra are sequentially shifted up for visual clarity	103
Figure 7.7	Comparison of harmonic intensity in the case of (a) fullerene plasma and (b) In plasma.	104
Figure 7.8	Variation of the harmonic intensity with number of laser shots in the case of nanoparticle-containing target. The target is irradiated at same place.	105
Figure 7.9	AFM images of the silver deposition in the case of : a) weak ($I \sim 10^{10}$ W/cm ²) excitation, and b) strong ($I \sim 10^{13}$ W/cm ²)	108

excitation of targets. The horizontal and vertical axes show the scan sizes of the two images, whereas the vertical bar at right shows the colour coding for different sized nanoparticles.

Figure 7.10	Comparison of the HHG spectra from a) silver mono-particles, b) in-situ produced silver nanoparticles, and c) from coated silver nanoparticles. The intensity of HHG emission is normalized for comparison. The curves b and c are shifted vertically for visual clarity.	109
Figure 8.1	Laser spectrum when no glass plate is inserted (blue) and when glass plate is inserted in the path of focussing laser pulse (red).	115
Figure 8.2	Bandwidth comparison of HHG (a) from normal laser pulse and (b) from laser pulse after passage through glass plate. Inset shows the expanded view of 17 th harmonic for the two cases.	116
Figure 8.3	Broadening of harmonic spectrum with increase of laser intensity. The harmonic spectrum for higher laser intensity has been shifted up for the ease of visual inspection.	119
Figure 8.4	Variation in harmonic bandwidth with harmonic order	121
Figure 9.1	Electron recombination energy normalized to ponderomotive energy vs. tunnelling phase of electron for (a) only fundamental laser pulse (b) two-colour laser pulse with 2% SH field and (c) two-colour laser pulse with 15% SH field.	127
Figure 9.2	Schematic of the experimental setup	128
Figure 9.3	HHG spectra from Ag plasma at : (a) single-colour (800 nm) pump, (b) orthogonally polarized two-colour pump, and (c) parallel polarized two-colour pump. Side lobes of the odd harmonics in the (a) correspond to the second-order diffraction lines of strong high-order harmonics.	130
Figure 9.4	CCD images of the harmonic spectra obtained from the silver plasma using : (a) two-colour laser pulses from circularly polarized fundamental radiation and (b) two-colour pump from linearly polarized fundamental radiation	131
Figure 9.5	Harmonic spectra obtained from carbon plasma plume using the two-colour pump scheme in the case of negatively chirped (thick line) and positively chirped (thin line) pulses of fundamental radiation.	132
Figure 9.6	Harmonic spectrum from indium plasma using the two-colour pump	133
Figure 9.7	CCD images of the harmonic spectra generated in C ₆₀ plasma using: (a) single-colour fundamental pump (800 nm), (b) two-colour pump (800 nm + 400 nm), and (c) single-colour SH pump (400 nm). The data were collected under similar experimental conditions.	133
Figure 9.8	HHG spectra from excitation with a) strong two-colour pump (b) single-colour fundamental pump (800 nm), and (c) two-colour pump with reduced efficiency through tilting the SH crystal. One may see that odd harmonics reappear with the reduction in SH intensity. The spectra are normalized and shifted vertically to facilitate visual comparison	135

List of tables

Table 2.1	Parameters of the Ti:sapphire laser	30
Table 2.2	Laser parameters during experiment	38
Table 3.1	Optimized laser parameters for high order harmonic generation experiments	51
Table 5.1:	Estimates of various factors contributing to phase-mismatch, coherence length, and absorption length, for different harmonic orders, to calculate the intensity scaling exponent.	82
Table 6.1	Comparison between observed cut-off and calculated harmonic cut-offs	91

Chapter 1

High order harmonic generation : An overview

The nonlinear interaction of an ultrashort laser pulse with matter generates coherent radiation at multiples (harmonics) of the laser frequency. The frequency of the generated radiation extends into the XUV region. This phenomenon is known as high order harmonic generation (HHG) [1].

A brief literature survey of the theoretical and experimental research work carried out in the field of HHG is presented in this chapter. In Section 1.1, a brief introduction to the HHG process is given. Section 1.2 describes some theoretical aspects of the various physical processes responsible for HHG. Finally, a brief review of the experimental work that has been carried out in HHG worldwide is presented in Section 1.3.

1.1. Introduction

High order harmonics can be generated by the interaction of ultrashort pulses (duration $\tau \sim 10^{-12} - 10^{-15}$ s) with gaseous media (laser intensity $I_L \sim 10^{13} - 10^{15}$ W/cm²) [2] or with solid surfaces (typically $I_L > 10^{17}$ W/cm²) [3]. While the interaction of ultrashort laser pulses with a gaseous medium generates only odd harmonics (due to inversion symmetry of the nonlinear process), the same with solid surfaces generates odd as well as even harmonic orders due to breaking of the symmetry at the plasma-vacuum interface. In both the cases, the harmonics propagate along the direction of the refracted / reflected laser beam. In our studies, as we have worked on HHG from underdense plasma plumes, which is like HHG in a gaseous medium, we will be mainly discussing the properties of HHG from gaseous targets.

The interaction of an ultrashort laser pulse with a gaseous medium results in the generation of odd harmonics of the laser frequency. The maximum order of the generated harmonic could be very large and the harmonic wavelength may extend right into the deep XUV - water window spectral range. The harmonic spectrum consists of only odd harmonics, intensity of which decreases rapidly for the first few orders, and thereafter remains nearly constant, which is referred to as the "intensity plateau". The intensity plateau of the harmonics is followed by a sharp "cut-off" where the intensity of harmonics drops rapidly to zero within a few harmonic orders. The process of harmonic generation is generally understood through the semi-classical model known as the "three-step model" which will be discussed in Section 1.2.

Since the process of harmonic generation is phase locked with the driving laser pulse, the generated harmonics have specific properties such as high degree of coherence, and ultra-short pulse duration (few tens of attosecond) [4]. These properties of harmonics, along with their ability to get focussed to diffraction-limited spot sizes [5], make them an ideal high-intensity, ultrashort coherent XUV source. Several applications of HHG have been realized, such as generation of attosecond pulses [4], measurement of ultrafast photo-recombination cross sections [6], probing of rotational dynamics of molecules [7], detection of molecular structure [8], etc. Many other applications have been predicted, such as strong field fast alignment of molecules [9], achievement of ultrahigh focussed intensities [5], etc.

In view of their potential applications, the HHG remains an active area of research. There are mainly three lines of research in HHG studies: 1) increasing the overall intensity of the HHG, 2) increasing the cut-off harmonic order, and 3) making certain harmonics much more brighter than the adjacent ones. Conventionally, the harmonics are generated by the interaction of ultrashort laser pulses with noble gases.

This technique has drawback of very limited number of target materials (i.e. noble gases) for experimentation. We have used plasma plumes for the generation of high order harmonics which have properties similar to gases but opens up a large number of target materials for exploration so that conversion efficiency and harmonic cut-off could be maximized. It also allows one to study HHG in materials like fullerenes, carbon nanotubes and other nano-particles, which is not possible via gaseous route.

1.2. Theoretical background

The theoretical description of HHG mainly comprises of models explaining the HHG from two different types of interactions namely HHG from gaseous plasma and HHG from solid surfaces. In sub-sections 1.2.1 and 1.2.2, we discuss the HHG from gases in terms of single atom model (or semi-classical model), and the propagation of harmonic radiation in the plasma. In sub-section 1.2.3, we discuss a model for HHG from solid surfaces.

HHG from gaseous media have certain salient features such as, a peculiar intensity pattern in which the intensity of harmonics decreases rapidly for first few orders and then remains constant upto a very high order and thereafter it decreases rapidly to form a well-defined cut-off, generation of only odd harmonics, and vanishing of HHG radiation when laser polarization is made circular. On the other hand, the salient features of HHG from solid surfaces are (a) monotonic decrease in intensity with increasing harmonic order and (b) the harmonic intensity is much higher for p -polarized lasers compared to s -polarized laser pulses.

1.2.1. Semiclassical model for HHG in gases

The single atom theory of HHG in gases can be understood through a semiclassical model, usually known as the three-step process [10, 11]. The model, first proposed by Corkum *et al* [10] taking into account the electron trajectories under the influence of laser field, later on improved by Lewenstein *et al* [11] by proposing a quantum mechanical picture of electron trajectories, is depicted in Fig. 1.1.

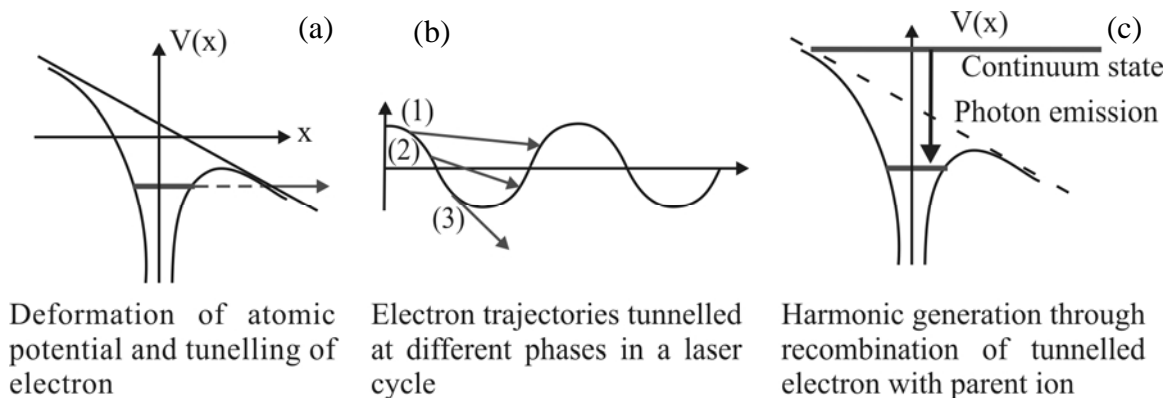


Fig. 1.1: Three-step model of high order harmonic generation [2]

In simple words, the model explains the HHG process in three steps. First, the potential well of the atom, when exposed to the external laser field, gets distorted. The electron which was earlier bound inside the atom can now tunnel out of the potential barrier (Fig. 1.1a). Depending on tunnelling phase, the electron may strike back or may never return to the parent atom, the latter situation is shown by trajectory 3 in Fig. 1.1b. In the former case, when tunnelled electron re-collides with the parent nucleus, it generates a photon with the energy equal to the sum of instantaneous kinetic energy of the electron and ionization potential of the parent atom. It is worth noting here that during this process there are two phases of tunnelling for which the kinetic energy of re-colliding electron is same. Interestingly, the electron which had tunnelled earlier strikes the atom later than the electron which had tunnelled later. These trajectories are known as long and short trajectories and depicted as (1) and (2) in Fig. 1.1b. All the harmonic

orders except for the cut-off harmonic order can be generated by either of the two electron trajectories. For the cut-off order, the two trajectories merge into one.

A simple particle trajectory analysis (Fig. 1.2) reveals the above stated fact. In the computational analysis, it was observed that only the electrons tunnelled (by a cosine electric field) between 0 and $\pi/2$ phase will return to the parent nuclei under the influence of laser field, whereas the electrons tunnelled between phase $\pi/2$ and π will not return to the parent ion. It was found that the electrons tunnelling out at phase $\sim\pi/10$ will generate the harmonic photon with maximum energy. The instantaneous kinetic energy of this electron is equal to 3.17 times the ponderomotive energy (U_p) of the electron in laser field. Thus the maximum energy of harmonic photon is

$$h\nu_{\max} = I_p + 3.17U_p \quad \dots\dots\dots (1.1)$$

where I_p is the ionization potential of the atom. The ponderomotive energy is the average energy of a free electron oscillating under the action of laser field and can be given by the expression

$$U_p = 9.33 \times 10^{-14} I (W / cm^2) \lambda^2 (\mu m^2) \quad \dots\dots\dots (1.2)$$

From the above discussion it is clear that the electrons tunnelled out between phase 0 to $\pi/10$ from long trajectories whereas the electrons tunnelled out between phase

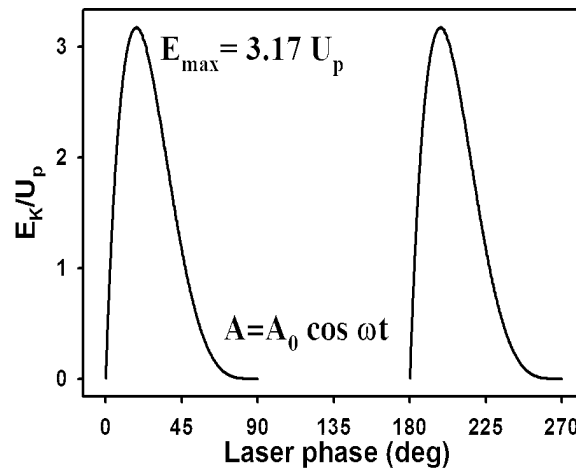


Fig. 1.2: Electron recombination energy vs. laser phase

$\pi/10$ to $\pi/2$ will form short trajectories. It is intuitive that the process is identical in each half of the laser cycle and due to this symmetry, the photons of energy equal to the odd multiple of laser photon energy (*i.e.* odd harmonics) add constructively, even harmonics add destructively, and all other wavelengths add with random phase. This is depicted schematically in Fig. 1.3. As a result, the interaction of a laser pulse during its passage through the gaseous medium results in only odd harmonic generation. At this point, one may also see the effect of circular polarization on HHG. In this condition the tunnelled electrons would never return to its parent atom/ion and one would not observe HHG. Since circular polarization can be written as the sum of two plane polarizations with $\pi/2$ phase difference, any electron tunnelled in such field will be brought back to parent atom/ion by one component of the laser field whereas it would be laterally shifted by the other component of the laser field. As a result the electron would never return to parent atom/ion.

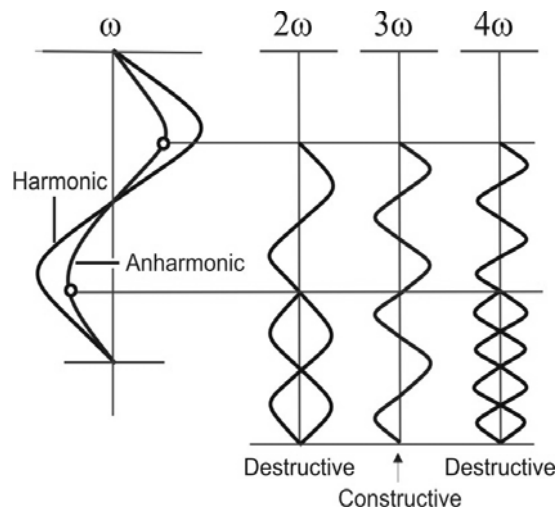


Fig. 1.3: Addition of the harmonic field with propagation results in generation of only odd harmonics

It would appear from Eq. 1.1 that the cut-off of the harmonic radiation can be indefinitely increased by increasing the laser intensity, which is not true [12]. With the increase in laser intensity, the deformation of the atomic potential increases and hence the ionization probability of the atom increases. After a certain intensity, the ionization

probability becomes close to unity. Further increase in laser intensity results in rapid ionization in the medium, increasing the electron density in the plasma. This increases the phase mismatch between the laser pulse and harmonic radiation, which in turn limits further growth of harmonic intensity. Thus, the harmonic intensity can be increased only up to certain laser intensity referred to as the *saturation intensity*. The saturation intensity is higher for materials with higher ionization potential. It follows from Eq. 1.1 that for atoms/ions of a particular ionization state, the cut-off harmonic order is limited by the saturation intensity. Further, if one considers harmonic emitters of a higher ionization potential (either atoms of a different material or higher ionization species of the same material), the cut-off harmonic order can be increased.

The quantum mechanical treatment of above model [11], based on the solution of time dependent Schrödinger equation, visualizes the process of tunnelling of the electron, its acceleration, and subsequent recombination as a nonlinear dipole. The moments of these nonlinear dipoles are calculated by integrating the Schrödinger equation under approximations of single active electron, zero atomic potential for free electron, undepleted ground state, and saddle point method. First three approximations are the approximations for the formation of equations, while the last one is used to integrate the final equation. The saddle point method, also known as *method of steepest descent*, evaluates the integrals which have large exponents as a factor. The model approximates the integral as the value around the zero of the exponent. The integral can be written as (for large λ)

$$F(\lambda) = \int f(z) e^{\lambda S(z)} = \sqrt{\frac{2\pi}{\lambda S''(z_0)}} e^{\lambda S(z_0)} f(z_0) \dots\dots\dots(1.3)$$

The quantum mechanical treatment of three-step model is remarkably successful in describing a number of characteristics of HHG such as HHG cut-off, basic shape of

the HHG spectrum etc. The above description shows the process of HHG from single atom. In the following Section we discuss the effect of propagation on harmonics.

1.2.2. Propagation effects

The overall intensity of the high order harmonics produced in a medium is affected by the phase matching conditions during their propagation inside the gas/plasma medium. If the phase velocity of the laser radiation (fundamental) and the generated harmonic radiation is same, the field of the odd harmonics will add constructively throughout the medium length and the intensity of harmonic radiation will grow as square of the medium length. Since the refractive index of the medium for the fundamental radiation and generated harmonics is somewhat different, the phase velocities for the laser radiation and the harmonic radiation are also different. The difference in phase velocities of the two radiation fields gives rise to the phase mismatch between them, which restricts the quadratic growth of the harmonic intensity with the medium length. The phase matching effect on the high order harmonics generated in *gas medium* was first studied by L'Huillier *et al* [13]. The effect of phase mismatch on the harmonics generated in *plasma plumes* has been studied by us [14].

The field amplitude of the harmonic radiation after the propagation in the medium of length L_{med} may be written as

$$E_q = \int_0^{L_{med}} N_0 d(q\omega_L) dz \quad \dots\dots\dots (1.4)$$

where N_0 is the density of harmonic emitters (mainly neutrals and singly charged ions), and $d(q\omega_L)$ is the nonlinear dipole moment of the emitters for q^{th} harmonic of laser frequency ω_L . The intensity of the q^{th} harmonic can be written as

$$I_q = |E_q|^2 \quad \dots\dots\dots (1.5)$$

In the perfect phase matching conditions the intensity of the harmonics should increase as the square of the length of the generating medium. However, in reality, the phase mismatch between the laser radiation and the generated harmonics, and reabsorption of the harmonic photons restrict the quadratic growth of harmonic intensity with medium length. The phase mismatch between the laser and harmonic radiation is generated from the different phase velocities of laser and harmonic waves due to dispersion. The phase mismatch between laser and q^{th} harmonic order can be written as

$$\Delta k = qk_{Laser} - k_{Harmonic} \quad \dots\dots\dots(1.6)$$

Considering the phase mismatch between the harmonic radiation and the laser field, and re-absorption coefficient (α) of harmonic radiation in the plasma medium, the Eq. 1.5 will get modified as [14]

$$E_q = \int_0^{L_{med}} N_0 d(q\omega_L) \exp(i\Delta kz) \exp[-\alpha(L_{med} - z)] dz \quad \dots\dots\dots (1.7)$$

Various factors contribute to the phase mismatch such as atomic dispersion, plasma dispersion, Gouy dispersion, and the intensity dependent phase shifts in nonlinear dipole.

1.2.3. Harmonic generation from solid surfaces

HHG from solid surfaces can be understood from the ‘*moving mirror model*’ as described by von der Linde *et al* [15, 16] and Lichters *et al* [17]. According to this model, when a femtosecond laser pulse interacts with a solid surface, it generates very short scale length plasma. During the short interaction time with the laser pulse, the ions can be regarded as fixed positive background charges. Electrons in a skin depth layer experience strong electromagnetic forces and are driven back and forth across the vacuum boundary. The details of the electron spatial distribution are neglected and electron motion is represented by the motion of the critical density surface (i.e. the

reflecting surface or the "mirror"). This effective reflecting surface represents the moving mirror.

Consider the spectrum of light reflected from an ordinary optical mirror oscillating at a frequency Ω much smaller than the optical frequency ω_0 . The mirror motion produces a phase modulation, and the spectrum of the reflected light exhibits sidebands at multiples of the modulation frequency. If the mirror could be made to vibrate at $\Omega = \omega_0$ (Fig. 1.4), these modulation sidebands would represent optical harmonics of the fundamental optical frequency. The high order harmonics are generated by beating of moving mirror and the incident laser frequency. In this way, both even and odd harmonic orders are produced, with monotonically decreasing intensity. It is worth mentioning here that with the increase in the plasma scale length, the reflecting surface of oscillating mirror become hazy and the efficiency of harmonic generation process decreases [15].

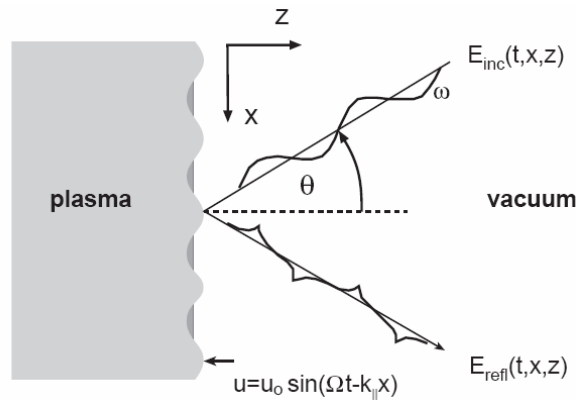


Fig. 1.4: Periodic modulation of solid surface by incident laser pulse resulting in emission of high order harmonics in the direction of reflected laser light [16]

In the nonrelativistic limit, for s-polarized light, there is no movement of electrons normal to target surface and hence there is no harmonic generation for s-polarized light or the harmonics are generated only by p-polarized light. However, at higher intensities, the interaction of laser with electron in the relativistic regime results in

figure-of-eight motion of the plasma electrons (Fig.1.5). Now there is electron oscillation in the direction normal to the target surface also. Thus, in the relativistic regime, the harmonic generation comes from both p -polarized and s -polarized light. However, the intensity of harmonics generated from p -polarized light is much larger than that from s -polarized light.

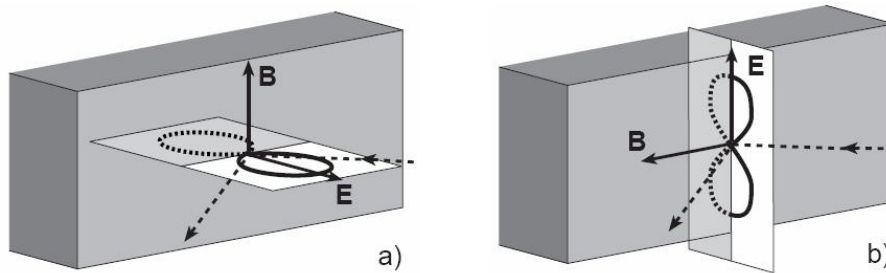


Fig. 1.5: *Fig.-of eight orbit of an electron for: (a) p -polarized light, (b) s -polarized light. [16]*

To increase the harmonic intensity from solid surfaces, it is required to increase the laser intensity. However, as the laser intensity is increased plasma is formed on the target surface by the pre-pulse present in the laser. This preplasma is generated a few nanoseconds before the arrival of the main laser pulse and hence has sufficient time to expand. Thus the formation of preplasma results in a long scale length plasma which in turn results in reduced harmonic conversion efficiency. Hence, in order to increase the harmonic conversion efficiency one needs to increase the laser pulse contrast.

In the next Section we discuss the experimental studies on HHG from gases, and solid surfaces.

1.3. Overview of experimental studies

The HHG studies are focussed towards increasing the harmonic conversion efficiency and the cut-off orders. As explained earlier, mainly two approaches are used for HHG *viz.* HHG from gaseous media and HHG from solid surfaces. We will discuss them briefly in the following sub-sections.

1.3.1. Harmonic generation in gases

Various media, such as gas jets, gas cells, gas filled hollow core fibres, and low ionized plasma plumes from laser ablated solids, were used in HHG experiments. These are discussed briefly in following subsections.

1.3.1.1. Harmonic generation from gas jets

A schematic of HHG from gas jets is shown in Fig. 1.6. A gas jet is generated by puffing the gas through a fast solenoid valve inside an evacuated chamber. Various nozzles can be used to change the density profile of the gas jet. High order harmonics are generated by focussing an ultrashort laser pulse at intensity $\sim 10^{13-15}$ W/cm² in the gas jet. These harmonics are then dispersed by a grazing incidence grating and recorded by a soft x ray detector (such as micro channel plate (MCP) and optical CCD camera combination, or a back illuminated x-ray CCD camera). Owing to its sensitivity and spatial resolution, MCP is the most widely used detector in this field. As one requires 10^{-5} - 10^{-6} mbar vacuum for operation of MCP, differential pumping is a necessary requirement in gas jet experiments.

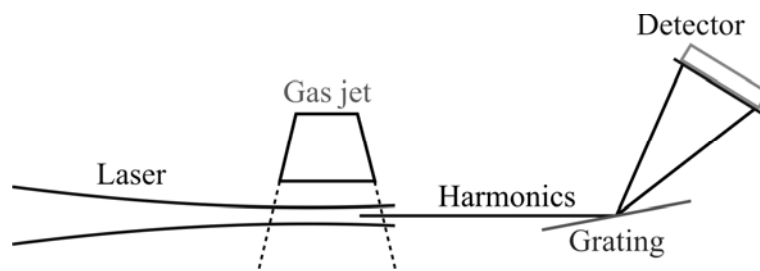


Fig. 1.6 : *Schematic of high order harmonic generation experiment from gas jets*

After the initial experiments of McPherson *et al* [18], the field has developed rapidly. Crane *et al* [19] at the Lawrence Livermore National Laboratory detected harmonics upto 45th harmonic of 600 fs frequency doubled 526 nm Nd:Glass laser in experiments with helium. In 1993, Macklin *et al* [20] reported harmonic generation up to 109th order of 125 fs 800 nm Ti:sapphire laser leading to sub-10 nm harmonic orders.

The high order harmonic emission was extended into the water window region (2.3 - 4.4 nm) by Z. Chang *et al* [12]. They observed the harmonic radiation up to 2.7 nm in He, associated with unresolved emission from harmonic number 297 [12]. Spielmann *et al* [21] have used few-cycle Ti:sapphire laser of ($\tau \sim 5$ fs) to extend the harmonic emission into water window region, and harmonics up-to photon energy ~ 400 eV were generated using helium gas jets.

A typical spectrum of the harmonics generated using laser pulses of ≥ 30 fs pulse duration is shown in Fig. 1.7a, where the harmonic emission in the plateau region followed by a sharp cut-off can be seen. Fig. 1.7b shows the harmonic emission using sub-10 fs pulses, continuum plateau extension can be observed in this figure extending the spectrum to sub-10 nm region [22].

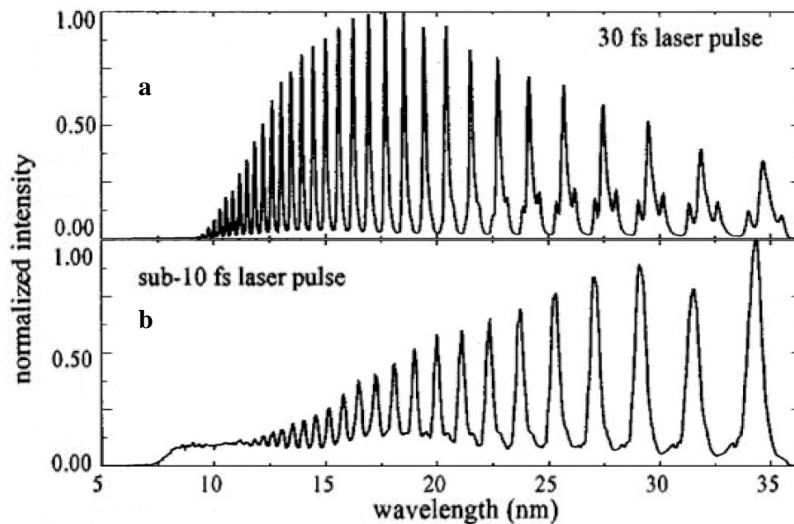


Fig. 1.7: High order harmonic spectrum for different values of laser pulse duration [22]

Gas jets are simple to generate but there are some limitations which compel researchers to look for other targets. First limitation is their small length. Mostly gas jets are ~ 5 -10 mm long. Hence if one wants to increase the harmonic emission intensity by increasing the length of the medium, it may not be easy to do this by using gas jets. Secondly, there is non-uniformity of the gas density along the laser propagation. Final

limitation comes due to the lack of laser guiding mechanism to sustain high peak power along the interaction length.

1.3.1.2. Quasi phase matched harmonic generation in hollow core fibres

Due to the above said limitations of the gas jets, gas filled hollow core fibres have been utilized to increase the conversion efficiency and cut-off of high order harmonic radiation [23, 24]. Hollow core fibres are glass capillaries of diameter $\sim 50\text{-}100\ \mu\text{m}$. These are filled with low pressure gases (few tens of mbar) to generate high order harmonics. The greater uniformity of the gas density, long interaction length (1-10 cm) due to laser guiding inside the fibre, and quasi phase matching (QPM) through the modulation of fibre diameter can be achieved in hollow fibres, resulting in better harmonic conversion efficiency.

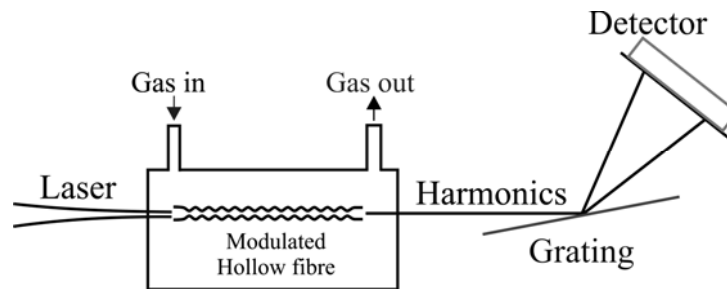


Fig. 1.8: HHG from modulated hollow core fibre

In order to get quasi-phase matching (QPM) the fibre surface is modulated, the modulation period is $\sim 1\text{-}2\ \text{mm}$. Modulation of the fibre surface results in the laser intensity modulation inside the fibre. The modulation in laser intensity results in modulation of electron density inside the fibre, which in turn results in different phase matching conditions in narrow and wide regions of the fibre. This results in QPM in HHG process and results in the enhancement of harmonic intensity.

Both, modulated and unmodulated fibres have been used for HHG. A schematic of the experimental setup for HHG using modulated hollow core fibres is shown in Fig.

1.8. Rundquist *et al* [23] were the first to use a hollow core fibre for HHG experiments. The fibre used in their experiment was unmodulated. The use of hollow core fibre results in 2 to 3 orders of magnitude enhancement in the intensity of the harmonics in the wavelength range of 17-32 nm. Later on, Paul *et al* [24] observed the extension in harmonic cut-off with the use of modulated hollow core fibres. The harmonic cut-off using 25 fs Ti:sapphire laser at an intensity 5×10^{14} W/cm², with straight hollow fibre filled with helium gas was ~ 14.5 nm [23], which extended to ~ 11 nm by the use of modulated fibre with modulation period ~ 1 mm and it further extends to ~ 7 nm by the use of modulated fibre with modulation period ~ 0.5 mm [24].

1.3.1.3. Harmonic generation from gas cells

As the production of hollow fibres and their alignment in the vacuum chamber is a cumbersome task, gas cells have been used as an alternative to the gas jets. Gas cells have the advantage of uniform density over the whole interaction region. They provide a longer interaction length and self-guiding mechanisms to enhance the laser intensity along the interaction length. A typical experimental setup utilizing a gas cell as target is shown in Fig. 1.9. Gas cells are usually made of glass and they have a sealed movable mechanism to vary the interaction length. The two sides of the gas cell are sealed with thin foils. The focussed laser punctures these foils and makes holes for entrance and exit. Thus alignment of the gas cell with the laser axis becomes an easy task. Various phase

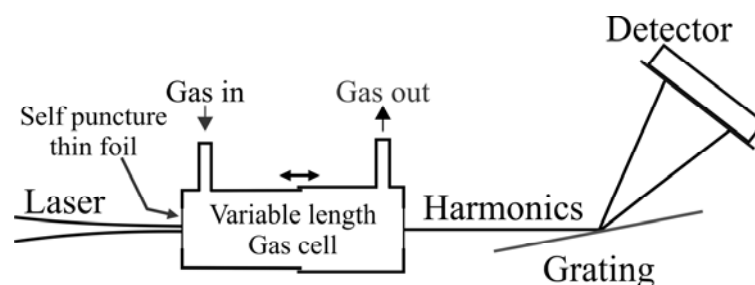


Fig. 1.9: Harmonic generation using variable length gas cells

matching and absorption effects have been studied using gas cells. For example, Lange *et al* [25] have observed periodic oscillations in harmonic intensity with gas pressure as shown in Fig. 1.10. From Eq. 1.7 it can be seen that as the pressure of the gas is increased, the harmonic intensity increases as the number of harmonic emitters are increased. However, with the increase in gas pressure, the phase mismatch between laser and harmonic radiation also increases. When the phase mismatch equals π , the harmonic intensity decreases to zero. If one increases the gas pressure further, the phase mismatch again increase beyond π and harmonic intensity start increasing. In this way an oscillatory harmonic intensity variation is observed, as seen from Fig. 1.10.

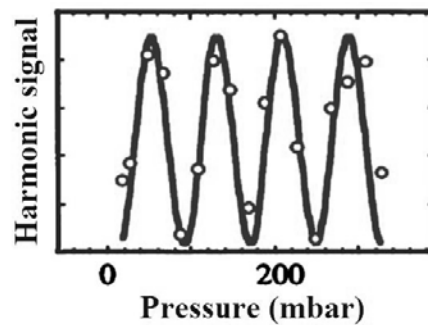


Fig. 1.10: Harmonic intensity with gas pressure [25]

For absorptive medium where the harmonic radiation is absorbed in the generating medium, the harmonic intensity oscillations were damped as shown by Tosa *et al* [26]. They used a 14 cm long gas cell, and harmonics were generated by self-guided laser beam. The harmonic intensity variation with the medium length is shown in Fig. 1.11. The harmonic intensity saturates for a gas cell of length 8 cm. Any further increase in the medium length results in damped oscillatory behaviour.

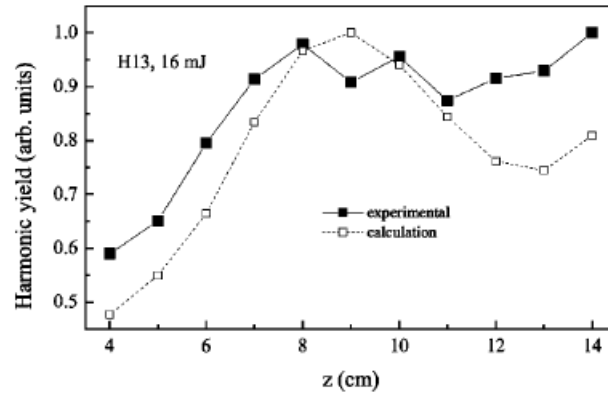


Fig. 1.11: Harmonic intensity variation with medium length [26]

1.3.2. Harmonic generation from plasma plumes

Due to the limited number of available gases in nature, the experimentation on the properties of high order harmonics with the properties of gas is limited. For generating high order harmonics, instead of using a gas jet, one can also use plasma plumes produced at the surface of solid targets on laser irradiation. This gives a wider scope for studying the effect of atomic properties on the HHG.

1.3.2.1. Laser ablated plasma plumes

The first experiments on HHG from laser ablated plasma plumes were done by Wahlström *et al* [27]. The plasma plume was formed by focussing a 55 mJ 100 ps Nd:YAG laser pulse on the surface of Na or K target. The harmonic generation up to 27th order was reported, however no plateau like pattern for high order harmonics was observed. Later on, Ganeev *et al* [28] reported plateau-like harmonic emission from the plasma plumes generated from the surface of various solid targets. In their studies, the highest harmonic order generated was 101st order of Ti:sapphire laser, which was observed using Mn targets [29]. In addition to the plateau-like harmonic emission, it was observed that in certain plasma plumes the intensity of particular harmonic orders was

much higher compared to the neighbouring harmonics [28]. This is known as *resonance enhancement* of harmonics and will be discussed in next sub-section.

Plasma plumes have certain advantages over the gas jets, such as less stringent vacuum requirements, ease of generation, and availability of large number of target materials. With the availability of large number of target materials, one can explore the nonlinear properties of the materials for efficient harmonic generation. The key feature that enables the generation of high order harmonics in plateau region is that, the plumes are low excited, and they mainly consists of neutral and singly charged particles and essentially behave like gases.

A schematic of the HHG setup from low laser ablated plasma plumes is shown in Fig. 1.12. The plume is generated by focussing a low intensity pre-pulse on the solid surface (the pre-pulse is usually a part of uncompressed laser radiation). This results in the generation of ablation plume mainly consisting of neutral and singly charged particles. After certain delay (~10-100 ns) when the plume is sufficiently expanded and cooled down, the fs laser beam is focussed in the plume. Nonlinear interaction between the laser and expanded plume results in HHG.

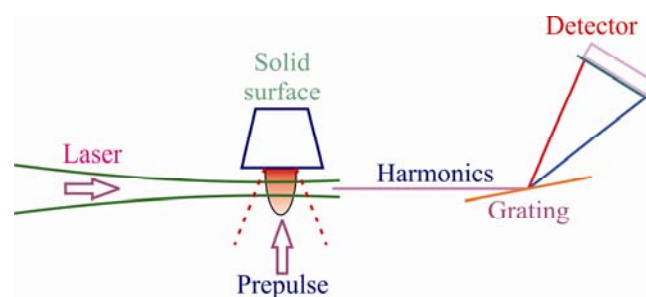


Fig. 1.12: Schematic of high order harmonic generation from laser ablated plasma plumes

1.3.2.2. Resonance enhancement of harmonics

The enhancement in the intensity of harmonic radiation remains an important aim of HHG experiments for their utilization in practical applications. Enhancement in the

intensity of single or bunch of harmonic orders through the overlapping of the harmonic wavelengths with atomic/ionic transitions is predicted theoretically by some groups [30, 31]. The use of low excited plasma plumes is especially promising for studying resonance enhancement of the intensity of particular harmonic orders, as the availability of large number of target material increases the probability of overlapping of atomic/ionic transitions with harmonic wavelengths greatly. Fig. 1.13 compares two high order harmonic spectra from 1) indium and 2) silver plasma plumes. One can see that the intensity of harmonics for silver plasma plume remains in a plateau whereas the intensity of the 13th H of indium was much enhanced compared to the neighbouring harmonic orders.

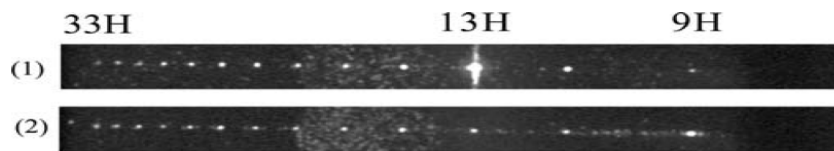


Fig. 1.13 High-order harmonic spectra from (1) indium and (2) silver plumes [28]

Similarly ~20 fold enhancement of 17th harmonic of Ti:sapphire laser pulse was observed (Fig. 1.13) in the experiments with the low excited plumes of tin [32]. It is also reported in the same work that this enhancement disappeared when the central wavelength of the pump laser was changed from 795 nm to 778 nm.

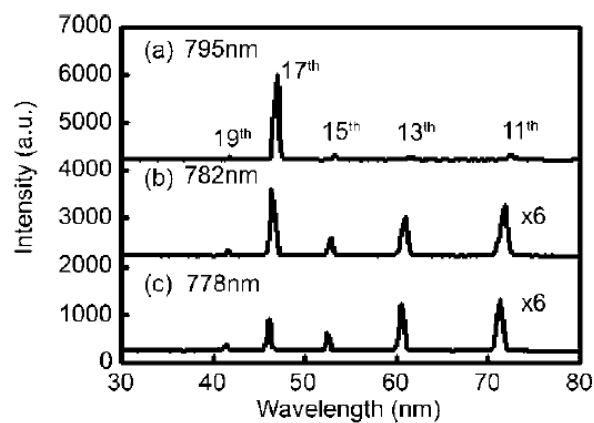


Fig. 1.14: Reduction in resonance enhancement with the change in driving laser wavelength [32]

As shown in Fig. 1.13, the resonance enhancement of high order harmonics may provide a good method to generate coherent XUV radiation. We have also observed 200x enhancement of the 13th order harmonic generated in our study of HHG from indium plumes [33] indicating that the technique may be used to substantially enhance the harmonic conversion. The theoretical views and experimental aspects of resonance enhancement in high order harmonics generated from plasma plumes will be discussed in more detail in Chapter 3.

1.3.3. Harmonics from solid surfaces

As mentioned earlier, the high order harmonics can also be generated from the interaction of ultrashort laser pulses with solid surfaces. The physical picture of HHG from solid surfaces has been discussed in Sec. 1.2.3. The reflection of laser light from oscillating plasma boundary results in the generation of all (odd as well as even) harmonic orders. As the harmonic intensity decreases monotonically with harmonic order, the cut-off depends on the sensitivity of the detector system. HHG from solids was observed for the first time by Carman *et al* [34] using nanosecond pulses of CO₂ (10.6 μm) laser. Specularly reflected harmonics from solid surfaces up to the eighteenth order of Ti:sapphire laser (800 nm) were observed by von der Linde *et al* [16] using a 130 fs, 30 mJ Ti:sapphire laser. Norreys *et al* [35] have observed harmonic emission up-to 75th order with a 1053 nm, 2.5 ps Nd:Glass laser. In this case, the harmonic radiation was spread over a large solid angle. Ganeev *et al* [36] have observed high order harmonic emission from the solid surfaces using 27 ps Nd:Glass laser pulses. It was observed that harmonics were generated by both *p*- and *s*-polarizations of laser in non-relativistic limit, contradictory to the theoretical expectation. The observed anomaly was explained in

terms of the role of Faraday rotation of laser polarization through self-generated magnetic field in plasma [36].

In the quest for ever higher order of harmonic generation, Dromey *et al* [37] have reported the generation of high order harmonics up to 850th order of 1053 nm, 600 fs Vulcan laser. The pre-pulse contrast was enhanced using double plasma mirror to $> 10^{11}$. It is reported that cut-off of harmonic emission decreases considerably if the plasma mirror setup is removed. In the line of earlier studies Dromey *et al* have found that although, the harmonic intensity decreases monotonically with harmonic order, the slope was smaller. It was observed that the decrease in harmonic intensity follows a power law $I_q \propto q^p$ where $p \approx 5.5-3.3$ in the non-relativistic limit. However, the value of p in the present experiment was reduced to $\approx 3.0-2.0$ due to relativistic effects [37]. Since the value of p decreases with increasing intensity, the high intensity lasers are desirable for efficient HHG from solid surfaces. On the other hand, as discussed earlier, in the case of the gaseous targets it is not possible to increase the harmonic intensity simply by increasing the laser intensity, as the increase in laser intensity results in rapid ionization of gas atoms thereby reducing the number of harmonic emitters and the harmonic intensity saturates. This makes solid surfaces a strong contender for HHG with ultrahigh intensity lasers. The HHG from solids is also free from the phase matching effects as the harmonics generated from solid surfaces do not propagate inside the medium, resulting in more coherent emission.

As discussed earlier for the generation of efficient specularly reflected HHG from solid surfaces, besides high intensity of the laser, steep density gradient plasma is also required [15, 37]. Creating a sharp plasma boundary becomes a formidable task with ultrahigh intensity lasers as the intensity of pre-pulse even at contrast of 10^7 is sufficient to create preplasma, thereby creating a shallow density profile. Special techniques such

as use of plasma mirrors are employed to increase the contrast further [37]. A schematic of the setup for HHG using solid surfaces is given in Fig. 1.15. Plasma mirrors are polished glass surfaces. The laser beam is incident over these surfaces under loosely focussed condition. The pre-pulse cannot create plasma at this condition and hence the reflectivity of the surface is poor and most of the laser energy is transmitted. With the arrivals of the main pulse, plasma is created at the surface and the surface act as a plasma mirror for the main pulse. Thus, the reflected pulse is without much pre-pulse, and hence the contrast of the laser pulse is improved.

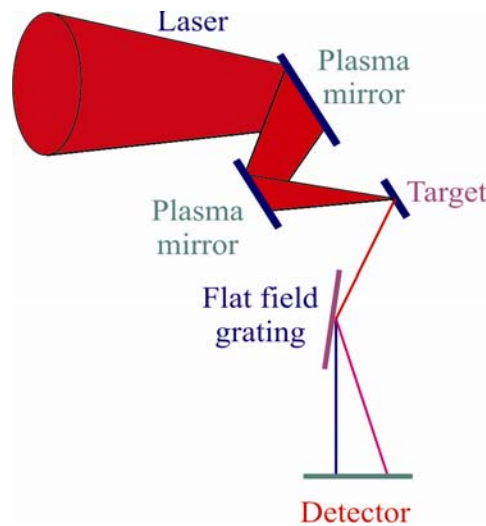


Fig. 1.15: Schematic of HHG from solid surfaces by using double plasma mirrors to reduce pre-pulse [37]

Bibliography

1. C. Winterfeldt, and G. Gerber, “Optimal control of high-harmonic generation”, *Rev. Mod. Phys.* **80**, 117 (2008).
2. P. Balcou *et al.* “High-order-harmonic generation: towards laser-induced phase matching control and relativistic effects”, *Appl. Phys. B* **74**, 509 (2002).
3. U. Teubner and P. Gibbon “High-order harmonics from laser-irradiated plasma surfaces”, *Rev. Mod. Phys.* **81**, 445 (2009).

4. F. Krausz and M. Ivanov, "Attosecond physics" *Reviews of Modern Physics* **81**, 163 (2009).
5. S. Gordienko, A. Pukhov, O. Shorokhov and T. Baeva "Coherent focussing of high harmonics: A new way towards the extreme intensities", *Phys. Rev. Lett.* **94**, 103903 (2005).
6. C. Jin, A. T. Le and C. D. Lin "Isolated attosecond pulse emission in the plateau region of high-order harmonics driven by a 7 fs 800 nm laser field", *Phys. Rev. A* **79**, 053413 (2009).
7. S. Ramakrishna, and T. Seideman, "High-order harmonic generation as a probe of rotational dynamics" *Phys. Rev. A* **77**, 53411 (2008).
8. T. Kanai, E. Takahashi, Y. Nabekawa, and K. Midorikawa, "Observing molecular structures by using high-order harmonic generation in mixed gases" *Phys. Rev. A* **77**, 41402 (2008).
9. A. Abdurrouf, and F. H. M. Faisal, "Theory of intense-field dynamic alignment and high-order harmonic generation from coherently rotating molecules and interpretation of intense-field ultrafast pump-probe experiments" *Phys. Rev. A* **79**, 23405 (2009).
10. P. B. Corkum, "Plasma perspective on strong field multiphoton ionization", *Phys. Rev. Lett.* **71**, 1994 (1993).
11. M. Lewenstein, Ph. Balcou, M. Yu. Ivanov, Anne L'Huillier, and P. B. Corkum, "Theory of high-harmonic generation by low-frequency laser fields", *Phys. Rev. A* **49**, 2117 (1994).

12. Z. Chang, A. Rundquist, H. Wang, M. M. Murnane, and H. C. Kapteyn, "Generation of coherent soft x rays at 2.7 nm using high harmonics", *Phys. Rev. Lett.* **79**, 2967 (1997), Erratum: *Phys. Rev. Lett.* **82**, 2006 (1999).
13. A. L'Huillier, X. F. Li, and L. A. Lompré, "Propagation effects in high-order harmonic generation in rare gases", *J. Opt. Soc. Am. B* **7**, 527 (1990).
14. H. Singhal, V. Arora, B. S. Rao, P. A. Naik, U. Chakravarty, R. A. Khan, and P. D. Gupta "Dependence of high-order harmonic intensity on the length of preformed plasma plumes", *Phys. Rev. A* **79**, 023807 (2009).
15. D. von der Linde and K. Rzàzewski "High-order optical harmonic generation from solid surfaces", *Appl. Phys. B* **63**, 499 (1994)
16. D. von der Linde, "Generation of high order optical harmonics from solid surfaces", *Appl. Phys. B* **68**, 315 (1999).
17. R. Lichters, J. Meyer-ter-Vehn, A. Pukhov, "Short-pulse laser harmonics from oscillating plasma surfaces driven at relativistic intensity", *Phys. Plasmas* **3**, 3425 (1996).
18. A. McPherson, G. Gibson, H. Jara, U. Johann, T. S. Luk, I. A. McIntyre, K. Boyer, and C. K. Rhodes, "Studies of multiphoton production of vacuum-ultraviolet radiation in the rare gases", *J. Opt. Soc. Am. B* **4**, 595 (1987).
19. J. K. Crane, M. D. Perry, S. Herman, R. W. Falcone, "High-field harmonic generation in helium", *Opt. Lett.* **17**, 1256 (1992).
20. J. J. Macklin, J. D. Kmetec, and C. L. Gordon, "High-order harmonic generation using intense femtosecond pulses", *Phys. Rev. Lett.* **70**, 766 (1993).

21. Ch. Spielmann, N. H. Burnett, S. Sartania, R. Koppitsch, M. Schnurer, C. Kan, M. Lenzner, P. Wobrauschek, F. Krausz, "Generation of coherent x-rays in the water window using 5-femtosecond laser pulses", *Science* **278**, 661 (1997).
22. L. Poletto G.e Tondello, and P. Villoresi, "High-order laser harmonics detection in the EUV and soft x-ray spectral regions", *Rev. Sci. Instrum.* **72**, 2868 (2001).
23. A. Rundquist, C. G. Durfee, Z. Chang, C. Herne, S. Backus, M. M. Murnane, H. C. Kapteyn, "Phase matched generation of coherent soft x-rays", *Science* **280**, 1412 (1998).
24. P. M. Paul, E. S. Toma, P. Breger, G. Mullot, F. Audebert, Ph. Balcou, H. G. Muller, P. Agostini "Observation of a train of attosecond pulses from high harmonic generation", *Science* **292**, 1689 (2001).
25. H. R. Lange, A. Chiron, J. F. Ripoche, A. Mysyrowicz, P. Breger, and P. Agostini, "High-order harmonic generation and quasiphase matching in xenon using self-guided femtosecond pulses", *Phys. Rev. Lett.* **81**, 1611 (1998).
26. V. Tosa, E. Takahashi, Y. Nabekawa, and K. Midorikawa, "Generation of high-order harmonics in a self-guided beam" *Phys. Rev. A* **67**, 063817 (2003).
27. C. G. Wahlstrom, S. Borgstrom, J. Larsson, and S.-G. Pettersson, "High-order harmonic generation in laser-produced ions using a near-infrared laser", *Phys. Rev. A* **51**, 585 (1994).
28. R. A. Ganeev, M. Suzuki, M. Baba, H. Kuroda, "Generation of strong coherent extreme ultraviolet radiation from the laser plasma produced on the surface of solid targets", *Appl. Phys. B* **81**, 1081 (2005).

29. R. A. Ganeev, L. B. E. Bom, J. C. Kieffer, M. Suzuki, H. Kuroda, and T. Ozaki, “Demonstration of the 101st harmonic generated from a laser-produced manganese plasma”, *Phys. Rev. A* **76**, 023831 (2007).
30. D B Milošević, “High-energy stimulated emission from plasma ablation pumped by resonant high-order harmonic generation”, *J. Phys. B* **40**, 3367 (2007).
31. P. V. Redkin and R. A. Ganeev, “Simulation of resonant high-order harmonic generation in a three-dimensional fullerene like system by means of a multi-configurational time-dependent Hartree-Fock approach”, *Phys. Rev. A* **81**, 063825 (2010).
32. M. Suzuki, M. Baba, R. Ganeev, H. Kuroda, and T. Ozaki “Anomalous enhancement of a single high-order harmonic by using a laser-ablation tin plume at 47 nm”, *Opt. Lett.* . **31**, 3306 (2006).
33. R. A. Ganeev, H. Singhal, P. A. Naik, V. Arora, U. Chakravarty, J. A. Chakera, R. A. Khan, I. A. Kulagin, P. V. Redkin, M. Raghuramaiah, and P. D. Gupta, “Harmonic generation from indium-rich plasmas”, *Phys. Rev. A* **74**, 063824 (2006).
34. R. L. Carman, D. W. Forslund, and J. M. Kindel, “Visible harmonic emission as a way of measuring profile steepening”, *Phys. Rev. Lett.* **46**, 29 (1981).
35. P. A. Norreys *et al*, “Efficient extreme UV harmonics generated from picosecond laser pulse interactions with solid targets”, *Phys. Rev. Lett.* **76**, 1832 (1996).
36. R. A. Ganeev, J. A. Chakera, M. Raghuramaiah, A. K. Sharma, P. A. Naik, and P.D. Gupta, “Experimental study of harmonic generation from solid surfaces irradiated by multi-picosecond laser pulses”, *Phys. Rev. E* **63**, 026402 (2001).
37. B. Dromey *et al*, “High harmonic generation in the relativistic limit”, *Nature Phys.* **2**, 456 (2006).

Chapter 2

Experimental setup and diagnostic system

The laser used in the present experimental study is a 10 TW, 45 fs, 10 Hz Ti:sapphire laser system. In this chapter, we present a brief description of this laser and the characterization of various parameters of the laser pulse. This is followed by the description of experimental arrangement for high order harmonic generation, their detection and measurement.

2.1. Ti:sapphire laser system

The laser used in the experimental study is a chirped pulse amplification (CPA) [1] technique based commercial Ti:sapphire laser system. The oscillator generates nanojoule pulses of ~ 20 fs duration at 75 MHz. A block diagram of the laser system is shown in Fig. 2.1. Generation of such small duration pulses is made possible by a mode-locking technique known as *Kerr-lens mode-locking* (KLM) [2]. This technique exploits the self-focussing of the laser pulses inside the lasing medium due to Kerr effect for the generation of femtosecond pulses. In such oscillators, initially the laser is in continuous free running mode. Then the laser cavity is disturbed externally. The disturbance of laser cavity results in the generation of very short duration pulse known as ‘coherent spike’. Coherent spike is a noise pulse for which all the lasing modes are inherently locked. Due to its small duration, the coherent spike has highest intensity and hence it undergoes largest self-focussing (due to Kerr effect) inside the laser crystal, and it gets amplified inside the lasing medium. The pulse duration of coherent spike would then be increased due to dispersion, by the laser crystal and air path. These factors introduce positive

dispersion in the laser pulse and to compensate these dispersions, passive components that provide negative dispersion are required. Prism pairs [3] and chirp mirrors [4] are generally employed for such applications. In this way one gets a stable femtosecond laser pulse having repetition rate corresponding to the optical path of the laser oscillator.

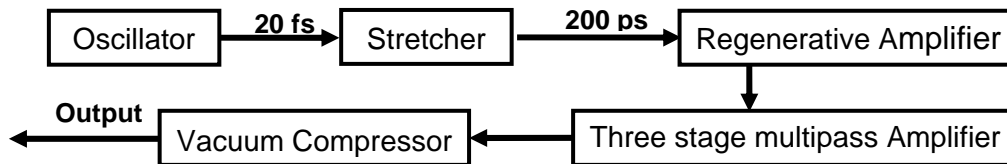


Fig. 2.1 Block diagram of the Ti:sapphire laser system

These pulses are then stretched using a pulse stretcher. The pulse stretcher uses a grating pair and a cylindrical mirror (known as Öffner type stretcher [5]), introduces positive linear chirp in the laser pulse and increases its duration from ~ 20 fs to ~ 200 ps. In a positive linearly chirped pulse, the wavelength of the pulse decreases linearly in time *i.e.* the initial portion of the pulse has longer wavelengths and the later portion of the pulse has shorter wavelengths.

The stretched pulse is injected into a regenerative (regen.) amplifier which is a low gain multipass amplifier that works in small signal amplification regime. In our case, the single pass gain of the regenerative amplifier is ~ 2 , whereas the overall gain of the amplifier is $\sim 10^5$. Its high gain is because it is basically a seeded oscillator. The energy of the seed pulse gets amplified to few micro joules in the regenerative amplifier [6]. The regen. amplifier is cavity dumped every 100 msec (*i.e.* at 10 Hz or at lower rep-rate, as desired).

In addition to the main pulse, there are laser pre-pulses present before the main pulse. The pre-pulses present in the regen. output pulse are mainly of two types, 1) amplified spontaneous emission (ASE), generated by the amplification of spontaneous emission in regenerative amplifier and 2) pre-pulse generated by the leakage of the pulse

ejector during the round trips in the regen. amplifier. To reduce the pre-pulse level, a *pulse cleaner* is used. The pulse cleaner consists of a fast Pockels cell which rotates the polarization of the laser pulse by 90° for a small time window of about 5 ns. This pulse is then passed through a polarizer. The polarizer rejects the pre-pulses and passes the main laser pulse (which is rotated by 90° by the Pockels cell), resulting in reduction of pre-pulse level. The rejection ratio of the pre-pulse depends on the extinction of the polarizers and switching of the Pockels cell. This pulse is then amplified in two bow-tie multipass amplifiers (one pre-amplifier and the other main amplifier) to achieve its final energy of ~ 600 mJ.

The amplified stretched pulse is then allowed to pass through a pulse compressor resulting in a laser pulse of 45 fs duration, and energy ~ 450 mJ. The pulse compressor employs a parallel grating pair along with a retro mirror to compensate the positive chirp of the laser pulse [7]. The negative chirp introduced by the pulse compressor depends on the separation between the two gratings. As one increases the separation the negative chirp is increased and at optimum value of the grating separation, the negative chirp introduced by the compressor compensates the positive chirp of the stretched laser pulse. Increasing/decreasing the grating separation from this optimum value results in negatively/positively chirped pulses. It may be noted that the pulse is not compressed to its original duration at oscillator. This is due to the reduction of pulse spectrum through gain narrowing during the amplification of the laser pulse [8].

The energy and repetition rate of the laser can be varied by changing the gain of multi-pass amplifiers and the ejection frequency of the pulse ejector, respectively. In the Table 2.1, we summarize the important parameters of the laser system.

Laser Parameter	Value
Pulse duration	45 fs (minimum)
Wavelength	790 nm \pm 10 nm (central)
Bandwidth	20 nm
Repetition rate	1, 2, 3, 5, 10 Hz, or single
Energy per pulse	Upto 450 mJ
Power	Upto 10 TW
Maximum intensity	Upto 4×10^{18} W/cm ²

Table 2.1 Parameters of the Ti:sapphire laser

2.2. Characterization of the laser pulse

Prior to any laser-plasma interaction experiment, it is essential to characterize the laser pulse for its various parameters viz. the pulse energy, spectrum, duration, beam divergence, and the pre-pulse contrast ratio, as these parameters influence the interaction process. The laser energy can be measured by standard pyro-electric energy meters. In the following, a brief account of the techniques for measuring the remaining parameters, and actual measurements are presented.

2.2.1. Laser spectrum

The spectrum of the final laser pulse was measured using an optical spectrograph with wavelength range 570 nm - 1100 nm. A typical spectrum of the laser pulse is shown in Fig. 2.2. The measured laser spectrum has a peak wavelength at 790 nm and bandwidth (FWHM) of about 20 nm ($\Delta\lambda$). The temporal profile of the laser pulse is expected to be hyperbolic secant squared (sech^2) type. This profile is generated because such pulses self-maintain their envelope (known as soliton pulses) during propagation in a chirp compensating system [9]. Applying uncertainty principle to the hyperbolic secant squared (sech^2) pulses, the product of frequency bandwidth and pulse duration should be $\Delta\nu \cdot \tau \geq 0.315$ [10], (or $\Delta\lambda(\text{nm}) \cdot \tau(\text{fs}) \geq 660$ for 790 nm laser). As per this relation the

expected smallest pulse duration comes out to be ~ 34 fs, which is smaller than the observed pulse duration of ~ 45 fs. The larger duration of observed pulse may be due to the nonlinear chirp in the laser pulse which cannot be compensated by the pulse compressor.

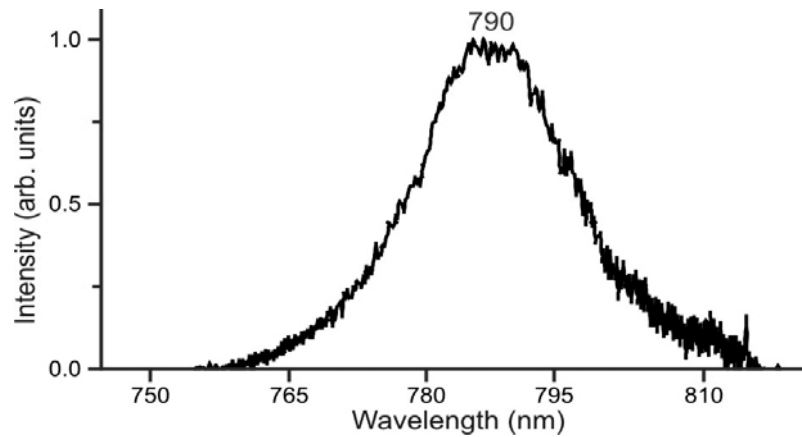


Fig. 2.2 : *A typical wavelength spectrum of the Ti:sapphire laser pulse*

2.2.2. Pulse duration measurement

Measurement of pulse duration is an important aspect of the ultrashort laser pulse - plasma interaction. Intensity autocorrelation method [11] is used to measure the duration of ultrashort laser pulses. In the second order autocorrelator shown in Fig. 2.3a, a beam splitter splits the incoming laser beam into two, which are then passed through a nonlinear crystal for second harmonic generation. If the two beams overlap both in space and time, a second harmonic beam is generated in the direction mid-way between the two beams (non-collinear phase matching). The temporal overlap of the two beams is achieved by the adjustment of the delay line of one arm of the autocorrelator. The angle between two beams and the laser pulse duration together determine the spatial width of the second harmonic correlated beam. A ray diagram of the intensity autocorrelator is shown in Fig. 2.3.

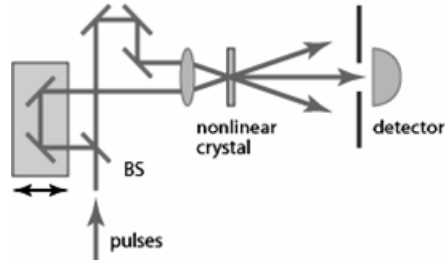


Fig. 2.3 A schematic of second order autocorrelator

The detector shown in Fig. 2.3 is a space resolved detector like a CCD camera. A ray diagram for the generation of autocorrelation trace from the overlap of the two ultrashort pulses is shown in Fig. 2.4. Only in the case of spatial and temporal overlap of two beams, the central second harmonic pulse is generated, known as autocorrelator trace. As mentioned earlier, the width of the central trace depends on the duration of the laser pulse and the temporal profile of the laser pulse. In a way, the measurement of the autocorrelation trace width does not give full information about the ultrashort pulse, as one has to know (or assume) the shape of the laser pulse in order to know the exact duration of the pulse.

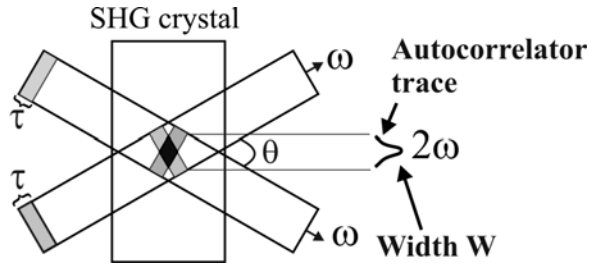


Fig. 2.4 Generation of autocorrelator trace in SHG crystal

The width of the autocorrelator trace (W) is related to the pulse width τ (FWHM) of the laser pulse and the cross-over angle θ between the two overlapping beams (see Fig. 2.4) by the relation [11]

$$\tau = \frac{2 W \sin(\theta / 2)}{K c} \dots\dots\dots (2.1)$$

where K is a constant which depends on the exact temporal shape of the laser pulse, and c is the velocity of light. For a hyperbolic secant squared (sech^2) pulse, $K = 1.55$. Fig. 2.5 shows a typical autocorrelator signal and its trace obtained using *Promise* software.

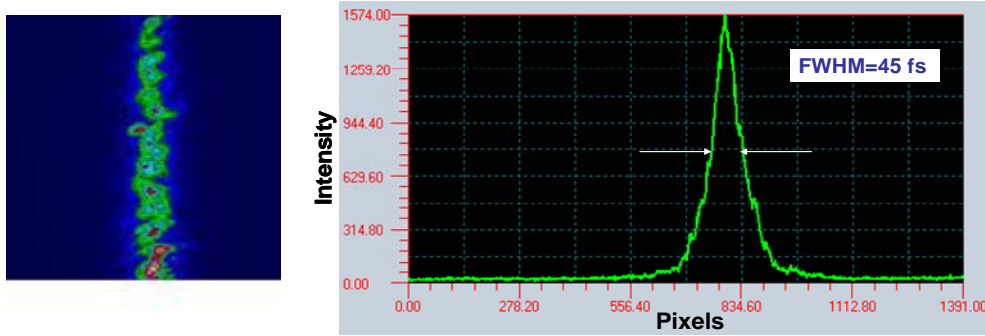


Fig. 2.5 (a) Autocorrelator signal, and (b) its trace using “*Promise*” software

Precise measurement of the cross-over angle θ is a difficult task and some error is always involved with such measurement. We have used another simple approach for the calibration of time axis with the CCD pixels. In this method, a small delay is introduced in one of the laser pulses. The peak of autocorrelation trace is shifted by the amount of the delay. The difference between the two autocorrelation peaks directly gives the time delay in terms of the CCD pixel. For example, if the delay between two pulses is changed by $10 \mu\text{m}$, the peak of overlapping pulse is shifted by ~ 33.3 fs. Thus the pixel shift of autocorrelator trace is equal to 33.3 fs. This method gives an accurate means of the measurement of the pulse duration. In this geometry, the formula for pulse duration measurement gets modified as

$$\tau = \left(\frac{W(\text{pixel})}{K} \right) \times \text{calibration factor} \left(\frac{\text{fs}}{\text{pixel}} \right) \dots\dots\dots (2.2)$$

The measured pulse duration was 45 fs.

2.2.3. Beam divergence measurement

In laser-plasma experiments, peak intensity of the focussed laser beam on the target is an important parameter that governs the interaction processes. It is therefore necessary to measure the focal spot size, which is governed by the laser beam divergence and the focal length of the focussing optics. The peak laser intensity is given by

$$I_0 = E/\tau(\pi\omega^2) \quad \dots\dots\dots (2.3)$$

where E is the pulse energy, τ is the pulse duration, and ω is focal spot radius. The schematic of the laser beam divergence measurement is shown in the Fig. 2.6. The laser

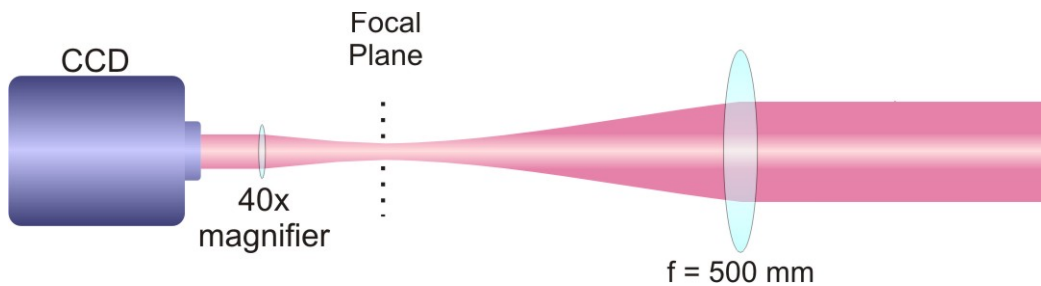


Fig. 2.6 Schematic of experimental setup for beam divergence measurement

focal spot on the target is magnified and imaged on a CCD camera using a microscope lens. To avoid any damage to the CCD sensor, the pulse energy prior to focussing the laser beam was reduced by reflecting the beam from multiple glass surfaces. The FWHM diameter ($2\omega_0$) of the focal spot was measured to be $\approx 18 \mu\text{m}$ for a lens of focal length 500 mm. Since the laser focal spot diameter is equal to the product of the laser beam divergence (θ) and the focal length (f) of lens as $f \times \theta$, one gets the full divergence of the final laser beam to be 36 micro-radians. Fig. 2.7 shows the measured focal spot of the laser. One can see that the spot is nearly circular and the intensity profile of the laser spot is close to Gaussian. It should be noted here that insertion of any filter in the path of the laser distorts the shape of the focal spot. Hence we have used multiple reflections from

anti-reflection windows (surface quality $\sim \lambda/10$) to reduce the laser intensity to desired levels.

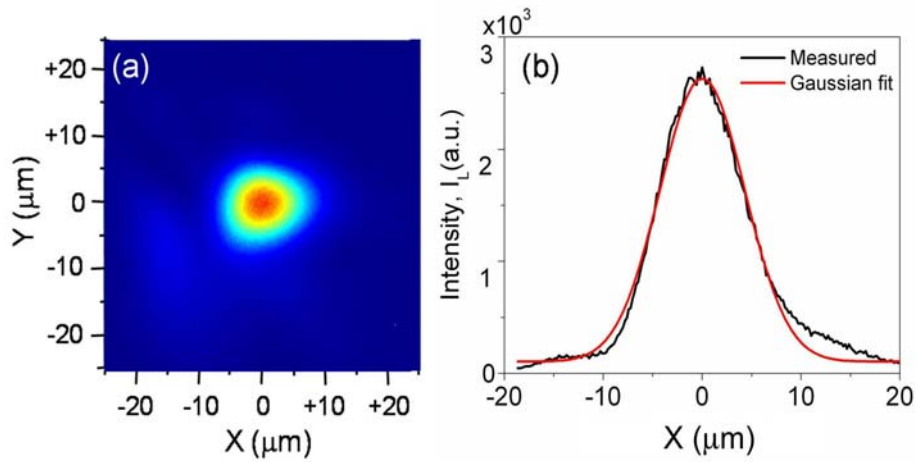


Fig. 2.7 a) Magnified image of laser focal spot on CCD, b) intensity profile of the laser spot closely matching the Gaussian fit.

After measurement of these parameters (i.e. laser pulse duration, beam divergence, and laser energy), we can now estimate peak intensity of the laser pulse (with a lens of focal length 500 mm) to be $\sim 10^{18}$ W/cm².

2.3. Experimental setup

A schematic of the experimental layout is shown in Fig.2.8. In this experiment the laser was operated at lower power of ~ 3 TW corresponding to a laser energy of ~ 150 mJ per pulse. To generate the plasma plume, a part of the uncompressed laser beam

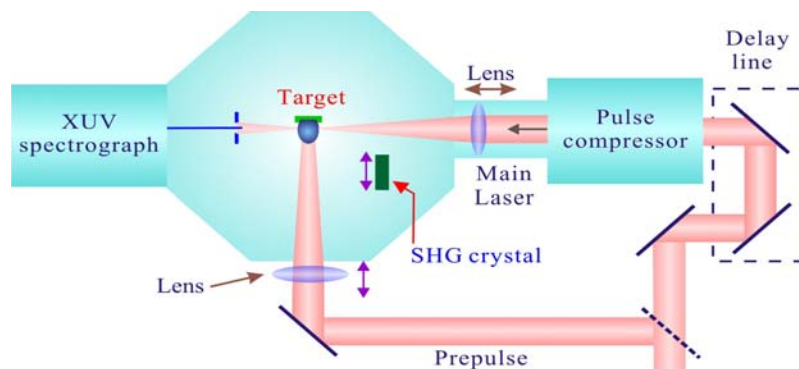


Fig. 2.8 Schematic of the experimental setup

(pulse energy of ~ 20 mJ, pulse duration of 200 ps, central wavelength at 790 nm) was split from the main beam by a beam splitter. This beam was focussed at normal incidence by a $f/10$ spherical lens of 500 mm focal length on the surface of target, which was kept in a vacuum chamber evacuated to 10^{-5} mbar. The focal spot of the pulse at target surface was ~ 600 μm . The intensity of this beam (referred to as the “pre-pulse” beam) at the target surface was $\sim 10^{9-10}$ W/cm^2 . The interaction of the laser pulse with the target surface at these low intensities generates the plasma plume mainly consisting of neutrals and singly charged ions. The plasma plume serves as the medium for harmonic generation [12]. In one of our experiments the details of which will be discussed in Chapter 7, we have generated the plasma plumes by focussing the prepulse at intensity $\sim 10^{13}$ W/cm^2 .

The laser pulse transmitted from the beam splitter was passed through a delay line and then passed through the vacuum compressor to generate the 45 fs pulse (will be referred as main pulse). This pulse has energy ~ 130 mJ. The delay between pre-pulse and the main pulse could be adjusted in the range of 6 ns to 130 ns by changing the length of the delay line. The main laser pulse was focussed in the preformed plasma plume using a spherical lens of focal length 500 mm, and its intensity in the plume was kept at 10^{15} – 10^{16} W/cm^2 . The intensity was adjusted by changing the position of the focussing lens. At the best focus of the lens the intensity of the laser can reach to $\sim 10^{18}$ W/cm^2 . However increasing laser intensity beyond the optimum range of 10^{15} – 10^{16} W/cm^2 reduces the intensity of harmonics. This will be further discussed in Chapter 5. Positive or negative chirp could be introduced in the laser pulse by changing the separation between the two gratings in the compressor. In this way, we could generate up to 15 ps long negatively chirped pulse and upto 5 ps long positively chirped pulse.

The interaction of the focussed laser beam with the preformed plasma plumes results in high order harmonic generation. The harmonic radiation was detected by a flat field XUV spectrograph of variable spectral range. The XUV grating disperses the HHG spectrum in the horizontal direction after its passage through a slit. The spectrograph went through many improvements during the course of the work. More details about the spectrograph are given in the next sub-section.

Various targets were used to generate the plasma plumes. These targets can be broadly divided into two parts : a) bulk targets (such as Ag, In, Cr, Mn etc.) and b) nanostructured targets (such as C₆₀, carbon nanotubes, nanoparticles of Ag, Au, etc.). The plasma plume generated from the interaction of the pre-pulse and target surface mainly consists of neutral atoms or singly charged ions (in the case of bulk materials) or mildly heated nanoparticles (in the case of nanostructured targets). One can place bulk surface / nanostructured target surface on a target holder of 4 mm width and 50 mm length. The targets of approximately 4 mm × 4 mm size were used. Multiple targets were placed on the holder so that the properties of HHG from these targets could be studied without breaking the vacuum. The emission from plasma plume was imaged through a port to record the optical spectrum of the plasma plumes.

To study the HHG from an elongated plasma plume, the pre-pulse beam was focussed on the target surface using an assembly of two crossed cylindrical lenses of focal lengths 550 mm and 450 mm. This combination gave a focal spot of 2 mm × 300 μm (FWHM). The intensity of pre-pulse at target surface was $\sim 10^9$ W/cm². The length of plasma plume was varied using a variable width slit placed before the lens assembly. The length of plasma plume was varied in the range of 0.8 mm to 2 mm in step size of 0.4 mm.

The laser parameters used in experimental study are summarized in Table 2.2.

Laser Parameter	Value in Experiment
Repetition rate	1 Hz, 10 Hz
Delay between pre-pulse and main pulse	6 ns to 120 ns
Energy (main pulse)	130 mJ
Energy (pre-pulse)	20 mJ
Intensity (main pulse)	10^{15} – 10^{18} W/cm ²
Intensity (pre-pulse)	10^9 – 10^{13} W/cm ²
Main pulse duration	45 fs to 15 ps
Pre-pulse duration	~ 200 ps

Table 2.2 Laser parameters during experiment

2.4. XUV spectrograph for harmonic detection

The generated harmonics were detected by an in-house developed XUV spectrograph. In the initial configuration the spectrograph comprised of a dispersing element and an imaging system. A schematic of the XUV spectrograph is shown in Fig 2.9. The dispersing element of the spectrograph was a variable line-spacing flat field grating which focussed the dispersed spectrum at a flat surface normal to its plane. To image the dispersed spectrum, an assembly of micro-channel plate (MCP) and optical CCD camera was used. The MCP, placed at the focal plane of the grating, converted the XUV signal to blue-green fluorescent signal, which was then imaged onto a CCD camera [12]. The MCP-CCD assembly was mounted on a bellows to facilitate translation of the detector assembly in the direction of dispersion. This allows selection of a suitable

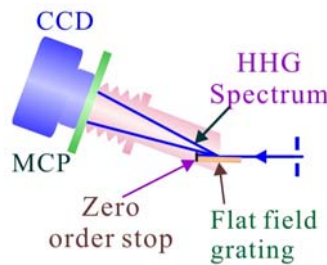


Fig. 2.9 A Schematic of XUV spectrograph

spectral range required for a particular experimental study. A typical spectrum of high order harmonic generation from the silver plasma plume using the above spectrograph is shown in Fig. 2.10.

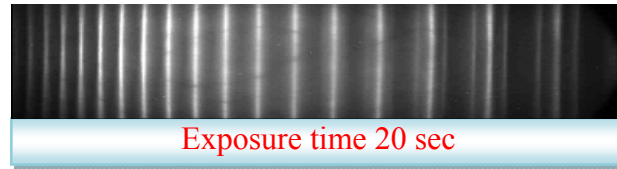


Fig. 2.10: Typical spectrum from the XUV spectrograph

The above spectrograph was later on modified to achieve higher sensitivity of detection through focussing of the line spectrum [13]. A schematic of this setup is shown in Fig 2.11. A cylindrical grazing incidence mirror was introduced before the flat field

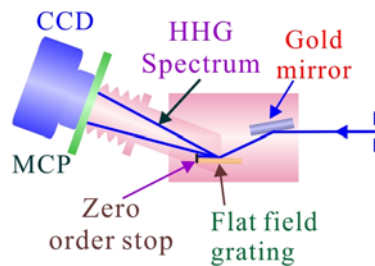


Fig. 2.11 A schematic of the improved XUV spectrograph

grating which focuses the dispersed spectral lines to points, thereby making the setup ~10 times more sensitive than the earlier one. A typical spectrum of the high order harmonic radiation from the silver plume recorded using this setup is shown in Fig. 2.12

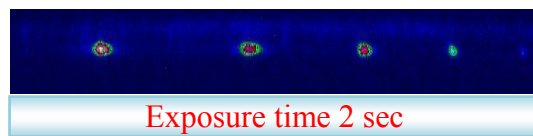


Fig. 2.12: Typical spectrum from the improved XUV spectrograph

From the next chapter onwards, we shall discuss our experimental findings of HHG from plasma plumes in the plateau region, and the various processes used for the optimization of the HHG yield and cut-off.

Bibliography

1. D. Strickland and G. Mourou, "Compression of amplified chirped optical pulses", *Opt. Commun.* **56**, 219 (1985).
2. D. E. Spence, P. N. Kean, and W. Sibbett, "60-fsec pulse generation from a self-mode-locked Ti:sapphire laser", *Opt. Lett.* **16**, 42(1991).
3. R. L. Fork, O. E. Martinez, and J. P. Gordon, "Negative dispersion using pairs of prisms", *Opt. Lett.* **9**, 150 (1984).
4. R. Szipöcs, K. Ferencz, C. Spielmann, and F. Krausz "Chirped multilayer coatings for broad-band dispersion control in femtosecond lasers", *Opt. Lett.* **19**, 201 (1994) .
5. G. Cheriaux, P. Rousseau, F. Salin, and J. P. Chambaret "Aberration-free stretcher design for ultrashort-pulse amplification" *Opt. Lett.* **21**, 414 (1996).
6. G. Vaillancourt, T. B. Norris, J. S. Coe, P. Bado, and G. A. Mourou, "Operation of a 1-kHz pulse-pumped Ti:sapphire regenerative amplifier", *Opt. Lett.* **15**, 317 (1990).
7. E. Treacy, "Optical pulse compression with diffraction gratings", *IEEE J. Quant. Electr.* **5**, 454 (1969).
8. A. E. Siegman, "*Lasers*", University Science books, USA, p 359 (1986).
9. L. F. Mollenauer, R. H. Stolen, and J. P. Gordon, "Experimental observation of picosecond pulse narrowing and solitons in optical fibres", *Phys. Rev. Lett.* **45**, 1095 (1980).

10. P. Lazaridis, G. Debarge, and P. Gallion, “Time–bandwidth product of chirped sech^2 pulses: application to phase–amplitude-coupling factor measurement”, *Opt. Lett.* **20**, 1160 (1995).
11. A. Brun, P. Georges, G. Le Saux and F. Sain, “Single-shot characterization of ultrashort light pulses”, *J. Phys. D: Appl. Phys.* **24**, 1225 (1991).
12. H. Singhal, R. A. Ganeev, P. A. Naik, V. Arora, U. Chakravarty, and P. D. Gupta, “Dependence of high order harmonics intensity on laser focal spot position in preformed plasma plumes”, *J. App. Phys.* **103**, 013107 (2008).
13. H. Singhal, R. A. Ganeev, P. A. Naik, J. A. Chakera, U. Chakravarty, H. S. Vora, A. K. Srivastava, C. Mukherjee, C. P. Navathe, S. K. Deb, and P.D. Gupta, “High order harmonic generation in plasma plume of *in situ* laser produced silver nanoparticles”, *Phys. Rev. A* **82**, 043821 (2010).

Chapter 3

Parametric optimization of harmonic generation in laser ablated plasma plumes

The high order harmonic generation (HHG) from the interaction of an intense ultrashort laser pulse with a nonlinear medium would, in general, depend on the parameters of the medium and the laser used. In HHG from gases, it has been commonly observed that the intensity of harmonics decreases rapidly for first few orders and then remains constant or decreases slowly upto some very high order (as mentioned earlier, this region is referred to as the *intensity plateau*), followed by a sharp cut-off [1-6]. Intensity and cut-off of the generated harmonics depend on ionization potential and density of the gas, and intensity and pulse duration of the laser. When the laser ablated plasma plume is used as the nonlinear medium, the ionization state and density of the plume interacting with the high intensity laser pulse will be governed by the pre-pulse laser intensity, the time delay between the pre-pulse and the high intensity laser pulse, and the distance of the interaction region from the target surface. In the earlier experiments [7-12], the high order harmonics up-to 27th order were observed through the interaction of intense ultrashort laser with strongly excited plasma plumes. In these experiments the intensity of the harmonics decreased monotonically with increasing harmonic order, and no plateau like emission pattern of harmonics was observed. This may be the result of poor phase matching conditions due to high electron density inside the plasma plumes.

For high efficiency harmonic generation, we have used low-excited plasma plumes which are expected to behave similar to a gas medium. In this chapter, we present results of our experiments on the characterization of high order harmonics generated from low-excited plasma plumes. We have also carried out parametric

optimization of harmonic generation with respect to various laser and plasma parameters, viz. pre-pulse laser intensity, main laser pulse intensity, the time delay between the two pulses, and the distance between the target surface and the axis of the main laser beam. The results are presented in Section 3.2.

3.1. Characterization of generated harmonics

Plasma plumes were produced from planar silver targets (strips of 2 mm width) irradiated by Ti:sapphire laser pre-pulse of ~ 200 ps duration. Although the maximum intensity of the main laser pulse was $\sim 10^{18}$ W/cm² in the focal region, the peak intensity in the plasma plume was kept much smaller by changing the position of laser focus with respect to the centre of plasma plume. Generated high order harmonics were analysed by the XUV spectrometer as described in previous chapter.

A typical image of harmonic spectrum from a silver plasma plume, produced at a pre-pulse intensity of $\sim 2 \times 10^{10}$ W/cm² and using main pulse of 10^{15} – 10^{16} W/cm² intensity, is shown in Fig. 3.1a [13]. In the initial setup (shown in Fig. 2.9), when the XUV spectrograph did not have the grazing incidence focussing mirror, the harmonics were seen as straight lines. Since wavelength separation between harmonic orders decreases with increasing harmonic order, the harmonics appear as an intensity comb with decreasing separation as one move from lower harmonic orders to higher orders. Intensity scan of Fig. 3.1a (i.e. the harmonic spectrum) is shown in Fig. 3.1b. The odd harmonics are seen from 21st to 61st order, over a spectral range of 13 to 38 nm. The harmonics are seen riding over a continuum which is due to some scattered radiation entering the XUV spectrograph. In the later experiments, this scattered radiation was much more effectively suppressed. The satellites appearing on both the sides of the locations of the lower order harmonics are due to the second order diffraction of the intense higher order harmonics. It was observed that, as expected theoretically, the harmonic emission vanished when the laser polarization was made circular.

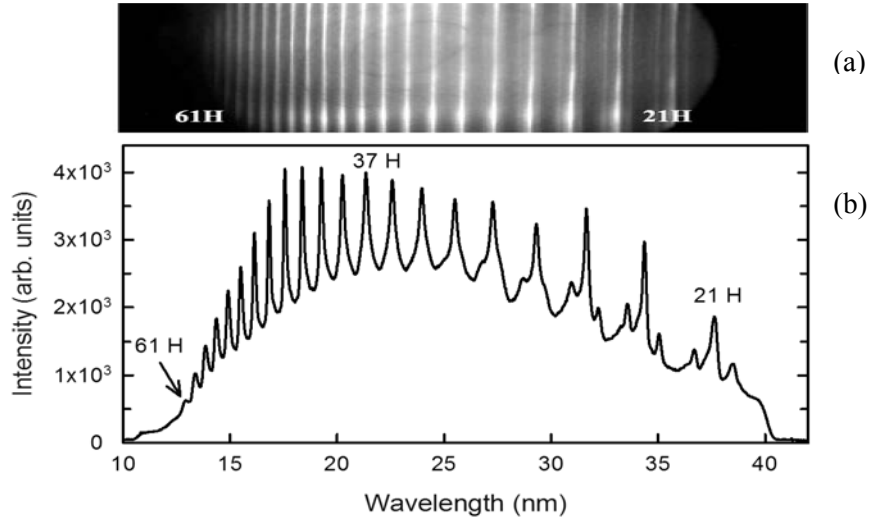


Fig. 3.1 Harmonic spectrum from silver plasma plume in the range of 13 to 38 nm. (a) A typical image of the harmonics and (b) its intensity scan across a horizontal line

As discussed in Section 1.2.1, the cut-off harmonic order can be given by the relation [14]

$$h\nu_{\max} = I_p + 3.17U_p \quad \dots\dots\dots (3.1)$$

The laser intensity in the plasma plume during the experiment was $\sim 4 \times 10^{15}$ W/cm² ($U_p \sim 235$ eV), for which the cut-off order comes to about 500th harmonic of the laser. The experimentally observed lower harmonic cut-off would indicate that the laser intensity responsible for harmonic generation is well below the peak intensity. It is inferred that HHG essentially occurs from leading edge of the laser pulse. As will be described in Chapter 4, this inference is established from observation of shift in harmonic wavelengths when chirp was introduced in the laser pulse. Next, the dependence of harmonic cut-off on the ionization potential of the target materials will be discussed in more detail in Chapter 6.

The spectral identification of harmonic orders was done using a strong plasma transition of Al²⁺ at 14.4 nm ($2p^5 3p^2 (^2P^\circ) - 2p^6 3s (^2S)$) as a wavelength marker. Once one harmonic order is identified, all the others could be uniquely assigned through

constantly decreasing separation with harmonic order, governed by the dispersion factor of the spectrograph. In addition to this, there is a strong 13th H ($\lambda = 61$ nm) from indium plasma plume (Fig. 3.2) which may also serve as a wavelength marker [15]. Occurrence of the enhanced 13th H in Indium plasma plume has been studied in detail, and same is presented in next chapter.

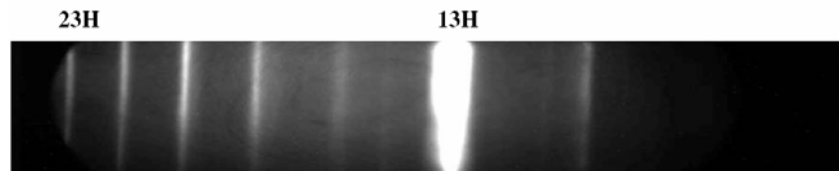


Fig. 3.2 Intense 13th harmonic order generated in indium plasma plume at ($\lambda=61$ nm)

The preparation of low-excited plasma plumes is crucial for efficient generation of high order harmonics. In our experiments, the laser focussing conditions were adjusted such that the plasma plume, prior to its interaction with the femtosecond laser pulse, predominantly consisted of the neutrals and small amount of singly charged ions. This was confirmed from spectral analysis of plasma emission in the visible and UV region. Fig 3.3 shows emission spectrum from indium plasma plume recorded using a fibre optic spectrograph [16]. Traces 1 and 2 shows the optical spectra for high and low excitations of the plasma plume. While only plasma emission was seen for the plume conditions for trace 1, strong harmonic generation was observed from plasma plume corresponding to trace 2. In trace 1, the two strongest lines at 525 nm and 565 nm are identified as transitions of In^{2+} and In^{1+} respectively [17]. On the other hand, in trace 2, the two prominent lines at 410 nm and 451 nm correspond to spectral transitions in neutral indium [17]. Thus a low excited plasma plume predominantly consisting of neutral atoms is suitable for HHG. The increase in free electron density in the plasma plume with increasing excitation produces a large phase mismatch between the

fundamental laser beam and the generated harmonics, leading to poor harmonic conversion.

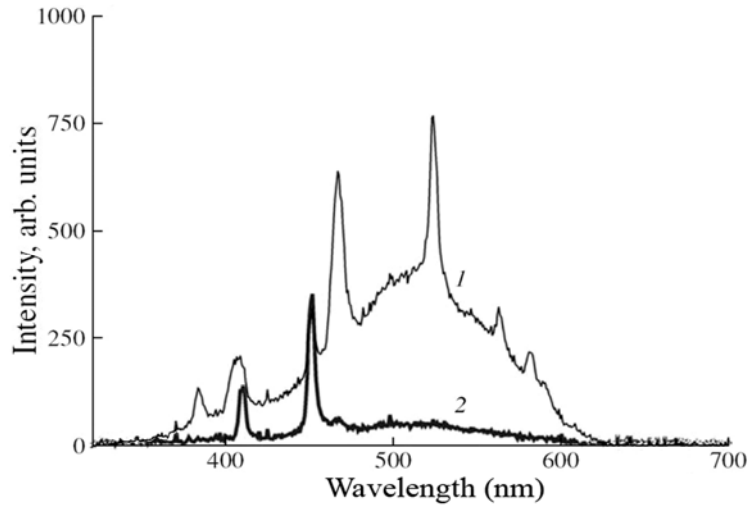


Fig. 3.3 *Optical spectrum from indium plasma plume: 1) shows the strong excitation conditions, 2) shows weak excitation conditions*

The temporal characteristics of plasma emission in the above two conditions were also recorded using a fast photodiode. Fig 3.4 shows the temporal profile of the plasma emission in the two conditions. It is seen that for the high-excited plasma, the optical emission lasts for several tens of nanoseconds. On the other hand, the optical emission from the low-excited plasma plume occurs for a much smaller duration of ~ 5 ns. Thus in the latter case, the main laser pulse interacts with a cooled down plasma.

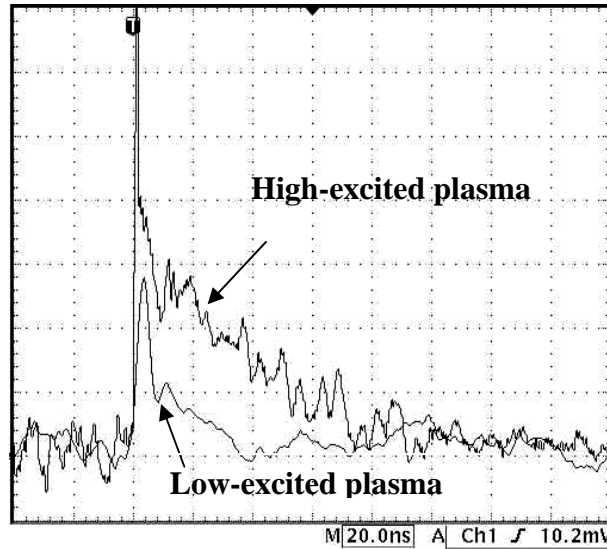


Fig. 3.4 Temporal characteristics of optical emission from low and high excited plasma plumes

3.2. Intensity optimization of harmonics with respect to various laser and plasma parameters

To optimize the conditions for high intensity harmonic generation, firstly the effect of laser intensity of pre-pulse producing the plasma plume was studied. Fig. 3.5 shows the variation of the intensity of the 35th harmonic with the pre-pulse laser intensity. It was observed that the harmonic intensity was maximum for a pre-pulse laser intensity of $\sim 10^{10}$ W/cm². This was true for all other harmonics as well. At this pre-pulse laser intensity, the plasma plume predominantly consisted of neutral atoms and singly charged ions. A decrease in the harmonic intensity was observed when the pre-pulse laser intensity was increased beyond 2×10^{10} W/cm². This is attributed to the generation of multiply charged ions in highly excited plasma plumes. This correspondingly results in higher free electron density in the plasma plume, which leads to increased phase mismatch between the harmonics and the fundamental laser radiation. The effect of phase mismatch on the intensity of high order harmonics will be further discussed in Chapter 5.

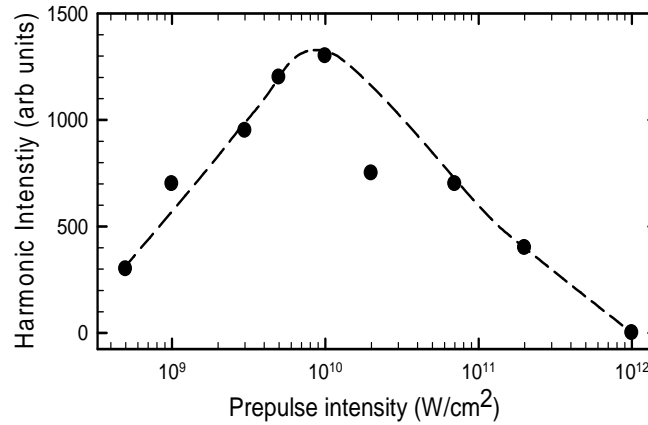


Fig. 3.5 Variation of the intensity of the 35th harmonic with the pre-pulse laser intensity. The dashed curve is to guide the eye.

Next, the optimization of the high harmonic generation was carried out with respect to the delay between the pre-pulse and the main laser pulse. For example, the variation of the intensity of the 13th harmonic from indium plasma plume with respect to the time delay between the pre-pulse and the main laser pulse is shown in Fig. 3.6 [15]. It is seen that the harmonic intensity increased rapidly up to a delay of ~30 ns and thereafter remained approximately constant up to the maximum delay of 57 ns used in the experiment. For efficient harmonic generation, it is necessary to have a good overlap between the plasma plume, expanding away from the target, and the main laser pulse, propagating at certain separation from the target surface. Hence, one would expect the optimum delay to increase with the atomic weight of the target elements. It was observed that the light materials (like boron, carbon) generate intense harmonics at small delay (~20 ns), and the heavier materials (such as copper, silver, indium, gallium, manganese, etc.) require larger delay (~60 ns). In the later experiments on lead target, the delay had to be increased to ~110 ns for efficient harmonic generation.

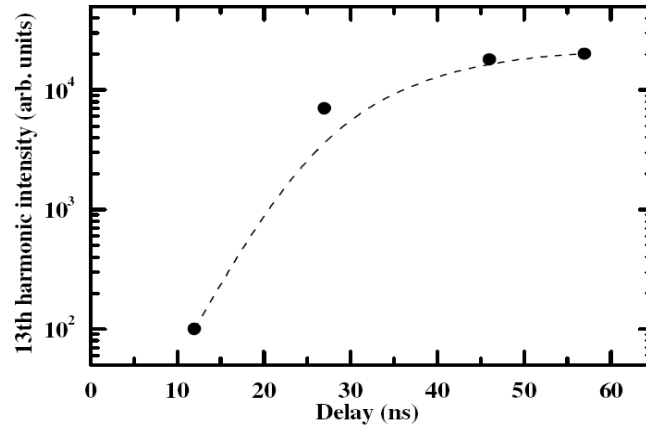


Fig. 3.6 Variation of the intensity of the 13th harmonic from indium plasma plume with respect to the time delay between the pre-pulse and the driving laser pulse. The dashed curve is to guide the eye.

The variation of harmonic intensity as a function of the distance of the femtosecond laser beam from target surface was also studied. Fig. 3.7 shows the dependence of the 21st harmonic intensity from silver plasma plume on the distance of the axis of the femtosecond laser beam from the target surface. The harmonic intensity is seen to be maximum at a distance of $\sim 100 \mu\text{m}$. This observation could be understood from the fact that the intensity of the generated harmonic radiation depends on the density of the plume. As the axis of main laser pulse is shifted away from the target surface, the density of the plasma medium decreases hence the harmonic intensity decreases. When the main laser pulse passes close to the target surface, the high temperature plasma produced by wing of this pulse adds to the pre-formed plasma plume. As discussed earlier, a large phase mismatch occurs in highly excited plasma plume resulting in smaller harmonic conversion.

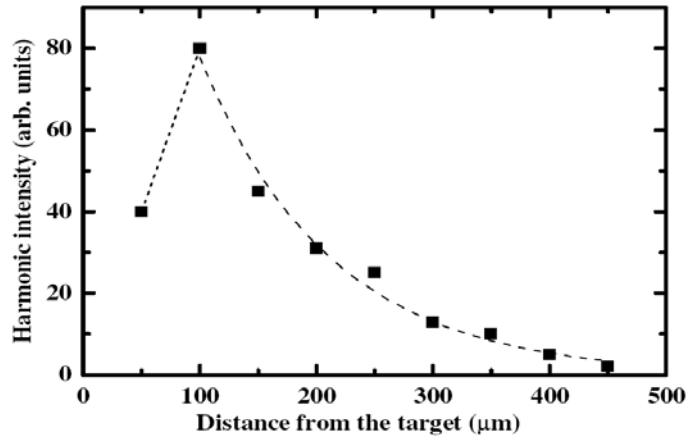


Fig. 3.7 Variation of the 21st harmonic intensity as a function of the distance between the target surface and the axis of the main laser beam.

Finally the intensity of HHG was also optimized for the location of the plasma plume with respect to the focus position of the main laser beam. Fig. 3.8 shows the dependence of the 21st harmonic intensity on the focal position of the driving laser radiation in a silver plasma plume [18]. It is seen that the HHG nearly vanished when the laser is focussed in the centre of the plume. More intense harmonics were produced when the laser beam was focussed after the plasma plume. The observed effect could be understood from phase mismatch between the fundamental and harmonic radiation. Analysis of various factors resulting in phase mismatch is provided in Chapter 5.

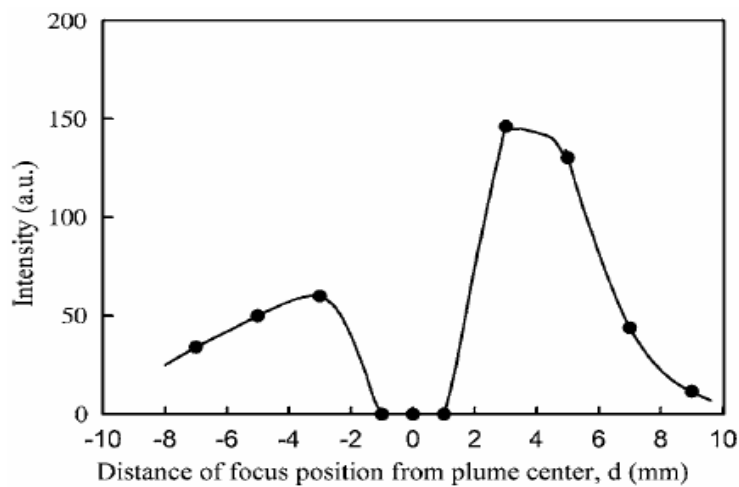


Fig. 3.8 Dependence of the 21st harmonic intensity on the focal position of the driving laser radiation.

Harmonic generation for various studies presented in following chapters was carried out in low excited plasma plumes under the following optimized conditions. These optimized values vary slightly from target to target hence range of optimized values is given in the table.

<i>Laser Parameters</i>	<i>Optimized value</i>
Pre-pulse intensity	$\sim 10^9 - 10^{10} \text{ W/cm}^2$
Time delay between the pre-pulse and Main laser pulse	$\sim 57 \text{ ns}$
Distance of axis of main laser beam from target surface	$\sim 100 \mu\text{m}$
Intensity of main laser beam in plasma plume	$\sim 10^{15} - 10^{16} \text{ W/cm}^2$

Table 3.1 *optimized laser parameters for high order harmonic generation experiments*

Bibliography

1. A. McPherson, G. Gibson, H. Jara, U. Johann, T. S. Luk, I. A. McIntyre, K. Boyer, and C. K. Rhodes, "Studies of multiphoton production of vacuum-ultraviolet radiation in the rare gases", *J. Opt. Soc. Am. B* **4**, 595 (1987).
2. J. K. Crane, M. D. Perry, S. Herman, R. W. Falcone, "High-field harmonic generation in helium", *Opt. Lett.* **17**, 1256 (1992).
3. J. J. Macklin, J. D. Kmetec, and C. L. Gordon, "High-order harmonic generation using intense femtosecond pulses", *Phys. Rev. Lett.* **70**, 766 (1993).
4. C. Winterfeldt, and G. Gerber, "Optimal control of high-harmonic generation", *Rev. Mod. Phys.* **80**, 117 (2008).
5. P. Balcou *et al.* "High-order-harmonic generation: towards laser-induced phase matching control and relativistic effects", *Appl. Phys. B* **74**, 509 (2002).

6. Ch. Spielmann, N. H. Burnett, S. Sartania, R. Koppitsch, M. Schnurer, C. Kan, M. Lenzner, P. Wobrauschek, F. Krausz, “Generation of coherent x-rays in the water window using 5-femtosecond laser pulses”, *Science* **278**, 661 (1997).
7. K. Krushelnick, W. Tighe, S. Suckewer, “Harmonic generation from ions in underdense aluminium and lithium–fluorine plasmas”, *J. Opt. Soc. Am. B* **14**, 1687 (1997).
8. R.A. Ganeev, V.I. Redkorechev, T. Usmanov, “Optical harmonics generation in low-temperature laser-produced plasmas”, *Opt. Commun.* **135**, 251 (1997).
9. W. Theobald, C. Wülker, F.R. Schäfer, B.N. Chichkov, “High-order harmonic generation in carbon vapor and low charged plasma”, *Opt. Commun.* **120**, 177 (1995).
10. Y. Akiyama, K. Midorikawa, Y. Matsunawa, Y. Nagata, M. Obara, H. Tashiro, K. Toyoda, “Generation of high-order harmonics using laser-produced rare-gas-like ions”, *Phys. Rev. Lett.* **69**, 2176 (1992).
11. S. Kubodera, Y. Nagata, Y. Akiyama, K. Midorikawa, M. Obara, “High-order harmonic generation in laser-produced ions”, *Phys. Rev. A* **48**, 4576 (1993).
12. C.-G. Wahlström, S. Borgström, J. Larsson, S.-G. Pettersson, “High-order harmonic generation in laser-produced ions using a near-infrared laser”, *Phys. Rev. A* **51**, 585 (1995).
13. R. A. Ganeev, H. Singhal, P. A. Naik, U. Chakravarty, V. Arora, J. A. Chakera, R. A. Khan, M. Raghuramaiah, S. R. Kumbhare, R. P. Kushwaha, and P. D. Gupta, “Optimization of the high-order harmonics generated from silver plasma” *Appl. Phys. B* **87**, 243 (2007).

14. M. Lewenstein, Ph. Balcou, M. Yu. Ivanov, Anne L'Huillier, and P. B. Corkum, "Theory of high-harmonic generation by low-frequency laser fields", *Phys. Rev. A* **49**, 2117 (1994).
15. R. A. Ganeev, H. Singhal, P. A. Naik, V. Arora, U. Chakravarty, J. A. Chakera, R. A. Khan, I. A. Kulagin, P. V. Redkin, M. Raghuramaiah, and P. D. Gupta "Harmonic generation from indium-rich plasmas" *Phys. Rev. A* **74**, 063824 (2006).
16. R. A. Ganeev, P. A. Naik, H. Singhal, U. Chakravarty, V. Arora, J. A. Chakera, M. Raghuramaiah, R. A. Khan, S. R. Kumbhare, R. P. Kushwaha, and P. D. Gupta, "Control of the Intensity of a Single Harmonic Generated in Laser Plasma by Varying the Chirp of Intense Femtosecond Pulses" *Opt. and Spectr.* **102**, 949 (2007).
17. NIST Atomic Spectra Database *ver. 4*, (2010).
18. H. Singhal, R. A. Ganeev, P. A. Naik, V. Arora, U. Chakravarty, and P. D. Gupta "Dependence of high order harmonics intensity on laser focal spot position in preformed plasma plumes", *J. App. Phys.* **103**, 013107 (2008).

Chapter 4

Resonance intensity enhancement of harmonics and wavelength tuning

In Chapter 3, we have described high order harmonic generation from low excited plasma plumes and the experimental determination of the laser and plasma conditions for achieving maximum intensity of harmonics and high value of cut-off order. As mentioned earlier, a typical spectrum of the high order harmonics consists of a broad plateau of odd harmonics followed by a sharp cut-off. The conversion efficiency of the harmonics in the plateau region under similar condition has been estimated to be $\sim 10^{-6}$ [1]. In view of their low energy, these harmonics have limited applicability. Hence, it is necessary to increase the conversion efficiency of the HHG.

While the harmonic emission from the plumes of some materials showed a broad plateau of odd harmonics, for few other materials, the HHG spectrum in the plateau region exhibited a much higher intensity of a particular harmonic order as compared to the neighbouring ones. For instance, as shown in Fig. 3.2 of Chapter 3, the intensity of 13th H (~ 61 nm) generated in indium plasma plume was ~ 200 times higher compared to that of the neighbouring harmonic orders [2]. This is attributed to resonance enhancement of a particular harmonic order. In this chapter we present an experimental study of intensity enhancement of some particular harmonic orders in various plasma plumes, and discuss the physical processes responsible for this behaviour. It is also demonstrated that the frequency of the harmonic radiation can be tuned (to a limited extent) by changing the chirp of the laser pulse. It is also shown that this tuning can be used to bring a particular harmonic order into/out of resonance.

4.1. Occurrence of strongly enhanced single harmonic orders

We have performed experimental studies and observed the resonance enhancement in the intensity of single harmonic orders generated in various plasma plumes [2–4]. The experimental observations are shown in Fig. 4.1, where the enhanced harmonic orders could be seen. It was observed that the 13th, 21st, 29th Harmonic generated in In, InSb, Cr plumes are enhanced by factor of ~200, ~20 and ~25 respectively, compared to neighbouring harmonic orders. The intensity of resonantly enhanced harmonic orders was 5 – 200 times more than the neighbouring harmonics in

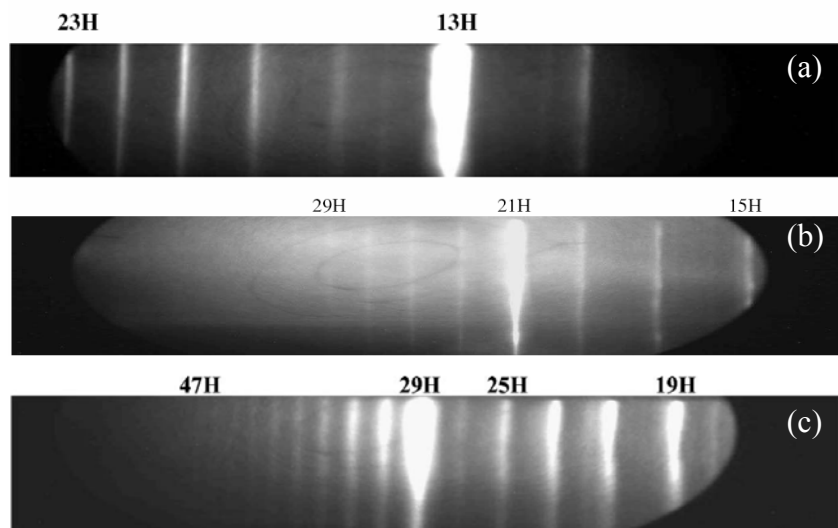


Fig. 4.1 High harmonic spectrum as recorded on the CCD camera for (a) indium plasma, (b) InSb plasma (c) Cr plasma

plateau region. It was also noted that the resonance enhancement of the particular harmonic order does not change with the change in laser intensity. It rather depends on the material constituting the plasma plume. To further establish the role of target element on resonance enhancement of particular harmonic order, we have performed an experimental study with three targets, namely GaAs, As and GaP. The results of the study are presented in Fig. 4.2. Here one can see that the 27th H from GaAs plume (under certain laser chirp conditions (as discussed in the Section 4), is enhanced compared to neighbouring harmonics. The study was repeated with As and GaP respectively. It

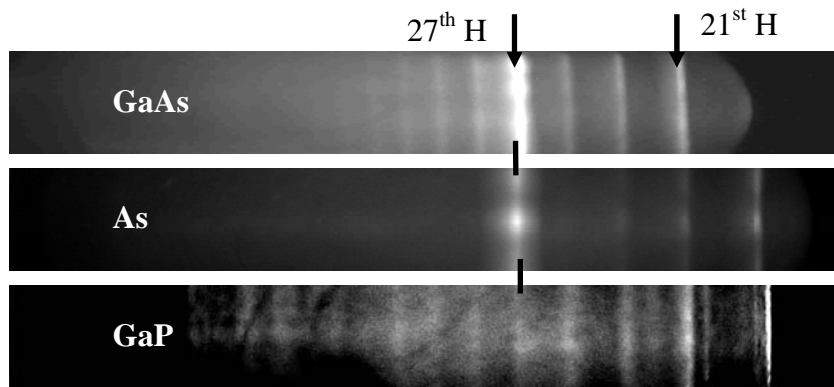


Fig. 4.2 Comparison of resonance enhancement of particular harmonic order, from GaAs, As and GaP plume, shows the role of target element on resonance enhancement.

was observed that same harmonic was enhanced (under similar chirp conditions) in As plume, whereas no enhancement was observed in the case of HHG from GaP plasma plume. The observation indicates that, in the case of HHG, molecular structure does not effect the resonance enhancement of particular harmonic order. In addition to this one can see that intensity of high order harmonics generated from GaAs plume was larger than that from both As plume and GaP plume. This indicates that the intensity of the generated harmonics depends on the target properties and may possibly be enhanced by using different morphology of the target materials.

The possibility of enhancement of the high-order harmonics in gaseous media using the atomic and ionic resonances has been extensively studied theoretically [5–8]. At the same time, for the plumes generated at the surface of some solid targets, the resonance conditions between the harmonic wavelength and the excited states of the neutrals and the singly charged ions, can lead to a considerable enhancement of the harmonic yield for some specific harmonic orders. The availability of a much wider range of target materials for this purpose increases the possibility of the resonance of an ionic transition with a harmonic order. Simulations have also shown that under resonant conditions it is possible to enhance the harmonic yield significantly [9].

Qualitatively, the observed intensity enhancement of a particular harmonic order can be attributed to the increase in nonlinear response of the plasma medium due to near coincidence of the harmonic wavelength with some strong radiative transition in the atoms and ions present in the plasma plume. Several such transitions have been identified, such as in the case of indium the transition at 19.92 eV (62.24 nm), corresponding to the $4d^{10} 5s^2 \ ^1S^0 \rightarrow 4d^9 5s^2 5p \ (^2D) \ ^1P^1$ transition of In^+ , lies close to the 13th harmonic wavelength (61.2 nm). The oscillator strength ('gf' value) of this transition has been calculated to be 1.11. The same can be said about the strong Sb^+ transition $4d^{10} 5s^2 5p^2 \ ^3P^2 \rightarrow 4d^9 5s^2 5p^3 \ (^2D) \ ^3D^3$ ($gf=1.36$, $\lambda =37.74$ nm), which is close to the 21st harmonic ($\lambda=37.85$ nm). It is possible that the Sb^+ transition in the InSb ion could be responsible for the observed enhancement of the 21st harmonic. Some strong transitions associated with Cr^+ ion in the region of 27.3 nm (29th harmonic) were reported in [4]. The theories proposed in [5–8] and computations in [9] are in line of our above discussed qualitative explanation of harmonic intensity enhancement.

4.2. Wavelength tuning of harmonics with laser chirp

High order harmonics are a good source of coherent XUV radiation having extremely short pulse duration. Although numerous harmonic wavelengths are generated, the applicability of such harmonic x-ray sources is restricted since only a discrete set of harmonic wavelengths, equal to the incident laser wavelength divided by odd integers, are available. On the other hand, synchrotron x-ray sources can provide continuously tunable incoherent x-ray radiation. Moreover, access to synchrotron sources is limited and they usually generate x-ray pulses longer than a few tens of picoseconds.

The addition of tunability to harmonic radiation would, therefore, offer a tunable, coherent, ultrashort x-ray source with peak brightness far greater than that of synchrotron

x-ray pulses. In principle, the harmonic wavelength can be tuned by changing the laser wavelength [1]. For the Ti:sapphire laser system used in this study, one can change the oscillator spectrum by a certain amount by tuning the laser cavity. However, this change cannot be directly transferred to the final laser spectrum due to gain narrowing and gain saturation processes. Moreover, it is also necessary to readjust the stretcher and compressor, which is a cumbersome process.

A much simpler approach to tune the harmonic wavelength without modifying the driving laser spectrum is by controlling the chirp of the fundamental radiation [2-4, 10, 11]. The chirp of the main laser pulse was varied by the adjustment of the separation between the gratings in the pulse compressor. A reduction in the grating separation from the chirp-free condition generates positively chirped pulses, and an increase provides negatively chirped pulses. The pulse duration of the laser was measured using the second order autocorrelator described in Chapter 2.

It was observed that the spectral tuning in the wavelengths of the high order harmonics, produced by the interaction of femtosecond duration laser radiation through low-excited plasma plumes, can be achieved through the chirp control of the driving laser radiation. Introduction of positive (negative) chirp in laser radiation results in the tuning of harmonic wavelengths towards red (blue) side of the spectrum [2].

For example, Fig. 4.3 demonstrates the tuning of 47th harmonic generated in silver plasma plumes with laser chirp. The signs in front of the laser pulse duration indicate its chirp, i.e. positive sign indicate positive chirp and vice-versa. It is seen that the wavelength shift of the harmonics (with respect to the no-chirp condition) increases with increase in the laser chirp. It may be noted that the data shown in Fig. 4.3 for different chirps is at different intensities, since the pulse duration changes but pulse energy and laser focussing conditions remain the same. It is pertinent to state here that

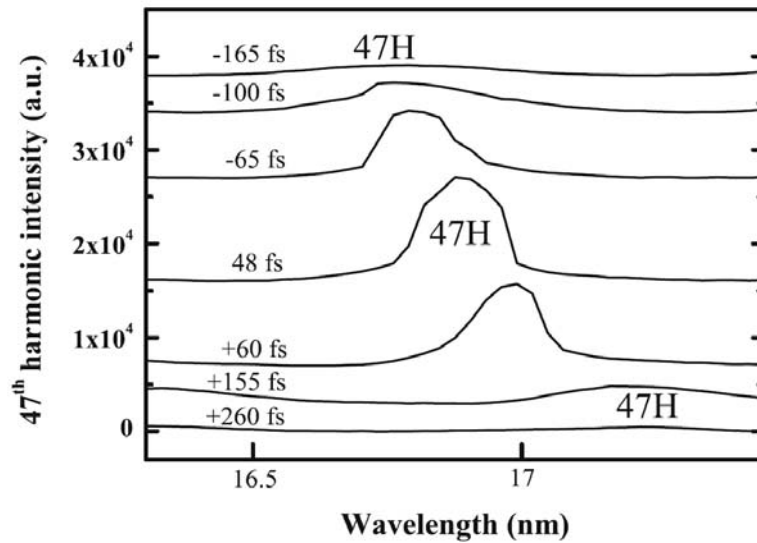


Fig. 4.3 Variation of the 47th harmonic wavelength for different chirp conditions of the driving radiation. Each curve is shifted vertically to avoid overlap for visual clarity

changing the laser intensity by changing the laser focussing conditions does not result in any wavelength shift in the harmonics spectrum. This observation establishes the fact that the key factor in the wavelength tuning of HHG spectra is the chirp control of the laser. One may see from Fig. 4.3 that with the change in laser chirp, the overall shift in peak wavelength of the 47th harmonic is ~ 0.8 nm. The amount of spectral shift in terms of the wavelength depends on the plasma medium and harmonic order. It was observed that the tuning of the harmonic wavelength decreases with increasing harmonic order. A tuning range of harmonic wavelength of up to ~ 2 nm (for 11th H) is obtained by variation of the laser chirp [10].

The above observed variation of wavelength shift of harmonics with laser chirp can be explained from the temporal analysis of the interaction of plasma plume with the chirped femtosecond laser pulse. As discussed in Chapter 3, the laser intensity inside the plasma plume is far greater than the saturation intensity [12]. In this intensity regime, the initial low intensity portion of the pulse interacts with the low excited plume and creates

harmonics efficiently. However, as the pulse intensity reaches its peak, due to rapid ionization of the plasma plume multiply charged ionic species are generated and the electron density inside the plasma plume increases. This leads to, a reduction in the population of the harmonic emitters (neutrals and singly charged ions), and increase in phase mismatch between the harmonics and the fundamental laser radiation, resulting in poor HHG by the trailing portion of the laser pulse. Thus, it is the leading edge of the pulse which contributes most to the HHG and hence the harmonics produced with positively/negatively chirped laser pulses were red/blue shifted (as the leading edge of the laser pulse have red/blue part of the laser spectrum) [10].

4.3. Resonance intensity enhancement of specific harmonics through wavelength tuning

It is shown in Section 4.1 that the HHG from plasma plumes of certain target materials can have resonantly enhanced harmonic orders and the matching of harmonic wavelengths with possible ionic transitions may be a reason behind such resonances. It is shown in Section 4.2 that change in laser chirp can tune the harmonic wavelengths. An experimental study was performed to study the effect of the laser chirp variation on the intensity of resonantly enhance harmonic orders. It was anticipated that the tuning of the high order harmonic wavelengths through laser chirp variation may result in detuning of harmonic orders from resonance conditions through mismatching the harmonic wavelengths with the ionic transitions. The same is experimentally observed and shown in Fig. 4.4. The intensity of the 13th harmonic generated in indium plasma plumes in the chirp-free case is ~ 200 times higher than that of the adjacent harmonics. This gets reduced to ~ 2 times higher than the intensity of neighbouring harmonics when generated from negatively chirped pulses of duration 250 fs. On the other hand, for the positively chirped pulses, the intensity of the 13th harmonic was similar to that in the chirp-free case.

It may be noted from Fig. 4.4 that the harmonic peaks shifted slightly toward the shorter wavelength side for the negatively chirped pulses [2].

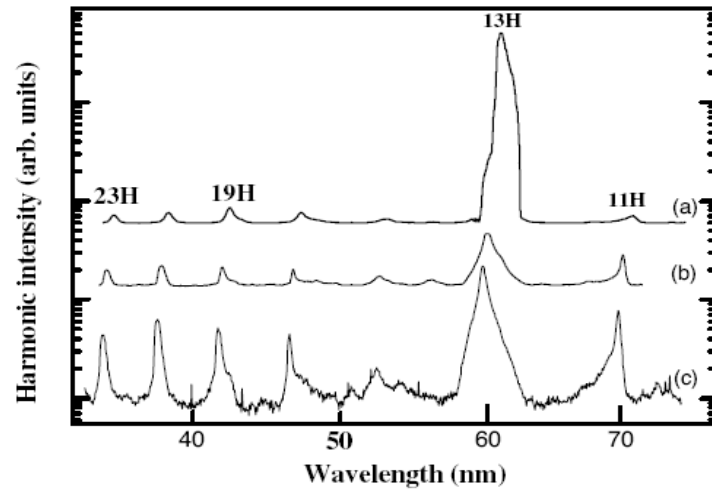


Fig. 4.4 Variation of the harmonic spectrum from indium plume with the pulse chirp and pulse width: (a) chirp-free 45-fs pulses, (b) negatively chirped 95-fs pulses, and (c) negatively chirped 250-fs pulses. Each curve is shifted vertically to avoid overlap for visual clarity.

Similarly, in the case of HHG from the plasma plumes of Cr, the enhancement in the intensity of 29th H and extinction of the 27th H was observed (Fig. 4.5a). The maximum ratio of the intensity of the 29th harmonic compared with that of the 31st was measured to be 23. It can be seen from Fig. 4.5c that at high negative chirp, the harmonic spectrum is so detuned from the resonances (which was causing the absorption of the 27th and the enhancement of the 29th harmonic intensity) that the intensity of the former has increased and that of the latter has decreased to make them comparable in intensity, which is expected in the plateau region when the resonances are absent [4].

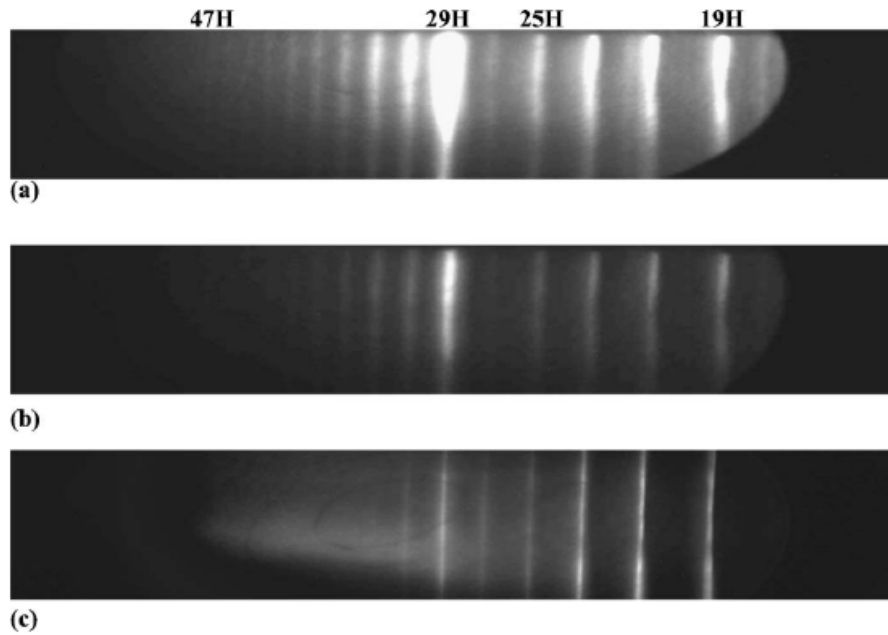


Fig. 4.5 Harmonic distribution of the Cr plume at different chirps of the driving pulse: (a) chirp-free 45 fs pulse, (b) and (c) negatively chirped 85 fs and 160 fs pulses.

It was also anticipated that in certain cases, a harmonic order which was initially not in resonant condition, through the tuning of the high order harmonic wavelengths by laser chirp variation, may tune into resonance. The same is observed in the case of plasma plumes of GaAs. It may be noted from Fig. 4.6 that in the chirp free case and for negatively chirped pulses, a featureless plateau like shape of high-order harmonics with a smooth decrease of harmonic intensity with increasing harmonic order was observed. However, with the introduction of positive chirp in the driving laser pulse, a strong enhancement of the 27th harmonic (29.4 nm) intensity compared to that of the neighbouring ones was observed. The intensity of the 27th harmonic belonging to the end-plateau region, generated from positively chirped 130 fs laser pulse, was ~6 to 7 times higher than the intensities of nearest harmonics. Hence the laser chirp control provides an important means of tuning the harmonics into resonances [3].

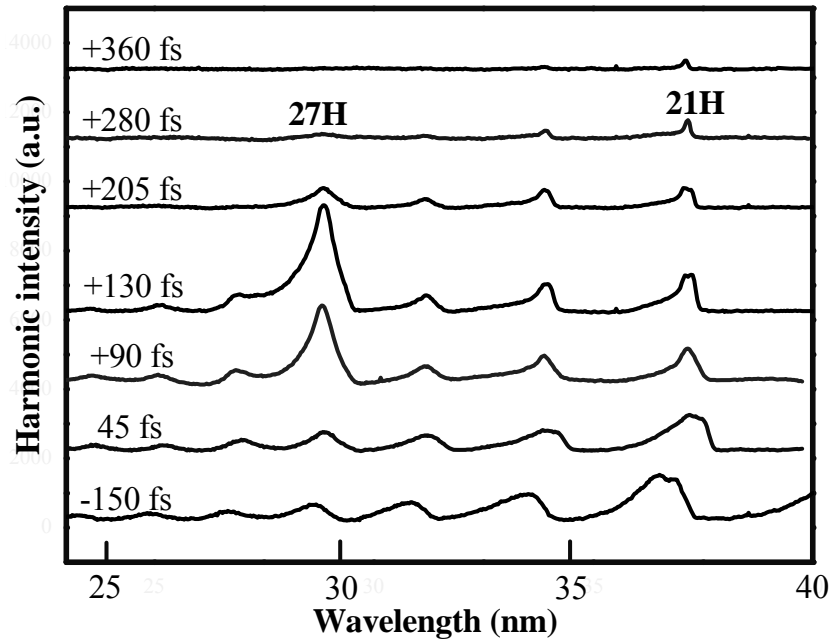


Fig. 4.6 Harmonic spectra from the GaAs plume as a function of pulse chirp and width. Each curve is shifted vertically to avoid overlap for visual clarity.

The tuning of harmonic wavelengths with change in laser chirp is thus an important tool for the generation of ultrashort, tunable, coherent x-ray source. Moreover, the interplay of harmonic resonances with laser chirp would be useful in making a harmonic source which can be made broadband or quasi monochromatic as per user requirement just by changing the laser chirp. Further, the appearance/disappearance of harmonic enhancement with laser chirp, establishes the role of atomic/ionic resonances in the enhancement of particular harmonic orders.

Bibliography

1. R. A. Ganeev, M. Suzuki, M. Baba, and H. Kuroda, "Generation of strong coherent extreme ultraviolet radiation from the laser plasma produced on the surface of solid targets", *Appl. Phys. B* **81**, 1081–1089 (2005)

2. R. A. Ganeev, H. Singhal, P. A. Naik, V. Arora, U. Chakravarty, J. A. Chakera, R. A. Khan, I. A. Kulagin, P. V. Redkin, M. Raghuramaiah, and P. D. Gupta “Harmonic generation from indium-rich plasmas” *Phys. Rev. A* **74**, 063824 (2006).
3. R. A. Ganeev, H. Singhal, P. A. Naik, V. Arora, U. Chakravarty, J. A. Chakera, R. A. Khan, P. V. Redkin, M. Raghuramaiah and P. D. Gupta, “Single-harmonic enhancement by controlling the chirp of the driving laser pulse during high-order harmonic generation from GaAs plasma”, *J. Opt. Soc. Am. B* **23**, 2535 (2006).
4. R. A. Ganeev, P. A. Naik, H. Singhal, J. A. Chakera, and P. D. Gupta, “Strong enhancement and extinction of single harmonic intensity in the mid- and end-plateau regions of the high harmonics generated in weakly excited laser plasmas”, *Opt. Lett.* **32**, 65 (2007).
5. C. Figueira de Morisson Faria, R. Copold, W. Becker, and J. M. Rost, “Resonant enhancements of high-order harmonic generation”, *Phys. Rev. A* **65**, 023404 (2002).
6. D. B. Milošević and W. Becker, “Role of long quantum orbits in high-order harmonic generation”, *Phys. Rev. A* **66**, 063417 (2002).
7. R. Taieb, V. Veniard, J. Wassaf, and A. Maquet, “Roles of resonances and recollisions in strong-field atomic phenomena. II. High-order harmonic generation”, *Phys. Rev. A* **68**, 033403 (2003).
8. D B Milošević, “High-energy stimulated emission from plasma ablation pumped by resonant high-order harmonic generation”, *J. Phys. B* **40**, 3367 (2007).

9. P. V. Redkin, M. K. Kodirov, and R. A. Ganeev, "Theoretical investigation of resonant nonperturbative high-order harmonic generation in indium vapors," *J. Opt. Soc. Am. B* **28**, 165 (2011).
10. R. A. Ganeev, P. A. Naik, H. Singhal, J. A. Chakera, P. D. Gupta, and H. Kuroda, "Tuning of the high-order harmonics generated from laser plasma plumes and solid surfaces by varying the laser spectrum, chirp, and focal position," *J. Opt. Soc. Am. B* **24**, 1138 (2007).
11. H. T. Kim, I. J. Kim, V. Tosa, Y. S. Lee, C. H. Nam, "High brightness harmonic generation at 13 nm using self-guided and chirped femtosecond laser pulses", *Appl. Phys. B* **78**, 863 (2004).
12. Z. Chang, A. Rundquist, H. Wang, M. M. Murnane, and H. C. Kapteyn, "Generation of coherent soft x-rays at 2.7 nm using high harmonics" *Phys. Rev. Lett.* **79**, 2967 (1997).

Chapter 5

Phase matching considerations in HHG

For any practical application of HHG as an ultrashort XUV coherent radiation source, it is desirable to have high conversion efficiency of the harmonics. As discussed in Chapter 4, the conversion efficiency of the high order harmonics, generated in low excited plasma plumes, could be increased by intensity enhancement of particular harmonic orders through atomic/ionic resonances. Moreover, since the HHG is a coherent process, the intensity of the harmonics would be greatly dependent on the phase matching between driving laser beam and the generated harmonic radiation. In the absence of any phase mismatch, the electric field of the harmonics generated at any point is in phase with the harmonics produced earlier (propagating with the fundamental) reaching that point. Under this condition, the intensity of the harmonics should increase quadratically with the increase in number of harmonic emitters (i.e. density of the medium) [1] or with the length of nonlinear medium (plasma plume in our case) [2]. However, in real conditions some phase-mismatch between the fundamental and harmonic radiations is always present. In a dispersive medium, the laser pulse and the harmonic radiation have different phase velocities and hence the electric field of the harmonics generated by the laser pulse in different parts of the medium will not add in phase, thereby restricting the expected quadratic growth of harmonic intensity with the medium length. If the phase mismatch becomes large, the harmonic intensity may even decrease, and with increasing phase mismatch, there may be intensity oscillations in the generated harmonics [3].

One of the factors responsible for the phase mismatch is the plasma dispersion. This arises due to the presence of free electrons in the plasma plume and the amount of

phase-mismatch depends on the density of free electrons. In a plasma plume, the free electrons may be present as a result of the residual ionization of the pre-pulse excitation or may be generated during the interaction of the plasma plume with femtosecond laser pulse. Interaction of the intense ultrashort laser pulse with plasma plume results in its rapid ionization thereby increasing the electron density inside the plasma plume. The rate of ionization of plasma plume depends on laser intensity and at very high laser intensity the electron density inside the plasma plume may become large enough to destroy the conditions for high order harmonic generation. The phase mismatch introduced by the plasma electrons may be controlled by controlling the intensities of pre-pulse at the target surface and the main femtosecond laser pulse inside the plasma plume.

In Chapter 3, we have discussed the parametric optimization of harmonic intensity with respect to the intensities of both pre-pulse and the main femtosecond laser pulse. It was observed that low excited plasma plume is cooled down in ~ 5 ns, which is much smaller than the time delay of ~ 57 ns between the pre-pulse and the main femtosecond pulse. The density of the free electrons due to residual ionization inside the medium would therefore be very small. Thus the main source of the free electrons inside the plasma plume is its ionization by the femtosecond laser pulse. Moreover, the transverse intensity profile of the laser pulse results in spatial electron density variation inside the plasma plume (higher in the centre and lower in the wings). Thus the plasma plume behaves essentially like a concave lens. The harmonic intensity detected by the XUV spectrograph will be affected by the refraction of harmonics by this lens. We have studied the effect of laser intensity and focussing conditions on high order harmonic generation and this is presented in Section 5.1

As mentioned earlier, in a dispersive medium like plasma plume, the phase mismatch between laser pulse and harmonic radiation would restrict the quadratic scaling

of harmonic radiation intensity with length of plasma plume. In addition to the plasma dispersion, the phase mismatch could arise due to atomic dispersion [2, 4], Guoy phase shift [5], and intensity dependent phase shift [4, 6]. Hence a study of the harmonic intensity scaling on the length of plasma plume can be useful in understanding of various factors contributing to phase mismatch. An experimental study on the dependence of harmonic intensity on medium length is performed and the results of the study are discussed in Section 5.2. An analytical explanation of the observed results based on the estimation of various phase mismatch factors is also presented.

5.1. Effect of laser intensity and focussing conditions

An experimental study has been performed to study the effect of the laser intensity and focussing condition of the femtosecond laser on HHG. The experimental arrangement for HHG and detection has already been explained in Chapter 2. The laser focus position with respect to the plume centre was varied by shifting the position of focussing lens of the femtosecond laser beam along the direction of laser propagation. A ray diagram depicting the propagation of the laser beam for three different focussing conditions is shown in Fig. 5.1. Figs. 5.1 a, b and c show the conditions when laser was focussed a) at the centre of the plasma plume, b) before the plasma plume and c) after the plasma plume respectively. The distance of focus position from the centre of the plasma plume is referred to as 'x'. For value of $x = 0$ the laser was focussed at the centre of the plasma plume. For negative/positive values of x the laser was focussed *before/after* the plasma plume. The dotted lines in the Fig. 5.1b and 5.1c represent the path of the femtosecond laser beam due to plasma induced defocusing. This aspect will be discussed later in this Section.

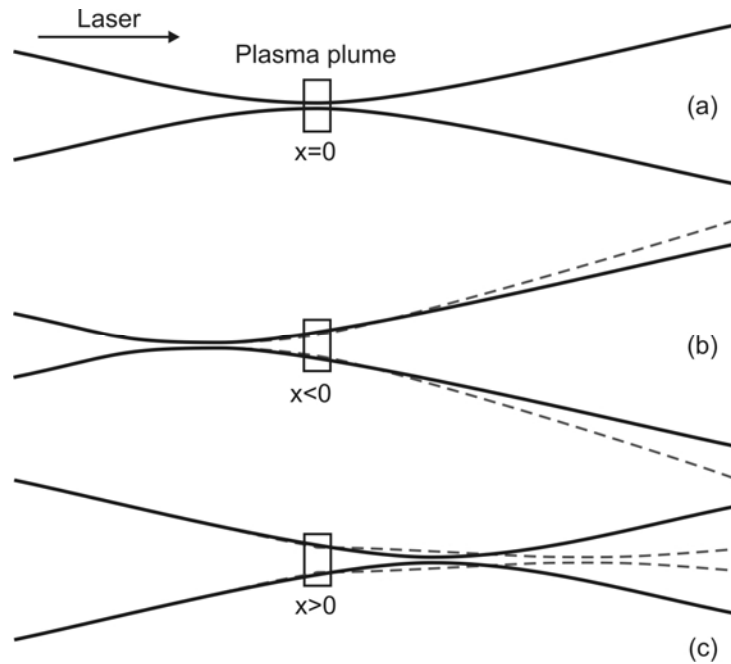


Fig. 5.1 Ray diagram showing the focusing geometry and effect of defocusing on the beam propagation under different focussing conditions.

The change in the intensity of the high order harmonics with the change in the laser focus position was studied. Fig. 5.2 shows the variation of 23rd harmonic intensity generated in silver plasma plumes with the change in focus position of the femtosecond laser beam with respect to the centre of plasma plume. It can be noted from the Fig. 5.2 that the harmonic emission vanishes when the laser beam is focussed at the centre of the

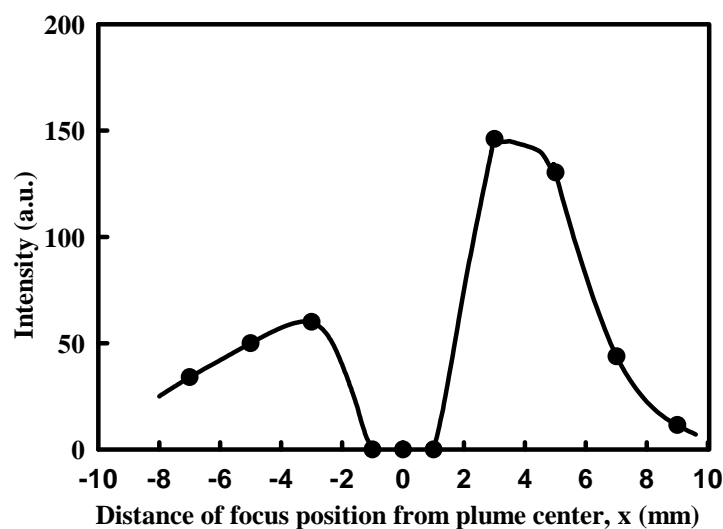


Fig. 5.2 Variation of the 23rd harmonic intensity with the change in focus position of the femtosecond laser w. r. to the centre of the plasma plume. The solid line is to guide the eye.

plasma plume, (*i.e.* $x = 0$). However, the harmonic emission appeared when the best focus position was moved away from the plume centre. The harmonic intensity showed a maximum for $x \sim \pm 3$ mm, and it decreased with further increase in value of $|x|$. The laser intensity at the centre of plasma plume for $x = \pm 3$ mm was $\sim 10^{16}$ W/cm². It is interesting to note that the peak harmonic intensity observed for $x = +3$ mm (*i.e.* when the laser is focussed after the plasma plume) is about 2.5 times larger than that of the peak at $x = -3$ mm. A similar behaviour was also observed for other harmonic orders.

Figure 5.3 shows the variation of the 41st harmonic intensity with x . Similar to the case of the 23rd harmonic, the harmonic emission vanished for $x = 0$ (*i.e.* the best focus at the centre of the plasma plume). However, in this case, the peak harmonic intensity appeared for a larger value of $x \sim \pm 5$ mm. The laser intensity at the centre of plasma plume for $x = \pm 5$ mm was $\sim 4 \times 10^{15}$ W/cm². This observation indicates that the optimum laser intensity for higher harmonic orders is smaller than that for the lower orders. It can also be noted from Fig. 5.3 that, while the peak harmonic intensity for $x = +5$ mm is higher than that for $x = -5$ mm, their ratio is smaller (~ 1.25) compared to the corresponding value for the 23rd harmonic shown in Fig. 5.2. These observations indicate

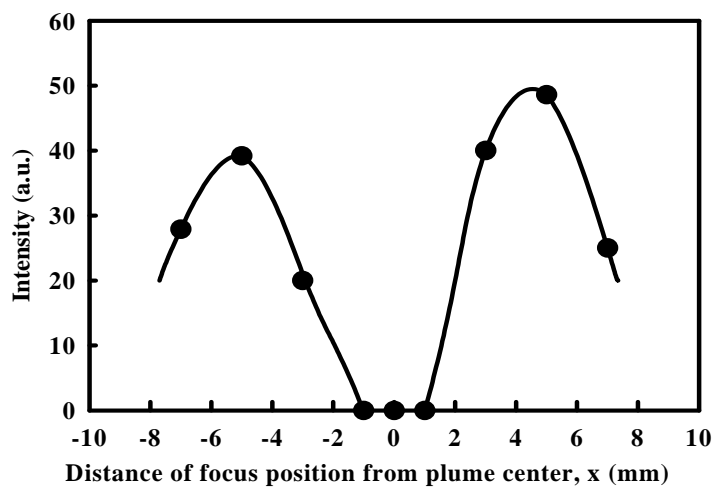


Fig. 5.3 Variation of intensity of 41st harmonic with the change in focus position of femtosecond laser w. r. to the centre of the plasma plume. The solid line is to guide the eye.

that the focal position of the femtosecond laser beam w. r. to the plasma plume is quite important for efficient harmonic generation, and the optimum position depends on the harmonic order.

The near disappearance of harmonic intensity for the laser beam focussed at the plume centre can be understood from the introduction of large phase mismatch between the laser and harmonic radiation, due to the high degree of ionization inside the plasma plume. The details of the phase mismatch will be discussed in following paragraphs. Similar study on high order harmonic generation from gas jets has been performed by Salieres *et al* [4]. Instead of near disappearance of harmonic intensity (as in our case) they have observed a small reduction in harmonic conversion efficiency when the laser was focussed at the centre of the gas jet, and two unequal peaks of harmonic intensities were observed around it. This could be understood from the fact that the peak laser intensity in their experiment was $\sim 6 \times 10^{14}$ W/cm², which was much smaller than our case. Thus the free electron density inside the gas jet and corresponding phase mismatch effects were also small.

Generation of high order harmonics from three-step model was discussed in Chapter 1. The processes of tunnelling, acceleration and recombination can be visualized as induction of a nonlinear dipole. The intensity of any harmonic order (say q^{th} order) of the laser of frequency ω_L , depends on the strength of the nonlinear dipole ($d(q\omega_L)$) [7]. If there are N_0 number of harmonic emitters, the intensity of the q^{th} harmonic after propagation through a medium of length L_{med} can be written as (considering laser is propagating in z direction)

$$I_q = \left| \int_0^{L_{med}} N_0 d(q\omega_L) dz \right|^2 \dots\dots\dots (5.1)$$

The term inside integral signifies the coherent addition of the electric field of q^{th} harmonic, and intensity of the harmonic is the square of its modulus. The observed

variation of harmonic intensity with laser intensity and focussing may be understood from the variation in the ionization condition in the plasma plume which affects the phase-matching between the laser pulse and the harmonic radiation. The Eq. 5.1 then gets modified as

$$I_q = \left| \int_0^{L_{med}} N_0 d(q\omega_L) \exp(i\Delta kz) dz \right|^2 \quad \dots\dots\dots (5.2)$$

where Δk is the phase mismatch factor. For small free electron density (compared to critical density n_{cr}) the plasma refractive index for laser pulse (μ_L) and its q^{th} harmonic (μ_q) can be written as

$$\begin{aligned} \mu_L &= \sqrt{1 - \frac{n_e}{n_{cr}}} = 1 - \frac{n_e}{2n_{cr}} \\ &= 1 - \frac{n_e e^2}{2\varepsilon_0 m \omega_L^2} \end{aligned} \quad \dots\dots\dots (5.3)$$

and

$$\begin{aligned} \mu_q &= 1 - \frac{n_e e^2}{2\varepsilon_0 m q^2 \omega_L^2} \\ &\approx 1 \quad (\text{For large 'q'}) \end{aligned} \quad \dots\dots\dots (5.4)$$

where n_e is the electron number density, e is electronic charge, ε_0 is the permittivity of free space, and ω_L is the laser frequency. Since the refractive index of the medium is different for the fundamental laser beam and the harmonic radiation, a phase mismatch is introduced between the two waves. The phase mismatch (Δk) between the laser pulse and harmonic radiation can be written as

$$\Delta k = k_q - qk_L \quad \dots\dots\dots (5.5)$$

where k_L is the wave-vector of laser and k_q is the wave vector for the q^{th} harmonic. The wave vectors can be written as

$$\begin{aligned}
k_L &= \frac{\mu_L \omega_L}{c} \\
&= \left(1 - \frac{n_e e^2}{2\epsilon_0 m \omega_L^2} \right) \frac{\omega_L}{c} \quad \dots\dots\dots (5.6) \\
k_q &= \frac{\mu_q \omega_q}{c} \\
&= \frac{q \omega_L}{c} \quad (\text{for large 'q'})
\end{aligned}$$

Distance over which the phase mismatch between the harmonic and fundamental radiation becomes π (*i.e.* $\Delta k L = \pi$) is referred to as coherence length (L_c). For q^{th} harmonic, L_c can be written as [8],

$$L_c = \frac{\pi}{\Delta k} = \frac{2\pi c \omega_L \epsilon_0 m}{q n_e e^2} \quad \dots\dots\dots (5.7)$$

The Eq. 5.2 can now be written as

$$I_q = \left| \int_0^{L_{med}} N_0 d(q \omega_L) \exp(i\pi \frac{z}{L_c}) dz \right|^2 \quad \dots\dots\dots (5.8)$$

It can be seen from Eq. 5.7 that the coherence length decreases with increased electron density and harmonic order. At high laser intensity, the coherence length decreases due to increase in n_e . Further, since at a fixed electron density, the coherence length is smaller for higher harmonic orders, the electron density for efficient harmonic generation for higher harmonic orders is smaller than that for lower orders.

The observed variation of the harmonic intensity with x can now be explained in terms of the physical picture of the effect of phase mismatch on HHG. As $|x|$ decreases from 8 mm to 0 mm, the peak laser intensity in the plasma plume increases from $\sim 10^{15}$ W/cm² to $\sim 10^{18}$ W/cm². The increase in laser intensity increases the nonlinear dipole moment of the atom and thereby increases the harmonic intensity. However, the increasing electron density in the plasma plume with the laser intensity increases the phase-mismatch, which reduces the harmonic intensity. The observed peak harmonic

intensity at $|x| = 3$ mm comes as a balance of these two effects. As $|x|$ is decreased from 3 mm to 0, the phase mismatch factor dominates, and harmonic intensity reduces.

The observation of peak harmonic intensity for the 23rd and 41st orders at different values of x [$x = \pm 3$ mm (Fig. 5.2) and $x = \pm 5$ mm (Fig. 5.3)] could be understood in terms of variation of coherence length with harmonic order. As seen from Eq. 5.7, the coherence length is proportional to $(n_e q)^{-1}$. Thus, for a given coherence length, the maximum acceptable electron density decreases for higher order harmonics and hence the optimum harmonic conversion should occur at a smaller laser intensity. In our experiment, the peak harmonic intensities for $q = 23$ and 41 occurred at $x = \pm 3$ mm and ± 5 mm for which the laser intensity at the plume centre was $\sim 10^{16}$ W/cm² and $\sim 4 \times 10^{15}$ W/cm² respectively.

Next, we examine the unequal peak intensity of harmonics for the same value of $|x|$ on the two sides of the plume centre. The radial intensity profile of a Gaussian beam results in a radial electron density profile with peak at the centre, and a corresponding refractive index profile with minimum at the centre (Eq. 5.3). This results in an outward curving of the wave-front of the laser beam leading to its defocusing. The plasma plume thus behaves like a concave lens resulting in defocusing of the femtosecond laser beam. As seen in Fig. 5.2, the peak harmonic intensity for the 23rd harmonic at $x = +3$ mm is 2.5 times larger compared to that for $x = -3$ mm. When the best focus position of the laser beam is before the plume, the defocusing effect in the plasma occurs in the already diverging part of the beam, resulting in an increased divergence (Fig. 5.1b) thereby reducing the harmonic intensity at the detector. On the other hand, for the opposite case, the defocusing occurs in the converging part of the laser beam. This shifts the focus of the laser beam (as well as that of the harmonics) towards the detector (Fig 5.1c) resulting in a higher intensity of the harmonics at the detector. A similar effect was seen for the

41st harmonic (Fig. 5.3), but the corresponding intensity ratio was smaller ~ 1.25 . As noted from Eq. 5.4, the refractive index for higher orders is closer to unity. Thus the defocusing is less pronounced for higher-order harmonics. Hence the ratio of the harmonic intensity on the two sides for 41st order harmonic is smaller as compared to that for the 23rd order harmonic.

5.2. Dependence of harmonic intensity on length of plasma plume

To study the effect of medium length on HHG from plasma plumes, an experimental study has been performed using elongated plasma plumes. The description of experimental setup is similar to that explained in Chapter 2 and experimental layout is same as in Fig. 2.8. In this experiment, we have used the XUV spectrograph without focussing mirror as shown in Fig 2.9. As explained in Chapter 2, two crossed cylindrical lenses of focal lengths 450 mm and 550 mm were used to focus the pre-pulse on target surface. These lenses generate a line focus of $2 \text{ mm} \times 300 \mu\text{m}$ (FWHM). The intensity of pre-pulse at the target surface was $\sim 10^{10} \text{ W/cm}^2$. Target used for this study was a silver strip of 2 mm width. The beam waist of the main femtosecond pulse was located at a distance (d) of 6.5 mm *after* the plasma plume, as shown in Fig. 5.4. The peak intensity of the fs laser pulse at the centre of the plasma plume was $\sim 2.5 \times 10^{15} \text{ W/cm}^2$. To study the effect of medium length on harmonic emission, length of the plasma plume was varied by inserting a slit of variable width in the centre of pre-pulse laser beam before the cylindrical lens assembly. The length of plasma plume was varied in the range of 0.8 mm to 2 mm in step size of 0.4 mm. All the other parameters were kept constant during the study.

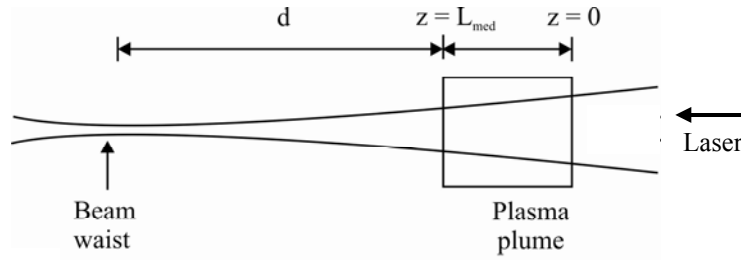


Fig. 5.4: The laser propagation geometry inside the plasma plume

The high-order harmonics, generated from silver plasma plumes, in the range of 15th to 47th order, covering a spectral range of 53 nm to 16 nm, were observed. The dependence of the harmonic intensity on the length of plasma medium was studied. Fig. 5.5 shows the variation of 21st, 33rd and 41st harmonic intensity with the length of plasma medium. The harmonic intensity (I_H) increases with the medium length (L_{med}), and it shows a length scaling of $I_H \propto L_{med}^p$, where the scaling exponent ' p ' is ~ 0.9 , 0.8 , and 0.7 for 21st, 33rd, and 41st harmonics respectively. These values of p are much smaller than 2.

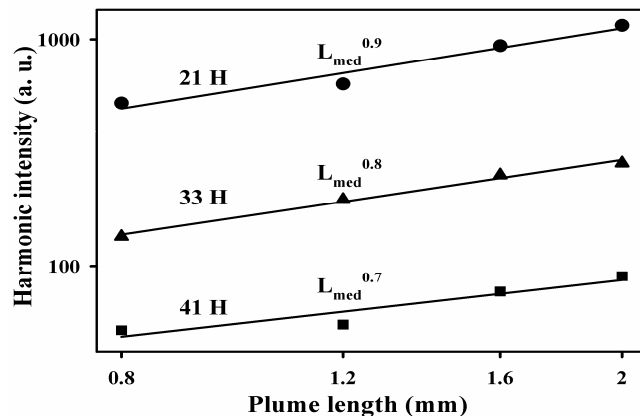


Fig. 5.5 Variation of the harmonic intensity with plume length

Next, we present the variation of harmonic intensity with harmonic order for medium lengths of 0.8 mm and 2 mm (Fig 5.6). It is seen from this figure that the intensity of harmonics decreases with increasing harmonic order. For instance, for the case of plasma plume length of 2 mm, the intensity of 41st order harmonic is ~ 13 times smaller than that of 21st order harmonic. However the decrease is slower for shorter

plume length, the ratio of the intensity of 21st harmonic to 41st harmonic is reduced to ~9.5 in the case of 0.8 mm plume length. Nevertheless, in both the cases, the harmonic emission deviates from the plateau-like emission behaviour observed in earlier studies with gas jets.

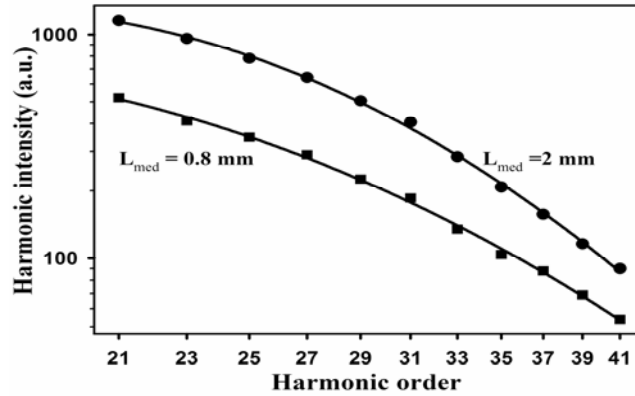


Fig. 5.6 Variation of harmonic intensity with harmonic order at two different medium lengths

5.3. Estimation of the effect of various phase mismatch factors

The above experimental results are now analysed from physical considerations involved in high order harmonic generation and growth of harmonic intensity with length of the medium. The intensity of the harmonic radiation after propagation in medium of length L_{med} is given by Eq. 5.8

$$I_q = \left| \int_0^{L_{med}} N_0 d(q\omega_L) \exp(i\pi \frac{z}{L_c}) dz \right|^2 \quad \dots\dots\dots (5.8)$$

Incorporating the re-absorption coefficient (α) of harmonic radiation in the plasma medium, the Eq. 5.8 will get modified as [9]

$$I_q = \left| \int_0^{L_{med}} N_0 d(q\omega_L) \exp\left(\frac{i\pi z}{L_c}\right) \exp[-\alpha(L_{med} - z)] dz \right|^2 \quad \dots\dots\dots (5.9)$$

where the location z is measured with respect to the entrance edge of the plasma plume. The term $\exp[-\alpha(L_{med} - z)]$ in Eq. 5.9 represents the re-absorption of harmonics generated at position z in the remaining plasma plume, where α is the absorption coefficient. For the sake of simplicity, we may assume the plasma plume to be of uniform density through its length so that Δk and α are not functions of z . This is reasonable since the electron density in plasmas produced during interaction of sub-nanosecond laser pulses scales with laser intensity as $I_L^{1/3}$ [10]. Thus the maximum density variation from the entrance / exit edge of the plasma plume with respect to its centre will be $\sim 15\%$ only. Similar to coherence length one may define absorption length as the distance over which the intensity of harmonic radiation is reduced to its $1/e$ value due to absorption during propagation. This L_{abs} can be expressed as

$$L_{abs} = \frac{1}{2\alpha} \quad \dots\dots\dots (5.10)$$

Finally after performing the integration, Eq. 5.9 can be expressed as

$$I_q = \left| N_0 d(q\omega_L) \exp\left[-\frac{L_{med}}{2L_{abs}}\right] \frac{\exp\left(\frac{i\pi}{L_{coh}} + \frac{1}{2L_{abs}}\right)L_{med} - 1}{\frac{i\pi}{L_{coh}} + \frac{1}{2L_{abs}}} \right|^2 \quad \dots\dots\dots (5.11)$$

This may be further simplified to

$$I_q = N_0^2 |d(q\omega_L)|^2 \frac{4(L_{abs}L_{coh})^2}{L_{coh}^2 + (2\pi L_{abs})^2} \left[1 + \exp\left[-\frac{L_{med}}{2L_{abs}}\right] - 2 \cos\left(\frac{\pi L_{med}}{L_{coh}}\right) \exp\left[-\frac{L_{med}}{2L_{abs}}\right] \right] \quad \dots\dots\dots (5.12)$$

It follows from the above expression that for given values of L_{coh} and L_{abs} , the harmonic intensity can be optimized with respect to the length of the plasma medium. Moreover, since in general, L_{coh} and L_{abs} vary with plasma density and harmonic order, one can make appropriate choices of the plasma density and medium length to achieve maximum

harmonic intensity for different orders of harmonics. One may note from Eq. 5.8 that harmonic intensity undergoes oscillations with a period of $2L_c$. Further as the effect of absorption is considered in Eq. 5.10 the harmonic intensity oscillations will be damped.

There are mainly four factors that contribute to phase mismatch [4] : 1) atomic dispersion [2, 4], 2) Gouy phase shift [5], 3) plasma dispersion, and 4) intensity dependent dynamical phase shift in non-linear dipole moment [4, 6].

Atomic dispersion refers to the variation in the refractive index of the gaseous medium for the fundamental and harmonic radiation. The corresponding phase mismatch Δk_a due to atomic dispersion can be written as

$$\Delta k_a = -(1 - \eta)N\pi c^2 q \omega_L \sum_k \frac{g_2}{g_1} \frac{1}{\omega_k^2 (\omega_k^2 - \omega_L^2)} A_k \quad \dots\dots\dots (5.13)$$

where N is the atomic density, η is fractional ionization, c is speed of light, g_2 and g_1 are statistical weights of the upper and lower states, ω_k , A_k are the transition frequencies and Einstein's coefficients for transitions of k^{th} level to ground state, q is the harmonic order and ω_L is the laser frequency.

The plasma dispersion arises due to presence of free electrons in the plasma. The phase mismatch due to plasma electrons can be calculated from Eqs. 5.3 and 5.4 as

$$\Delta k_{pl} = \frac{\eta N e^2 q}{c \omega_L \epsilon_0 m} \quad \dots\dots\dots (5.14)$$

where ϵ_0 is the permittivity of free space, e, m are electronic charge and mass respectively.

Another term contributing to the phase mismatch is Gouy phase shift. This arises due to the phase change in the focussing laser radiation during its propagation. Gouy phase mismatch between laser beam and the q^{th} harmonic during propagation through the medium length L_{med} can be written as [5]

$$\Delta k_G(z) = \frac{q-1}{L_{med}} \left[\tan^{-1} \frac{d + L_{med}}{z_R} - \tan^{-1} \frac{d}{z_R} \right] \dots\dots\dots (5.15)$$

Finally, the last term contributing to phase mismatch is the intensity dependent dynamical phase shift (IDP). The phase mismatch between harmonics emitted between two ends of the plasma medium can be written as [6]

$$\Delta k_{IDP} = -\frac{1}{L_{med}} C_{1,2} [I_L(d + L_{med}) - I_L(d)] \dots\dots\dots (5.16)$$

where the subscripts 1, 2 denote short and long trajectories respectively, $C_1 = 1 \times 10^{-14} \text{ cm}^2/\text{W}$ and $C_2 = 24 \times 10^{-14} \text{ cm}^2/\text{W}$ [6].

Overall phase mismatch Δk can be written as

$$\Delta k = \Delta k_a + \Delta k_G + \Delta k_{pl} + \Delta k_{IDP} \dots\dots\dots (5.17)$$

The coherence length L_{coh} may be estimated from overall phase mismatch as $L_{coh} = \pi/\Delta k$.

It can be noted that all the phase mismatch factors, except the IDP shifts, are proportional to harmonic order, and hence the coherence length decreases with increasing harmonic order. This will result in decrease of harmonic intensity with increasing harmonic order, as observed in our study (Fig. 5.6). Moreover, this decrease in the intensity of harmonic orders should be faster for longer plume length, as phase mismatch accumulated by higher harmonic orders with increasing length is higher.

Although no measurements of plasma density were made in the present study, an estimate of the same was taken from the earlier work on plasma plumes generated under similar conditions [11] to be $\sim 2 \times 10^{17} \text{ cm}^{-3}$. At this density, the absorption length of the XUV photons due to photoabsorption in neutral silver is calculated to be $\sim 2.0, 2.3, 2.5$ mm for 21st, 33rd, 41st harmonic orders respectively [12].

The coherence length L_{coh} of the plasma plume for different harmonic orders can be calculated from $\pi/\Delta k$, where different components of Δk are given in Eq. 5.17. An

exact calculation of the different phase-mismatch factors requiring detailed analytical calculations or computer simulations will be quite involved. However, gross estimates are made in the following to illustrate the relative importance of various factors [9]. Firstly, the atomic phase mismatch can be determined from Eq. 5.13. For silver, the major transitions contributing to refractive index are $^2P_{3/2} \rightarrow ^2S_{1/2}$ and $^2P_{1/2} \rightarrow ^2S_{1/2}$ ($4d^{10}5p \rightarrow 4d^{10}5s$) having transition wavelengths of 328 nm, and 338.3 nm, with corresponding spontaneous emission rates $A_k = 1.47 \times 10^8 \text{ s}^{-1}$, and $1.35 \times 10^8 \text{ s}^{-1}$ respectively [13, 14]. In low excited plasmas used for HHG, the degree of ionization is typically in the range of 5-10%. Taking an average value of 7.5% for a plasma plume of density $2 \times 10^{17} \text{ cm}^{-3}$, the atomic phase mismatch Δk_a can be estimated from Eq. 5.13 as -1.3, -2.0, -2.5 rad/mm for 21st, 33rd, 41st harmonic orders respectively. Similarly, the plasma phase mismatch Δk_{pl} is also estimated from Eq. 5.14 as 1.5, 2.4, 3.0 rad/mm for 21st, 33rd, 41st harmonic orders respectively.

Next, the Gouy phase is calculated from Eq. 5.15 as 0.15, 0.25 and 0.3 rad/mm for 21st, 33rd and 41st harmonic orders respectively. Further, the intensity dependent phase shifts Δk_{IDP} can be estimated from Eq. 5.16. The calculation is done using effective value of laser intensity responsible for harmonic generation and C_1 , since the short trajectory, which has less phase-mismatch, is the dominating trajectory for harmonic emission. Although the peak laser intensity at the plume centre is $\sim 2.5 \times 10^{15} \text{ W/cm}^2$, the effective laser intensity is governed by saturation effects [2]. The electron quiver energy corresponding to the maximum order of harmonic (47th) observed in our experiments is $\sim 16 \text{ eV}$. Using Eq. 1.1, the saturation intensity is estimated to be $\sim 2.7 \times 10^{14} \text{ W/cm}^2$. Assuming this as the effective intensity at the plume centre, for a Gaussian beam of geometry shown in Fig. 5.4, the change in laser intensity from the entrance to the exit of the plasma plume ($I_L(0) - I_L(L_{med})$) is $\sim -1.8 \times 10^{14} \text{ W/cm}^2$. The phase mismatch Δk_{IDP} is

now calculated using Eq. 5.16 as ~ 0.9 rad/mm. As stated earlier, this value is independent of the harmonic order.

The overall phase mismatch Δk , on adding up all the four contributions, comes out to be 1.25, 1.55, 1.7 rad/mm and the same is shown in Table 5.1. The corresponding coherence lengths (L_{coh}) are 2.5, 2.0, 1.9 mm for 21st, 33rd, and 41st harmonic orders respectively. The absorption lengths (L_{abs}) were estimated to be 2.0, 2.3, 2.5 mm for 21st, 33rd, and 41st harmonic orders, respectively. Using these values of L_{abs} and L_{coh} in Eq. 5.12, the harmonic intensities for different plume lengths were calculated and the least square fit of these values gives the length scaling exponent ' p ' to be 1.1, 0.9, and 0.8 for 21st, 33rd and 41st harmonic orders, respectively. These values are close to the experimentally observed scaling exponents and show a similar decreasing trend with harmonic order. The estimated values of scaling exponent will depend on the value of atomic density (N) and degree of ionization (η) of the plasma plume. The small difference in calculated scaling exponents with experimentally observed value may be due to the choice of number density used for calculation. Moreover, the plasma plume will also have a spatial density variation. Thus the simple estimations carried out here are able to reasonably illustrate the observed scaling of harmonic intensity with medium length for different harmonic orders.

Harmonic order	Δk_G rad/mm	Δk_{IDP} rad/mm	Δk_a rad/mm	Δk_{pl} rad/mm	Δk rad/mm	L_{coh} mm	L_{abs} mm	Scaling exponent
21	0.15	0.9	-1.3	1.5	1.25	2.55	2.0	1.1
33	0.25	0.9	-2.0	2.4	2.3	2.00	2.3	0.9
41	0.30	0.9	-2.5	3.0	2.5	1.85	2.5	0.8

Table 5.1: Estimates of various factors contributing to phase-mismatch, coherence length, and absorption length, for different harmonic orders, to calculate the intensity scaling exponent.

The value of scaling exponent ' p ' for all the three harmonic orders is smaller than 2 expected for a completely phase matched medium. The decrease in ' p ' occurs as the medium length approaches towards the coherence length. Since the coherence length is smallest for the 41st harmonic order, the value of ' p ' is also the smallest for this harmonic order. The above calculations also illustrate the faster decrease of harmonic intensity with harmonic order for longer plasma plume length. Since the coherence length decreases with increasing harmonic order, the phase mismatch accumulated during propagation through a longer plasma plume will increase with harmonic order at a higher rate. From the contributions of different factors to phase-mismatch, listed in Table 5.1, it can be clearly seen that the contribution of IDP is also quite significant. Contribution of this term can be reduced by reducing the intensity variation along the plasma plume, which can be achieved by increasing, the Rayleigh range (z_R) through the use of large f number of focussing optics.

Bibliography

1. L. A. Lompre, A. L'Huillier, M. Ferray, P. Monot, G. Mainfray, and C. Manus, "High-order harmonic generation in xenon: intensity and propagation effects", *J. Opt. Soc. Am. B* **7**, 754 (1990).
2. Ph. Balcou *et al.*, "High-order-harmonic generation: towards laser-induced phase matching control and relativistic effects", *Appl. Phys. B* **74**, 509 (2002).
3. H. R. Lange, A. Chiron, J. F. Ripoche, A. Mysyrowicz, P. Breger, and P. Agostini, "High-Order Harmonic Generation and Quasiphase Matching in Xenon Using Self-Guided Femtosecond Pulses", *Phys. Rev. Lett.* **81**, 1611 (1998).

4. P. Salieres, A. L'Huillier, P. Antoine, and M. Lewenstein, "Studies of the spatial and temporal coherence of high order harmonics", *Adv. At. Mol. Opt. Phys.* **41**, 83 (1999).
5. F. Lindner, G. G. Paulus, H. Walther, A. Baltuska, E. Goulielmakis, M. Lezius, and F. Krausz, "Gouy Phase Shift for Few-Cycle Laser Pulses", *Phys. Rev. Lett.* **92**, 113001 (2004).
6. Y. Tamaki, J. Itatani, M. Obara, and K. Midorikawa, "Optimization of conversion efficiency and spatial quality of high-order harmonic generation", *Phys. Rev. A* **62**, 063802 (2000).
7. M. Lewenstein, Ph. Balcou, M. Yu. Ivanov, A. L'Huillier, and P. B. Corkum, "Theory of high-harmonic generation by low-frequency laser fields", *Phys. Rev. A* **49**, 2117 (1994).
8. H. Singhal, R. Ganeev, P. A. Naik, V. Arora, U. Chakravarty, and P. D. Gupta, "Dependence of high order harmonics intensity on laser focal spot position in preformed plasma plumes" *J. Appl. Phys.* **103**, 013107 (2008).
9. H. Singhal, V. Arora, B. S. Rao, P. A. Naik, U. Chakravarty, R. A. Khan, and P. D. Gupta, "Dependence of high-order harmonic intensity on the length of preformed plasma plumes", *Phys. Rev. A* **79**, 023807 (2009).
10. P. Mora, "Theoretical model of absorption of laser light by a plasma", *Phys. Fluids* **25**, 1051 (1982).
11. R. A. Ganeev, H. Singhal, P. A. Naik, U. Chakravarty, V. Arora, J. A. Chakera, R. A. Khan, M. Raghuramaiah, S. R. Kumbhare, R. P. Kushwaha, and P. D. Gupta,

- “Optimization of the high-order harmonics generated from silver plasma”, *Appl. Phys. B* **87**, 243 (2007).
12. J. H. Hubbell, “Survey of photon-attenuation-coefficient measurements 10 eV to 100 GeV”, *At. Data Nu. Data Tables* **3**, 241 (1971).
 13. J. C. Pickering and V. Zilio, “New accurate data for the spectrum of neutral silver”, *Eur. Phys. J. D* **13**, 181 (2001).
 14. D. C. Morton, “Atomic Data for Resonance Absorption Lines. II. Wavelengths Longward of the Lyman Limit for Heavy Elements”, *Astrophys. J., Suppl. Ser.* **130**, 403 (2000).

Chapter 6

Improvement in stability of HHG and extension of cut-off order

High intensity of harmonic radiation and its stable operation are pre-requisites for any practical application of this radiation. In general, the harmonic intensity for laser ablated plasma plumes would depend on laser intensity variation and target surface conditions in different laser shots. In principle, one can have a highly stable laser and expose a fresh surface on the target for each shot to achieve nearly-stable harmonic intensity. However, for high repetition rate irradiation, large size targets may be required which sometimes may not be practical. Hence in earlier studies, experiments were performed by repeated irradiation of the same spot on the target for several laser shots. It was observed that harmonic intensity reduced by a factor of 2 after firing $\sim 20 - 30$ laser shots. Due to repeated ablation from the same area, the irradiated portion of the target recedes inwards so that its distance from the axis of the femtosecond laser beam increases. Hence the plasma produced from successive laser shots on the target would undergo a larger distance of expansion in reaching the axis of the femtosecond laser beam. The resulting reduction of plasma plume density in the interaction regime could be responsible for the observed decrease in harmonic intensity. In principle, this situation can be much improved by decreasing the amount of target material ablated in each shot. We have performed a study on stable harmonic generation by using a low energy pre-pulse laser beam focussed more tightly to achieve the same laser intensity. This study is presented in Section 6.1.

Next, the generation of coherent XUV radiation at shorter wavelengths through extension of HHG cut-off remains an area of active investigations [1]. As discussed in

Chapter 1, the cut-off harmonic order in high order harmonic generation from low excited plasma plumes is governed by ionization potential of the target material. A closed-form relation of harmonic cut-off order with the ionization potential of the atom is given by Chang *et al* [2]. In Section 6.2, we present an experimental study of cut-off harmonic order in plasma plumes of different target materials and compare the results with those expected theoretically [2]. A second plateau of harmonics was observed in plasma plumes of manganese. It was seen that the intensity and cut-off order in this second plateau could be increased by increasing the pre-pulse laser intensity and optimizing the intensity of femtosecond laser pulse. Results of this study and physical understanding of generation of second plateau in plasma plumes of some elements is also presented in Section 6.2.

6.1. Stable harmonic generation in plasma plumes

The experimental arrangement for HHG studies has been explained in Chapter 2. The high order harmonics were generated by focussing an intense femtosecond laser pulse inside a low-excited preformed plasma plume (Fig 2.8). This plasma plume was generated by loosely focussing a 30 mJ, 200 ps laser pulse on the target surface using a 500 mm plano-convex lens. The laser was focussed on target surface with a spot size of ~600 micron and the peak laser intensity at target surface was $\sim 10^{10}$ W/cm². In order to experimentally see the effect of reduction in the amount of ablated material on the stability of harmonic generation, the pre-pulse laser energy was reduced and the focal spot was made smaller to keep the same pre-pulse laser intensity. Specifically, the pre-pulse energy was reduced from ~30 mJ to ~7 mJ by inserting neutral density filters before the focussing lens, and the focussing was made tighter to a focal spot size ~300 microns. The harmonic spectra recorded for different number of laser shots fired on the same spot are shown in Fig. 6.1. It is seen that the intensity of HHG remains nearly same

even after ~ 1000 laser shots were fired at the same spot and it reduces by a factor of ~ 2 after ~ 2000 shots were fired on the same surface. Thus the stability of harmonic generation from pre-formed plasma plumes could be much improved by optimizing pre-pulse laser energy and focussing conditions.

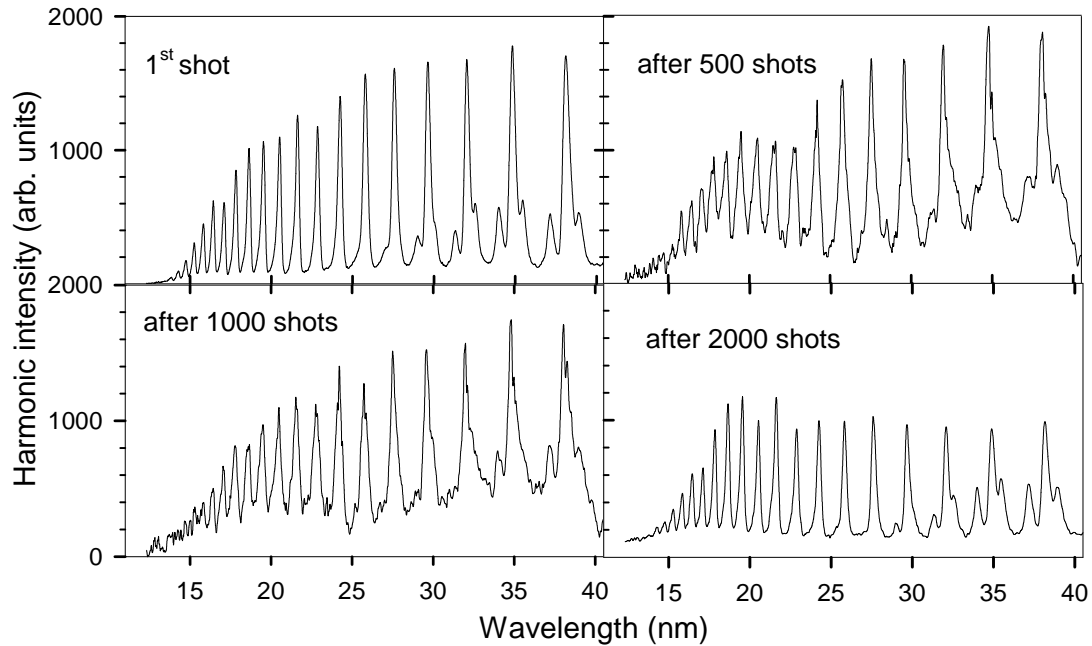


Fig. 6.1 HHG spectra recorded for different number of laser shots fired on the same spot

6.2. Study of harmonic cut-off order in plasma plumes of different targets and its extension through second plateau generation

The extension of harmonic cut-off remains an important area of investigation in view of various practical applications such as ultrafast x-ray dynamics and also for the understanding of the process itself. The cut-off of harmonic radiation depends on the intensity of the laser radiation and the ionization potential of the target material utilized. High order harmonic spectra were observed from the plasma plume of different target materials using the experimental setup shown in Chapter 2. The femtosecond laser intensity was optimized to achieve the maximum value of harmonic cut-off order for each material. The cut-off orders observed are indicated in parentheses : Ag(63), In(41),

Al(49). In the case of Cr, and Mn, it was found that harmonic emission shows a plateau like emission pattern which has cut-off at 27th, and 31st harmonic respectively, beyond which a second plateau of harmonics starts from 29th and 33rd harmonics respectively and extends to several harmonic orders. The harmonic emission from plasma plumes of Mn is shown in Fig. 6.2. It was observed that that with increase in the excitation of the Mn plume and increasing the intensity of femtosecond pulse the harmonic cut-off extends to 73rd harmonic order.

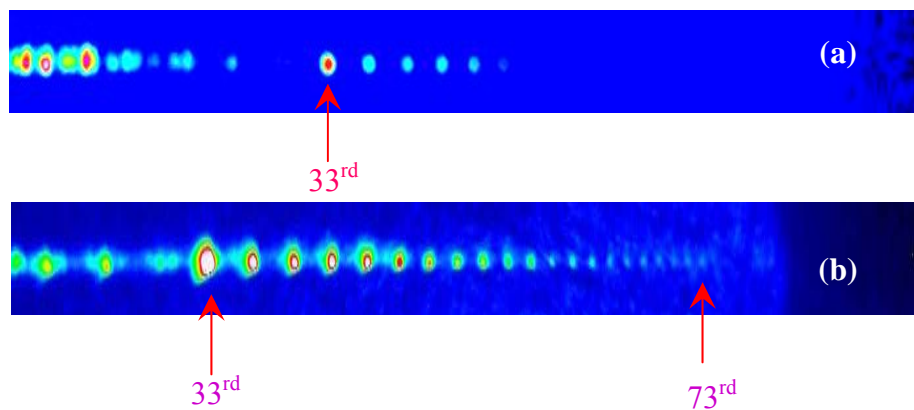


Fig. 6.2 Observation of second plateau in HHG from Mn plume (a) HHG before optimization (b) HHG after optimization

We now examine the observed experimental results in the light of theoretical predictions. As per three-step model discussed in Chapter 1, the energy of harmonic photon is equal to the sum of ionization potential of the atom/ion and the kinetic energy of the electron moving under the effect of laser field at the instant of its re-collision with parent ion. The maximum photon energy can be written as [3, 4]

$$h\nu_{\max} = I_p + 3.17U_p, \quad \dots\dots\dots (6.1)$$

where U_p is the ponderomotive energy and I_p is the ionization potential of the atom. The maximum ponderomotive energy possible for the HHG is corresponding to saturation intensity I_s as discussed in Chapter 1. The saturation intensity can be estimated from the ionization rates given by Ammosov-Delone-Krainov (ADK) [5] and an analytical

expression for the maximum harmonic cut-off energy $h\nu_c$ can be obtained in the closed form for laser intensities greater than saturation intensity [2].

$$h\nu_c = I_p + \frac{0.5I_p^{(3+a)}\lambda^2}{\left\{\ln\left[0.86\tau 3^{2n^*-1}G_{l,m}C_{n^*}^2 / (-\ln(1-p))\right]\right\}^2} \quad \dots\dots\dots (6.2)$$

where $h\nu_c$ and I_p are in eV, $a = 0.5$ (this factor is taken to correct the approximation used in the derivation of the saturation intensity), λ is the laser wavelength in μm , τ is the laser pulse duration in fs, p is the ionization probability defining the saturation intensity (here taken as 90%), and n^* is the effective principal quantum number. It is pertinent to state here that the approximation correction factor ‘ a ’ arises due to the deviation of atomic states from their ideal description. The expressions for n^* , C_{n^*} and G_{lm} are [5].

$$n^* = z^* \sqrt{\left(\frac{13.6}{I_p \text{ (eV)}}\right)} \quad \dots\dots\dots (6.3)$$

$$C_{n^*} = \left(\frac{2e}{n^*}\right)^{n^*} \frac{1}{\sqrt{2\pi n^*}} \quad \dots\dots\dots (6.4)$$

$$G_{lm} = \frac{(2l+1)(l+|m|!)}{6^{|m|} |m|!(l-|m|)!} \quad \dots\dots\dots (6.5)$$

where ‘ l ’ and ‘ m ’ are orbital and magnetic quantum numbers of outermost electron. The Eq. 6.2 predicts the observed cut-off harmonic orders from noble gases quite accurately [2].

Unlike gases where HHG is from neutral atoms, the harmonics from plasma plumes are generated mainly from neutral atom and singly ionized particles. Thus the harmonic cut-off order would depend on the second ionization potential of the atom. One can calculate the harmonic cut-off order for this situation using Eq. 6.2. For silver ions (Ag^+) $I_p = 21.45$ eV, $l = 2$, $m = 0$. At this point it is required to reconsider the applicability of the approximation correction factor ‘ a ’. For the original value of $a = 0.5$

used in Ref. 2 the harmonic cut-off from Ag^+ comes about 85 which is much higher compared to the observed cut-off of 63 (Chapter 3). This difference between the observed and calculated values of cut-off orders could be possibly due to a value of the approximation correction factor ‘ a ’ smaller than 0.5. This indeed may be true as the screening of nuclear charge is more effective in singly charged ions as compared to that for the corresponding neutral atoms. It is therefore reasonable to expect that the electronic states of singly charged ions are closer to their ideal description as compared to that for neutral atoms. The lower values of harmonic cut-off order of 63 for Ag^+ ions would fit well with theoretical calculation if ‘ a ’ is taken as 0.4. It was found that the harmonic cut-offs for various other elements calculated by this method are in excellent agreement with observed results (keeping the value of $a = 0.4$). Table 6.1 summarizes the comparison between observed and calculated cut-offs generated from 45 fs pulses [6].

Element	Observed cut-off	Species	Ionization potential (eV)	Calculated cut-off
Ag	63	Ag	7.57	9
		Ag^+	21.45	65
In	41	In	5.78	5
		In^+	18.9	45
Al	49	Al	6	5
		Al^+	18.8	55
GaAs	43	As	9.79	13
		As^+	18.5	45
Cr	27	Cr	6.76	7
	47	Cr^+	16.5	31
		Cr^{+2}	31	169
Mn	31	Mn	7.43	9
	73	Mn^+	15.6	32
		Mn^{+2}	34	290

Table 6.1 Comparison between observed cut-off and calculated harmonic cut-offs

The cut-off of harmonic radiation could further be increased by the HHG from doubly charged ions. In low excited plasma plumes the HHG from singly charged particles is observed. However, in certain cases it is possible to see the HHG even from doubly ionized states in plasma plumes. Since number of explorable nonlinear media for HHG in the case of plasma plumes is very large, it is possible to find some media which have larger nonlinear response for doubly charged ions. This phenomena is observed in the case of V, Mn where second plateau was observed during their interaction with femtosecond laser pulses [7]. In the case of V, the HHG upto 71st harmonic was observed which is possible only from doubly ionized particles. In the case of Mn, the harmonics upto 101st order were seen. As discussed earlier, in our experiments the harmonic was observed up to the 73rd harmonic order.

The HHG upto 31st harmonic is attributed to singly charged Mn ions. Normally the HHG from doubly charged ions could not be observed in other plumes but in this case the nonlinearity of HHG process from doubly ionized media is increased due to the large number of unpaired 'd' electrons in doubly ionized Mn. The calculated cut-off comes ~294 order which is high compared to observed cut-off of 101st harmonic this may be due to further reduction in the approximation correction factor a . The non-visibility of the HHG up-to 101st order in our case is due to less sensitivity of the detector at lower wavelengths. Further investigation and improvement in detection system is required to detect the highest harmonic order emitted from these plumes for better understanding of the process.

Bibliography

1. C. Winterfeldt, and G. Gerber, “Optimal control of high-harmonic generation”, *Rev. Mod. Phys.* **80**, 117 (2008).
2. Z. Chang, A. Rundquist, H. Wang, M. M. Murnane, and H. C. Kapteyn, “Generation of Coherent Soft X Rays at 2.7 nm Using High Harmonics” *Phys. Rev. Lett.* **79**, 2967 (1997).
3. P. B. Corkum, “Plasma perspective on strong field multiphoton ionization”, *Phys. Rev. Lett.* **71**, 1994 (1993).
4. M. Lewenstein, Ph. Balcou, M. Yu. Ivanov, Anne L’Huillier, and P. B. Corkum, “Theory of high-harmonic generation by low-frequency laser fields”, *Phys. Rev. A* **49**, 2117 (1994).
5. M. V. Ammosov, N. B. Delone, V. P. Krainov, “Tunnel ionization of complex atoms and of atomic ions in an alternating electromagnetic field”, *Sov. Phys.-JETP*, **64**, 1191 (1986).
6. H. Singhal *et al* “Study of high order harmonic cut-off in laser produced plasma plumes” Manuscript under preparation.
7. M. Suzuki, L. B. E. Bom, T. Ozaki, R. A. Ganeev, M. Baba, and H. Kuroda “Seventy-first harmonic generation from doubly charged ions in preformed laser-ablation vanadium plume at 110 eV”, *Opt. Express* **15**, 4112 (2007).

Chapter 7

HHG from nanoparticles-containing plasmas

High order harmonic generation from the interaction of ultrashort laser pulses with gaseous media is a well established method for the generation of ultrashort pulse, coherent radiation in the extreme ultraviolet (XUV) spectral range [1–3]. Various properties of HHG, such as XUV photon energy, the possibility of achieving diffraction limited focusing conditions [4], coherence, and ultrashort pulse duration make it a potential source for various practical applications. Many applications of HHG have been realized, such as generation of attosecond pulses [5], measurement of ultrafast photo-recombination cross sections [6], probing of rotational dynamics of molecules [7], detection of molecular structure [8], etc. Several other applications have been predicted, such as strong field fast alignment of molecules [9], achievement of ultrahigh focused intensities [4], etc.

In the previous chapters, we have described our studies on HHG from the interaction of low excited plasma plumes with ultrashort Ti:sapphire laser pulses. High-order harmonic generation from various plasma plumes were studied [10-12]. In Chapter 3 we have described the optimization of laser and plasma parameters to maximize the intensity of high order harmonics and the cutoff harmonic order [11]. In order to increase the practical applicability of the HHG, it is required to increase the conversion efficiency of the process which has been reported to be $\sim 10^{-6}$ [12]. In Chapters 4 & 5, we have presented studies on resonant enhancement of particular harmonic orders [13] and the use of elongated plasma plumes [14] respectively, to achieve higher intensity of harmonics. In this chapter, we describe high order harmonic generation from plasma plumes containing metal nanoparticles and fullerenes etc., possessing high nonlinear

optical properties, to increase the harmonic conversion efficiency. It was observed that under similar conditions of laser irradiation used for bulk targets, the nanoparticles containing plasma plumes produced harmonics predominantly in the range of 9th – 27th order (87 nm – 29 nm) with intensity ~100 times higher compared to those from bulk targets [15].

Section 7.1 presents the methods of preparation of substrates containing nanoparticles (to prepare plasma plumes for HHG) from nanoparticles powder. The results of harmonic generation from these nanoparticle targets are presented in Section 7.2. This section also includes results of harmonic generation from fullerenes containing plasma plumes. The HHG from fullerenes containing plasma plumes was similar to that from plasma plumes containing metal nanoparticles. Further, as discussed in Chapter 6, stable harmonic generation is an important requirement for the utilization of this radiation as an XUV source. The stability of the harmonic generation from nanoparticles / fullerenes depends on the interaction of nanoparticles / fullerene coating deposited on the substrates. This is also described in this section. Physical understanding of the observed enhancement in harmonic intensity in nanoparticles containing plasma plumes is also discussed.

Plasma plumes containing nanoparticles were also produced *in-situ* from the interaction of pre-pulse laser beam with bulk metals. Study of harmonic generation from such plasma plumes is given in section 7.3.

7.1. Preparation of nanoparticles-containing plasma plumes

The nanoparticles-containing plasma plumes for HHG studies were prepared by ablating the nanoparticles / fullerene containing substrates by a low intensity laser pre-pulse. The powder of nanoparticles / fullerene was mixed with either glue or an organic

medium and then pasted on a plane solid surface. In what follows we describe the preparation of nanoparticles / fullerene containing plasma plumes for our experiments on HHG.

The study of HHG using metal nanoparticles containing plasma plumes was mainly performed using Ag nanoparticles, and in some cases using Au, and SrTiO₃ nanoparticles. Commercially procured samples of Ag, Au and SrTiO₃ were used for preparation of targets. In addition, silver nanoparticles were also developed in-house by reducing silver nitrate with sodium borohydride and hydrogen peroxide in the presence of trisodium citrate. A capping agent polyvinyl pyrrolidone was used to prevent aggregation. The reaction took place at room temperature. At the end of the reaction, the solution turned blue. The absorption spectrum of the sample showed a peak at 638 nm.

The structure of the various nanoparticles was analyzed with a transmission electron microscope (TEM). Sample preparation for TEM observation was performed by preparing a suspension of the sample in methanol that was then dropped onto the copper-supported carbon film. To reduce agglomeration, the dilute nanoparticles emulsion was subjected to ultrasonic dispersion for approximately 10 minutes. The transmission electron microscope (Philips CM200) was operated at 200 kV accelerating voltage. The resolution of the TEM was ~ 2 Å. Fig 7.1 shows the TEM images of commercially procured Ag, and Au nanoparticles and in-house developed Ag nanoparticles. The samples of commercially procured Ag and Au nanoparticles have spherical shape with average particle size (APS) of ~ 10 nm and 14 nm (as shown in Fig. 7.1a and 7.1b respectively). The SrTiO₃ nanoparticles were also spherical and had an APS of 38 nm. On the other hand, the in-house developed Ag nanoparticles were predominantly of triangular shape (Fig. 7.1c) and had an APS of ~ 50 nm. Experimental studies on HHG using nanoparticles of different materials, sizes and shapes can provide

interesting in-sight into the properties of these nanostructured targets in enhancing harmonic intensity.

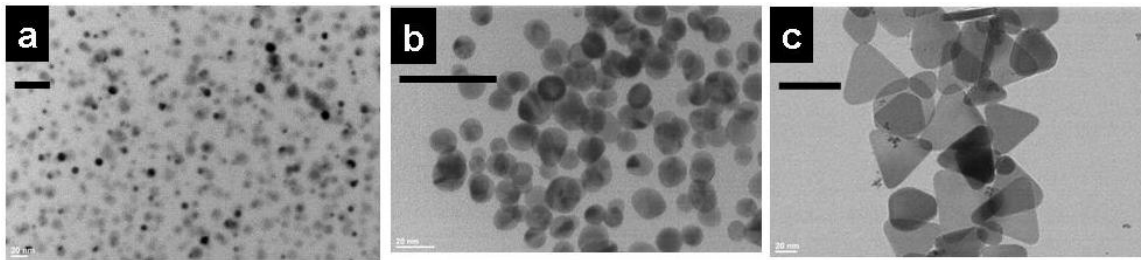


Fig. 7.1 TEM images of (a) commercially purchased Ag nanoparticles, (b) commercially purchased Au nanoparticles, (c) chemically prepared Ag triangle platelets. The size of black lines on the images is 50 nm

The nanoparticles substrates were prepared from the above nanoparticles. The nanoparticles were mixed with fast drying vacuum compatible glue and spread on a glass slide. The process was repeated several times to obtain a thick coating of nanoparticles on the glass slide. Although this was the easiest method to prepare substrate, the surface irregularities and the density variation of the nanoparticles is large in such substrates. All the metal nanoparticles substrates, except for triangular Ag nanoparticles substrates, were prepared in this manner. To obtain a smoother surface and more uniform density distribution of the nanoparticles across the whole substrate area, we mixed triangular Ag nanoparticles with polyvinyl alcohol (PVA) and then a layer of the solution was coated on the glass slide. When the solution dried up, another layer was applied over it. The process was repeated many times so that about 2 mm thick layer was formed. Alternatively, the substrate was prepared by the same method as explained above, except that the sample was dried in an oven at 60 °C. This process increased the density of Ag nanoparticles.

In order to take TEM images to check the presence of nanoparticles in laser ablated plasma plumes from the above substrates, the deposited material was sprinkled over water surface (by scratching the glass slide on which it was deposited). It was then

dispersed by an ultrasonic disperser and then the sample was caught on a carbon grid by fish-net method. The carbon grid was then dried and used as target in TEM. The TEM images of ablated material deposited on the glass plate showed morphological patterns (Fig. 7.2a) similar to the unirradiated nanoparticles (Fig. 7.1a). However, at pre-pulse intensities above 10^{10} W/cm^2 , the TEM images of the deposited sample showed the disintegrated nanoparticles (Fig. 7.2b). These studies revealed the range of pre-pulse laser intensities, which could be useful for maintaining the nanoparticles in the plasma plumes after laser ablation of nanoparticle-containing targets.

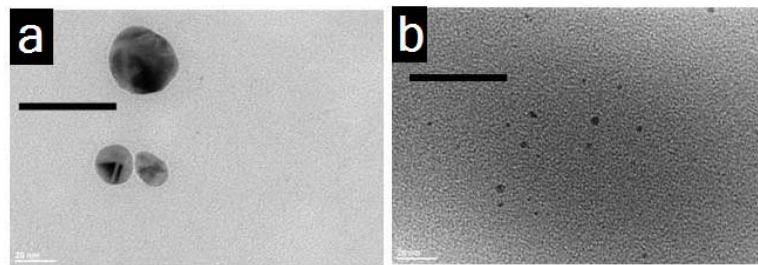


Fig. 7.2 TEM images of (a) deposited Ag nanoparticles obtained at low intensity of pre-pulse ($\sim 10^9 \text{ W/cm}^2$) and (b) deposited disintegrated Ag nanoparticles obtained at high intensity of pre-pulse ($\geq 1 \times 10^{10} \text{ W/cm}^2$). The size of black lines on the images is 50 nm

The targets for HHG from commercially available mixtures of fullerenes (98% of C_{60} and 2% of C_{70} powder, from Alfa Aesar) were made by two methods. In the first method, similar to the metal nanoparticles, the C_{60} powder was glued on the glass substrates using fast drying vacuum compatible glue. In second method, the C_{60} powder was mixed with PMMA. The ratio of C_{60} :PMMA was kept at $\sim 50:50$ weight parts. After dissolving the two components in the solution, the suspension was poured on the glass slides and dried in vacuum oven at 70°C . By this method, a homogeneous C_{60} -polymer composite film of thickness $\sim 1 \text{ mm}$ was obtained.

Figure 7.3a shows the TEM image of the edge of a C_{60} aggregated cluster powder. At some places, a regular spacing of the lattice planes was observed to be 0.6 and 0.8 nm for the C_{60} clusters, which is consistent with the lattice spacing of these face-

centred cubic structures [16]. The crystalline state of the fullerenes was verified by Fourier transform performed on TEM image (see the inset in Fig. 7.3a). Due to random position of the C_{60} powder in the grid, different electron diffraction patterns were observed from the same material. Analogous features remained in the case of the TEM of deposited debris of the fullerene powder after laser ablation at moderate intensities of the heating pre-pulse radiation ($\leq 7 \times 10^9 \text{ W/cm}^2$).

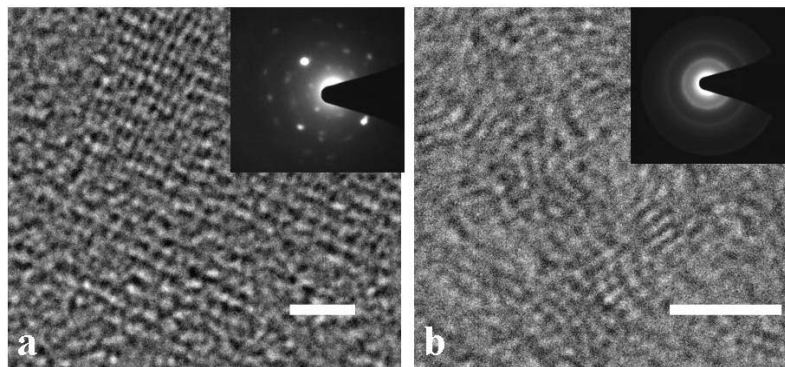


Fig. 7.3 (a) TEM image of C_{60} powder agglomerate before the deposition; (b) TEM image of deposited debris of C_{60} after strong excitation ($I = 1 \times 10^{10} \text{ W/cm}^2$) of fullerene-containing target. The scale lengths on the images correspond to 2 nm. In the insets, the Fourier transform patterns of the C_{60} crystalline nano-powder and debris are shown.

Another pattern of TEM of the debris of ablated fullerene powder appeared at the pre-pulse intensities above $1 \times 10^{10} \text{ W/cm}^2$. In that case, we observed different spacing of the lattice planes created on the surface of substrates and grids after laser ablation (Fig. 7.3b). The regular spacing of these lattice planes was 0.36 nm, which is close to the inter-planar lattice spacing of 0.34 nm for graphitic layers. TEM image presented in Fig. 7.3b pointed to the microstructure typical of carbon black: an intermediate structure between amorphous and fully graphitized carbon. The corresponding Fourier transform pattern also revealed a drastic difference with crystalline structure of the studied C_{60} samples (Fig. 7.3a). These studies also revealed the range of pre-pulse intensities, which could be useful for maintaining the fullerenes in the laser plumes after laser ablation of C_{60} -containing targets.

7.2. HHG from plasma plume containing nanoparticles / fullerenes

In this Section, we will discuss the HHG from plasma plumes containing various metal nanoparticles. The nanoparticles containing-plasma plumes were generated either by ablating the nanoparticles containing substrate or by nanoparticles generated *in situ* during the interaction of pre-pulse with metal surfaces.

7.2.1. HHG from plasma plumes of nanoparticle targets

Plasma plume was created from various substrates coated with nanoparticles of different materials as well as of different shapes using the experimental setup shown in Fig 2.8. For comparison with HHG from plasma produced from bulk materials, experiments were also done using silver and indium targets. The pre-pulse intensity and femtosecond laser pulse intensity were kept to be $\sim 10^9$ W/cm² and $\sim 10^{15}$ W/cm² respectively. It was observed that the harmonics generated from nanoparticles-containing plasma plumes were very intense in relatively lower orders, with a cut-off order of $\sim 27^{\text{th}}$ harmonic. Hence the MCP-CCD assembly in the XUV spectrograph was positioned to detect the lower order harmonics. Fig. 7.4 shows the harmonic spectrum from plasma plumes produced from substrates coated with Ag nanoparticles (triangular shaped nanoparticles mixed in PVA and dried in oven) and bulk silver. Harmonics in the range of 9th H to 19th H (governed by geometry of detector) are seen in Fig. 7.4. A typical HHG spectrum from silver nanoparticles is compared with the harmonic emission from plasma plume produced from bulk silver in Fig. 7.4. For better visibility, the intensity of HHG from bulk silver case is multiplied by 10. It can be clearly seen that harmonics (9th H to 19th H) from Ag nanoparticles plume are very strong compared to the corresponding harmonics from bulk silver. For example, the 9th harmonic from Ag nanoparticles is

~200 times stronger than that from bulk silver [15], whereas the average intensity enhancement in the range of 9th to 17th H order was ~25. This is an important observation which shows that materials in their nanoparticles form give much higher harmonic intensity compared to that in the bulk form. This implies that nano-size plays a crucial role in harmonic enhancement.

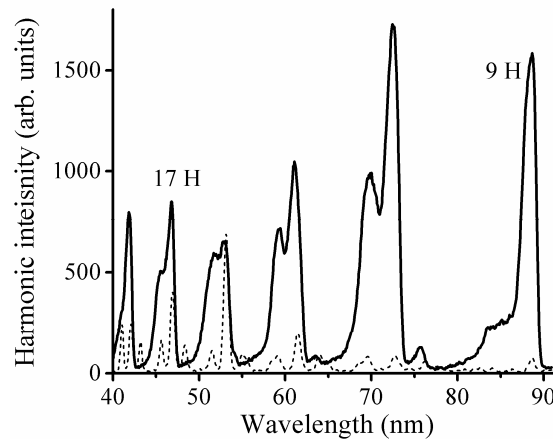


Fig. 7.4 Typical HHG spectra from silver nanoparticles (solid line) and bulk silver target (dashed line). The intensity of HHG spectrum from bulk Ag target is 10× multiplied for better visibility.

A comparison of HHG from Ag nanoparticles targets formed by different methods of preparation is shown in Fig. 7.5. The motivation for this study was to see if the matrix holding the nanoparticles on the substrate plays any significant role in governing the harmonic intensity. It can be seen from Fig. 7.5 that the intensity of harmonics is a little larger for the target prepared in PVA solution and dried in oven. This small increase in harmonic intensity is perhaps due to larger density of nanoparticles. Hence, silver nanoparticles containing targets prepared by this method were used in rest of the studies. It was observed that due to surface irregularities, the HHG intensity changes with the choice of target position for the formation of plasma plume. This effect was most prominent in the targets prepared by mixing nanoparticles with glue. Moreover, the HHG from these targets was least stable. It may be noted that the matrix (PVA or glue) without nanoparticles did not produce any significant

harmonics. This indicated that the job of the matrix is to get evaporated at low intensity of the pre-pulse, to release the nanoparticles which then interact with the main pulse and produce strong harmonics.

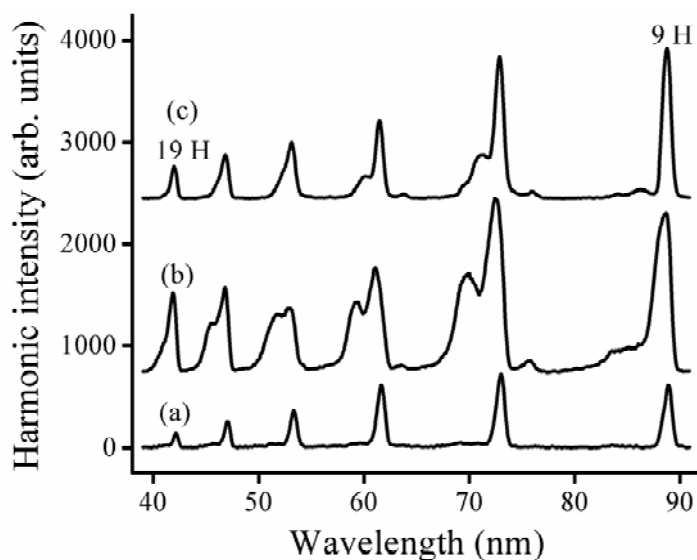


Fig. 7.5 Comparison of HHG yield from silver nanoparticles prepared in (a) PVA and dried naturally, (b) PVA and dried in oven, and (c) prepared by mixing nanoparticles with glue. The harmonic intensity from the nanoparticle target prepared in PVA and dried in oven is maximum. The spectra (b, c) are shifted up for visual clarity.

A comparison of relative intensity of HHG in various bulk and nanoparticles targets was also made, which is shown in Fig. 7.6. It can be seen that HHG intensity for bulk Ag and In is much smaller compared with nanoparticles targets (for low-order harmonics), except for resonantly enhanced 13th H of indium. Relative intensity and cut-off of HHG from various nanoparticles targets (Ag, SrTiO₃, and Au) were quite similar. This indicates that unlike in bulk targets, the material dependent effects in nanostructured targets are subdued.

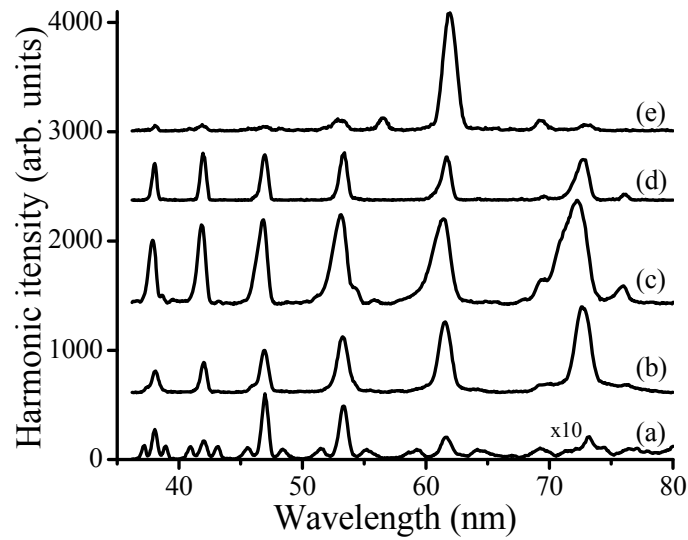


Fig. 7.6 Comparison of relative intensities of harmonics for (a) bulk Ag, (b) Ag nanoparticles, (c) SrTiO₃ nanoparticles, (d) Au nanoparticles, and (e) bulk In. The intensity of bulk Ag harmonics is multiplied by 10 for better visibility. The intensity of harmonics from nanoparticles is of the order of the enhanced 13th harmonic from indium plasma. The spectra are sequentially shifted up for visual clarity

7.2.2. HHG from plasma plumes of fullerene targets

Next, we present the results on harmonic generation from plasma plume containing fullerenes [17]. Figure 7.7a presents a typical HHG spectrum from plasma plume containing fullerenes at the same pre-pulse and main fs laser pulse intensities as in Section 7.2.1. Strong harmonics in the range 9th–17th H are observed. The intensities of these harmonics may be compared with the harmonic emission from plasma plume of indium (shown in Fig. 7.7b) produced under identical laser irradiation conditions. It is observed that the intensity of harmonics in the range of 9th–17th harmonic order from C₆₀ plumes is comparable to the intensity of 13th harmonic from the indium plume. As presented earlier in Fig. 7.6, the intensity of 13th H from indium plume is comparable to that from plasma plumes containing silver nanoparticles. These observations indicate that the HHG from plasma plume containing fullerenes is as strong as that from plasma plume containing metal nanoparticles. The physical explanation for high intensity

harmonic generation from fullerenes / nanoparticles compared to the bulk targets is presented in Section 7.4. Further, it may be noted here that the size and composition of these two types of nanostructures is quite different. Fullerenes are made from non-metal element carbon and other nanoparticles are made from metallic elements. The size of fullerenes is also quite small (~ 0.7 nm) compared to the metal nanoparticles (~ 10 nm). This observation indicates that in nanostructured targets in addition to the suppression of material specific properties, the dependence on size is also suppressed. It is required to explore this observation further by experimenting with nanoparticles of different materials and sizes.

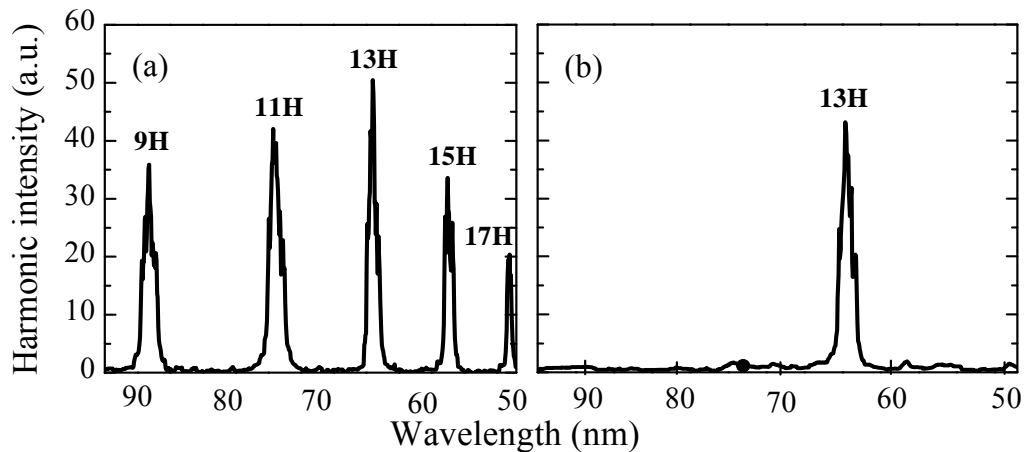


Fig. 7.7 Comparison of harmonic intensity in the case of (a) fullerene plasma and (b) In plasma.

7.2.3. HHG stability from nanostructured targets

The stability of HHG from silver nanoparticles has been studied. The variation of harmonic intensity with laser shots on the same place of nanoparticles-containing target is shown in Fig. 7.8. It can be seen that there is no significant fall in the intensity of the HHG up to ~ 40 laser shots. The stability of HHG process is greatly improved in the present study compared to the previous reports on harmonic generation using ablated nanoparticles [18]. Special target fabrication techniques described in previous Section

enable one to make thicker coating of nanoparticles on the substrate, resulted in increased stability of the HHG from silver nanoparticle targets. Intensity of the laser pre-pulse is also a factor concerning the stable harmonic generation from these targets. It was observed that when the pre-pulse intensity was increased to 3×10^9 W/cm² the harmonic intensity was increased due to higher concentration of ablated particles in the plasma plume, but increased depletion of the material from the coated substrate resulted in poor stability of HHG.

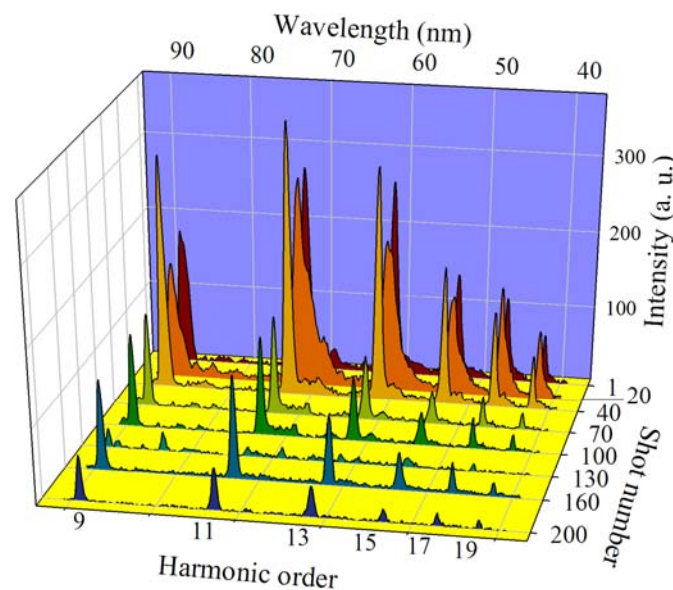


Fig. 7.8 Variation of the harmonic intensity with number of laser shots in the case of nanoparticle-containing target. The target is irradiated at same place.

7.2.4. Physical understanding of experimental results

High order harmonic generation has been understood in terms of so called three-step model [19-20]. The details of the HHG process in terms of this model are given in Chapter 1. One crucial step in this model is that the ionized electron has to recombine with the parent atom / ion. The increased efficiency of HHG from nanoparticles containing plasma plume targets can be understood in terms of enhanced recombination cross-section of the accelerated electron. This is discussed in the following paragraphs.

The average excursion length of the tunnelled electron before recombination is

$$\langle x \rangle = \frac{eE}{2m\omega^2} \dots\dots\dots(7.1)$$

where e and m are charge and mass of the electron and E and ω are electric field and frequency of the laser respectively. For our experimental conditions of main laser pulse intensity $\sim 10^{15}$ W/cm², the average electron excursion length is ~ 1.5 nm. This may be compared with average intra-atomic distance inside nanoparticles. Taking a near solid density of $\sim 6 \times 10^{22}$ particles/cc, the average particle distance (d) comes to be ~ 0.2 nm, which is much smaller than the average electron excursion length. From this, it follows that the electrons tunnelled inside the nanoparticle can not contribute towards HHG. Thus HHG comes predominantly from surface of the nanoparticle.

Further, the recombination probability of electron with atoms on the surface of nanoparticle would be governed by the size of electron wave-packet in comparison to intra-particle distance. For example, the kinetic energy of electron leading to emission of a 15th H photon from recombination with an Ag⁺ ion (ionization potential $I_p = 21.45$ eV) would be $h\nu - I_p = 1.82$ eV. The de-Broglie wavelength $\left(\lambda_e = \frac{h}{p} \right)$ for this electron is 0.9 nm which is much larger than the intra-particle distance of ~ 0.2 nm. The effective increase in recombination probability leads to high intensity of the harmonics from nanoparticles. This picture is also consistent with a fast decrease in the harmonic intensity beyond 29th order observed in our study as the de-Broglie wavelength (~ 0.25 nm) would become comparable to the intra-particle separation in the nanoparticle.

7.3. HHG from silver nanoparticles produced *in situ* during laser-matter interaction

It has been reported that the nanoparticles can be generated by the interaction of sub-nanosecond pulses with bulk metals at an intensity of $\sim 10^{13}$ W/cm² [21-22]. From the discussion in Chapter 3, it is clear that the laser intensity for the preparation of optimal plasma plumes for HHG is much different. In the latter case, the plasma plumes are prepared using the low-intensity pre-pulse ($I_{pp} \sim 10^9$ W/cm²) and predominantly consists of neutral and singly charged ions. Here, the free electron density inside the plasma plume is small to keep the phase mismatch between laser pulse and harmonic radiation, low. However, in the case of nanoparticles-containing plasma, the adverse phase mismatch effects of higher electron density may be compensated by the greater nonlinear response of the nanoparticles. This motivated us to explore the HHG from nanoparticles produced *in situ* in plasma plumes during their production with sub-nanosecond laser pulses.

The interaction of the pre-pulse (pulse duration $\tau \sim 200$ picosecond) with the silver target at intensity of $\sim 10^{13}$ W/cm² (which is also the maximum focusable intensity of the pre-pulse) generated the nanoparticles. The morphology of the ablated material was studied by the atomic force microscopy (AFM) of the deposited sample on a glass substrate kept at ~ 1 cm from the target surface. Fig. 7.9 shows the AFM images of the deposition, taken at two different intensities of the pre-pulse. Fig. 7.9a shows the AFM image of deposition at $\sim 10^{10}$ W/cm² (the optimal intensity for HHG from the plasma plumes containing monomers), no significant amount of nanoparticles is seen in the AFM. Fig 7.9b shows the AFM of deposition at $\sim 10^{13}$ W/cm². One can see good amount of nanoparticles present in the deposition. The mean size of nanoparticles was

30 nm. The sharp images of nanoparticles indicate that concentration of the deposited atomic layer containing single particles is insignificant.

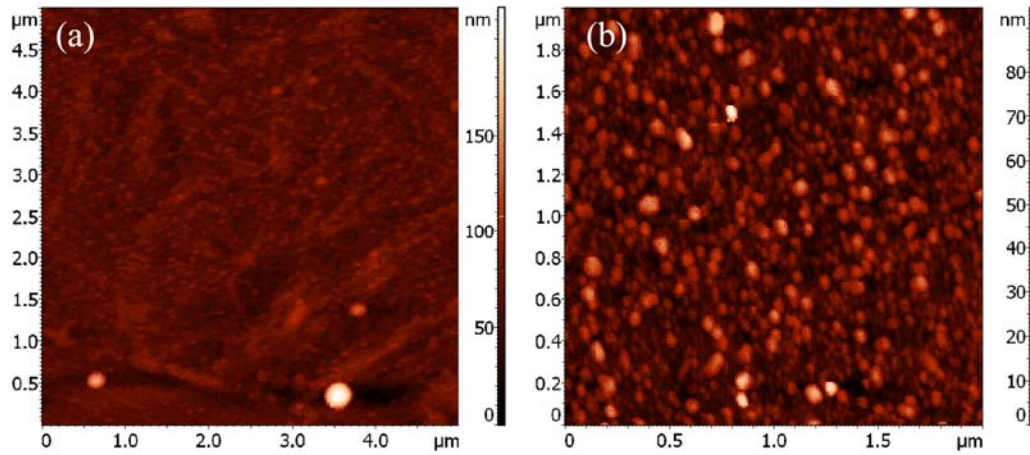


Fig. 7.9 AFM images of the silver deposition in the case of : a) weak ($I \sim 10^{10} \text{ W/cm}^2$) excitation, and b) strong ($I \sim 10^{13} \text{ W/cm}^2$) excitation of targets. The horizontal and vertical axes show the scan sizes of the two images, whereas the vertical bar at right shows the colour coding for different sized nanoparticles.

The experimental arrangement for HHG was discussed in chapter 2. The harmonic spectrum is detected by a microchannel plate (MCP). Usually at low intensity, the pre-pulse generates a very small amount of plasma emission which need not be filtered. In the present case, when the pre-pulse interact with the target at $\sim 10^{13} \text{ W/cm}^2$, the plasma emission generated from the interaction of high intensity pre-pulse with target surface was much stronger than the intensity of HHG itself. In order to filter the contribution of the plasma light, the MCP detector was gated by a short gate pulse of 15 ns.

The high order harmonics were generated from the interaction of the *in situ* produced nanoparticles with intense ultrashort laser pulse (main pulse) is shown in Fig. 7.10a [23]. The spectrum of HHG from *in situ* produced nanoparticles is compared with the HHG spectrum from bulk Ag plumes (Fig. 7.6a), and 10 nm (preformed) Ag nanoparticles (Fig. 7.6b). The intensity of HHG from the three targets is normalized and the spectra are shifted vertically for comparison of the spectral features. The low order

harmonics from bulk silver plume are also multiplied by a factor of 5 to increase their visibility. It is clearly seen from Fig. 7.10c that the intensity of 9th-15th harmonics is less compared to the 17th harmonic in the case of HHG from plasma plumes of bulk silver. On the other hand, the intensity of harmonics from the plasma plumes created on the coated silver nanoparticles decreases slowly from 9th harmonic to 17th harmonic (Fig. 7.10b). Comparison of the HHG spectral characteristics of Fig. 7.10a for the *in situ* produced nanoparticles with that from bulk silver and silver nanoparticles indicates that HHG in the *in situ* case is from Ag nanoparticles rather than from Ag mono-particles.

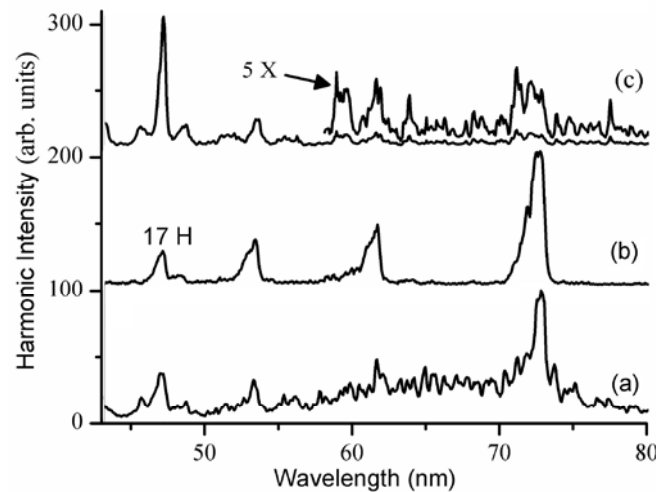


Fig. 7.10 Comparison of the HHG spectra from a) silver mono-particles, b) *in-situ* produced silver nanoparticles, and c) from coated silver nanoparticles. The intensity of HHG emission is normalized for comparison. The curves b and c are shifted vertically for visual clarity.

It was observed that as the intensity of pre-pulse on the bulk silver surface was increased from $\sim 10^9$ W/cm² to $\sim 10^{12}$ W/cm², the HHG spectrum gradually reduced and completely vanished. However, at a still higher intensity of $\sim 10^{13}$ W/cm², harmonics suddenly reappear, as the pre-pulse was focussed at tight focussing conditions. The intensity of harmonics generated from *in situ* produced nanoparticles is similar to the intensity of harmonics generated from bulk silver plume and ~ 10 times smaller than the harmonics generated from plasma plumes of silver nanoparticles coated targets. However,

since the size of the interaction medium for *in-situ* produced nanoparticles was considerably smaller ($\sim 40 \mu\text{m}$) compared to the size of the interaction medium for bulk silver targets or targets coated with silver nanoparticles ($\sim 600 \mu\text{m}$), the efficiency of HHG process in *in situ* produced nanoparticles is much higher compared to that of bulk silver targets and is comparable to that with silver nanoparticle coated targets. It has been shown in our earlier study that the intensity of harmonics increases with the length of plasma plume [14]. Hence creating longer plasma plume by using higher energy pre-pulse may increase the intensity of HHG from *in situ* produced nanoparticles, and make it comparable to or higher than the intensity of HHG from silver nanoparticles coated targets.

Bibliography

1. C. Winterfeldt, and G. Gerber, “Optimal control of high-harmonic generation”, *Rev. Mod. Phys.* **80**, 117 (2008).
2. U. Teubner and P. Gibbon “High-order harmonics from laser-irradiated plasma surfaces”, *Rev. Mod. Phys.* **81**, 445 (2009).
3. B. Dromey *et al*, “High harmonic generation in the relativistic limit”, *Nature Phys.* **2**, 456 (2006).
4. S. Gordienko, A. Pukhov, O. Shorokhov and T. Baeva “Coherent focussing of high harmonics: A new way towards the extreme intensities”, *Phys. Rev. Lett.* **94**, 103903 (2005).
5. C. Liu, Y. Zheng, Z. Zeng, R. Li, and Z. Xu, “Isolated attosecond pulse emission in the plateau region of high-order harmonics driven by a 7-fs 800-nm laser field”, *Phys. Rev. A* **79**, 043826 (2009)

6. C. Jin, A. T. Le and C. D. Lin, "Isolated attosecond pulse emission in the plateau region of high-order harmonics driven by a 7-fs 800-nm laser field", *Phys. Rev. A* **79**, 053413 (2009).
7. S. Ramakrishna, and T. Seideman, "High-order harmonic generation as a probe of rotational dynamics" *Phys. Rev. A* **77**, 53411 (2008).
8. T. Kanai, E. Takahashi, Y. Nabekawa, and K. Midorikawa, "Observing molecular structures by using high-order harmonic generation in mixed gases" *Phys. Rev. A* **77**, 41402 (2008).
9. A. Abdurrouf, and F. H. M. Faisal, "Theory of intense-field dynamic alignment and high-order harmonic generation from coherently rotating molecules and interpretation of intense-field ultrafast pump-probe experiments" *Phys. Rev. A* **79**, 23405 (2009).
10. R. A. Ganeev, P. A. Naik, H. Singhal, J. A. Chakera, P. D. Gupta, and H. Kuroda, "Tuning of the high-order harmonics generated from laser plasma plumes and solid surfaces by varying the laser spectrum, chirp, and focal position," *J. Opt. Soc. Am. B* **24**, 1138 (2007).
11. R. A. Ganeev, H. Singhal, P. A. Naik, U. Chakravarty, V. Arora, J. A. Chakera, R. A. Khan, M. Raghuramaiah, S. R. Kumbhare, R. P. Kushwaha, and P. D. Gupta, "Optimization of the high-order harmonics generated from silver plasma" *Appl. Phys. B* **87**, 243 (2007).
12. R. A. Ganeev, M. Suzuki, M. Baba, H. Kuroda, "Generation of strong coherent extreme ultraviolet radiation from the laser plasma produced on the surface of solid targets", *Appl. Phys. B* **81**, 1081 (2005).

13. R. A. Ganeev, H. Singhal, P. A. Naik, V. Arora, U. Chakravarty, J. A. Chakera, R. A. Khan, I. A. Kulagin, P. V. Redkin, M. Raghuramaiah, and P. D. Gupta, "Harmonic generation from indium-rich plasmas", *Phys. Rev. A* **74**, 063824 (2006).
14. H. Singhal, V. Arora, B. S. Rao, P. A. Naik, U. Chakravarty, R. A. Khan, and P. D. Gupta, "Dependence of high-order harmonic intensity on the length of preformed plasma plumes", *Phys. Rev. A* **79**, 023807 (2009).
15. H. Singhal, R. A. Ganeev, P. A. Naik, A. K. Srivastava, A. Singh, R. Chari, R. A. Khan, J. A. Chakera and P. D. Gupta, "Study of high-order harmonic generation from nanoparticles", *J. Phys. B* **43**, 025603 (2010).
16. W. Zhu, D. E. Miser, W. G. Chan, and M. R. Hajaligol, "Characterization of combustion fullerene soot, C₆₀ and mixed fullerene", *Carbon* **42**, 1463 (2004).
17. R. A. Ganeev, H. Singhal, P. A. Naik, J. A. Chakera, A. K. Srivastava, T. S. Dhami, M. P. Joshi, and P. D. Gupta, "Influence of C₆₀ morphology on high-order harmonic generation enhancement in fullerene-containing plasma" *J. Appl. Phys.* **106**, 103103 (2009).
18. R. A. Ganeev, M. Suzuki, M. Baba, M. Ichihara and H. Kuroda, "Low- and high-order nonlinear optical properties of BaTiO₃ and SrTiO₃ nanoparticles", *J. Opt. Soc. Am. B* **25**, 325 (2008).
19. P. B. Corkum, "Plasma perspective on strong field multiphoton ionization", *Phys. Rev. Lett.* **71**, 1994 (1993).

20. M. Lewenstein, Ph. Balcou, M. Yu. Ivanov, A. L'Huillier, and P. B. Corkum, "Theory of high-harmonic generation by low-frequency laser fields", *Phys. Rev. A* **49**, 2117 (1994).
21. R. A. Ganeev, U. Chakravarty, P. A. Naik, H. Srivastava, C. Mukherjee, M. K. Tiwari, R. V. Nandedkar, and P. D. Gupta, "Pulsed laser deposition of metal films and nanoparticles in vacuum using subnanosecond laser pulses", *Appl. Opt.* **46**, 1205 (2007).
22. S. Amoruso, G. Ausanio, R. Bruzzese, M. Vitiello, and X. Wang, "Femtosecond laser pulse irradiation of solid targets as a general route to nanoparticle formation in a vacuum," *Phys. Rev. B* **71**, 033406 (2005).
23. H. Singhal, R. A. Ganeev, P. A. Naik, J. A. Chakera, U. Chakravarty, H. S. Vora, A. K. Srivastava, C. Mukherjee, C. P. Navathe, S. K. Deb, and P.D. Gupta, "High order harmonic generation in plasma plume of *in situ* laser produced silver nanoparticles", *Phys. Rev. A* . **82**, 043821 (2010).

Chapter 8

Spectral broadening of the harmonic radiation

As discussed in Chapter 7, high order harmonics of higher intensity are produced using low excited plasma plumes containing metal nanoparticles and fullerenes in comparison to those from bulk targets [1]. This ultrashort duration (\sim fs) coherent XUV radiation can be used for ultrafast spectroscopic studies such as measurement of ultrafast photo-recombination cross sections [2], probing of rotational dynamics of molecules [3], and detection of molecular structure [4]. For such studies it is required that the harmonic wavelength should overlap with the wavelength of the atomic/ionic transition under consideration. Thus, tunability of the harmonic radiation is desired for the above applications. Partial tuning of harmonic wavelength can be accomplished by changing the spectrum [5] and chirp [6] of the femtosecond laser pulse. In this regard the generation of harmonics of large bandwidth would also be useful to facilitate easier overlap of the harmonic radiation with atomic/ionic transitions.

In this chapter, we present an experimental study on the generation of broadband high order harmonics through the use of larger bandwidth of pump laser pulse. The bandwidth of the laser was increased by a) self phase modulation (SPM) of the laser pulse by passing it through a glass plate and b) SPM of the laser pulse during its interaction with plasma plume containing nanoparticles. Section 8.1 describes the study on HHG from a spectrally broadened laser pulse during its passage through a 5 mm thick glass plate. In Section 8.2, we will describe our experimental study of generation of broadband harmonics from plasma plumes produced from nanostructured targets. In the latter case, the generation of broadband harmonics is explained from the broadening of

laser spectrum during the interaction of the femtosecond laser pulse with nanoparticles present in the plasma plume.

8.1. HHG using self-phase modulated laser pulse

High order harmonics were generated by spectrally broadened fs laser pulse. The experimental arrangement for HHG is explained in Chapter 2. The high order harmonics were generated by the interaction of fs laser pulse with preformed plasma plume. A 500 mm focal length lens was used to focus the fs pulse. The spectral broadening of the fs laser pulse was achieved by passing it through a 5 mm thick glass plate kept between the focussing lens and the plasma plume. The intensity of the laser pulse inside the glass plate was estimated to be $\sim 3 \times 10^{12}$ W/cm². The spectrum of the laser pulse with/without passing through the glass plate is shown in the Fig. 8.1. It is seen that the bandwidth (FWHM) of the laser spectrum increased from ~ 17 nm (normal pulse) to ~ 32 nm (phase modulated pulse) after its passage through the glass plate.

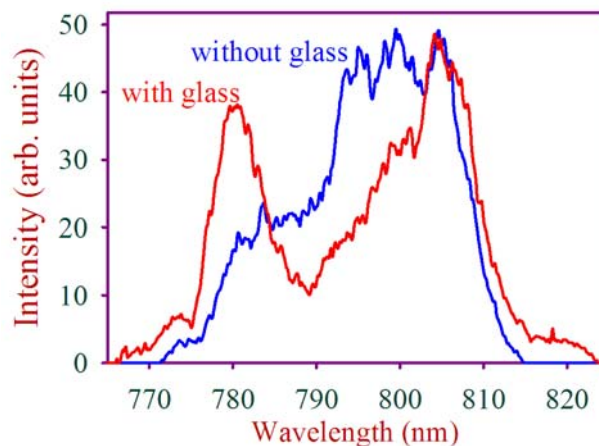


Fig. 8.1 Laser spectrum when no glass plate is inserted (blue) and when glass plate is inserted in the path of focussing laser pulse (red).

The harmonic spectrum was recorded from silver plasma plume for laser pulse with/without passage through the glass plate. The harmonic spectra are shown in Fig. 8.2. It is clearly seen that the spectral width of harmonics for the case of laser pulse passing

through the glass plate (Fig. 8.2b) is larger than that for the normal laser pulse (Fig. 8.2a). The inset in Fig 8.2 shows an expanded view of the 17th harmonic for the two cases. It is seen that the spectral width (FWHM) of the 17th harmonic increased from 0.4 nm to 0.7 nm for the case of laser pulse passing through the glass plate. It is further noted from the inset that the harmonic radiation is red shifted as compared to the harmonics from normal pulse. The observed increase in the bandwidth of the harmonic radiation (Fig. 8.2) is in nearly same proportion to that for the laser pulse.

The SPM of laser pulse results in its spectral broadening. This can be understood from the analysis of time varying laser field propagating through a nonlinear medium. The electric field of the laser can be expressed as

$$E = A(t) \exp(i(\omega_0 t + \phi)) \quad \dots\dots\dots (8.1)$$

where A(t) is the time envelope of the pulse. The frequency of the wave can be written as the time derivative of the exponent

$$\omega = \frac{d(\omega_0 t + \phi)}{dt} = \omega_0 + \frac{d\phi}{dt} \quad \dots\dots\dots (8.2)$$

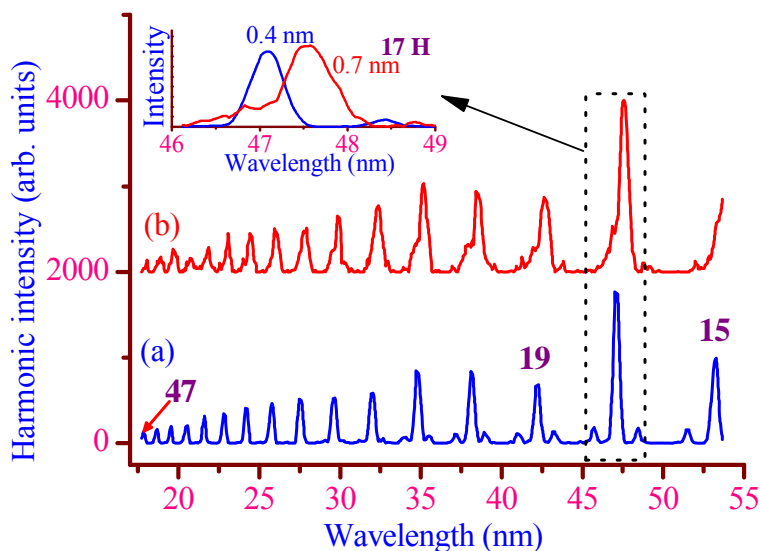


Fig. 8.2 Bandwidth comparison of HHG (a) from normal laser pulse and (b) from laser pulse after passage through glass plate. Inset shows the expanded view of 17th harmonic for the two cases.

From the above expression it can be noted that new frequencies are generated in a laser pulse with time varying phase. If this time dependence in the phase arises due to laser pulse itself, the phenomenon is known as *self phase modulation*. It is known that at high laser intensities, the refractive index of the medium becomes intensity dependent. The expression for refractive index can be written as

$$n = n_0 + n_2 I(t) \quad \dots\dots\dots (8.3)$$

where n_2 is the coefficient of nonlinear refractive index. The phase difference introduced in the laser pulse by a medium of length L , compared to the pulse passing through vacuum can be written as

$$\phi = \frac{2\pi}{\lambda} L - \frac{2\pi}{\lambda} (n_0 + n_2 I) L \quad \dots\dots\dots (8.4)$$

The time derivative of the Eq. 8.4 gives the additional frequencies generated in the laser pulse given by the following equation

$$\delta\omega = \frac{d\phi}{dt} = -2\pi n_2 \frac{L}{\lambda} \frac{dI}{dt} \quad \dots\dots\dots (8.5)$$

It should be pointed out here that the frequency shift in the laser pulse is visible only if the phase derivative is of the order of the laser frequency. In the case of ultrafast laser pulses, the intensity is a fast varying function of time hence new frequencies are generated in the laser pulse. One can see that for positive n_2 the leading edge of the pulse has additional red frequencies whereas the trailing portion of the pulse will have additional blue frequencies, thereby resulting in the generation of a positively chirped spectrally broadened laser pulse.

The laser spectral broadening can be estimated using Eq. 8.5. The non-linear refractive index n_2 for BK7 glass is $3.4 \times 10^{-16} \text{ cm}^2/\text{W}$ [7]. Taking a typical value of dI/dt of $\sim 10^{25} \text{ W cm}^{-2} \text{ sec}^{-1}$ the increase in bandwidth $\delta\omega$ turns out to be $\sim 100 \text{ THz}$. When this

is added to initial bandwidth 50 THz, the spectral bandwidth comes to be ~ 50 nm, which is on higher side to the observed value.

As explained in the above paragraphs, the laser pulse acquires a positive chirp on passage through a medium with positive nonlinear refractive index (n_2). Thus the high order harmonics produced from such laser pulses are also shifted towards red [6].

8.2. Harmonic generation from plasma plumes containing nanoparticles

In this Section we will discuss the broadband harmonic generation using nanostructured targets. The preparation and characterization of these targets have been discussed in Chapter 7. The nanostructured target used in this study was made by mixing triangular silver nanoparticles in a PVA-matrix and pasted on a glass substrate. The average particle size of triangular nanoparticles was ~ 50 nm. The plasma plume was created by focussing a laser pre-pulse of energy ~ 20 mJ and pulse duration ~ 200 ps at a spot size in the range of ~ 600 μm . The delay between the two pulses was kept at ~ 60 ns.

The harmonic yield was optimized by varying the different laser and plasma parameters. During these optimizations, it was observed that the bandwidth of harmonics could be increased by increasing the femtosecond laser intensity inside the plasma plume. Fig. 8.3 shows harmonic emission spectra generated at two laser intensities of $\sim 1.8 \times 10^{15}$ W/cm^2 and $\sim 3.5 \times 10^{15}$ W/cm^2 . The spectra are normalized and shifted vertically for better visual inspection. It can be seen that the spectral width of HHG was larger for higher laser intensity. For example, the spectral width of the 11th H is increased from ~ 1 nm to ~ 5 nm. It can also be seen from Fig. 8.3 that the spectral broadening of the harmonics occurs towards the blue side. These observations may result if the harmonics were produced from a spectrally blue-broadened laser pulse. This may indeed happen through self-phase modulation (SPM) of the laser pulse during its interaction with nanoparticles

in the plasma plume [8]. The phenomenon was observed in our earlier study of laser scattering from plasma produced in argon gas clusters [8]. In this experiment we had studied the interaction of Ar clusters with 25 picoseconds (ps) Nd:glass laser pulses. It

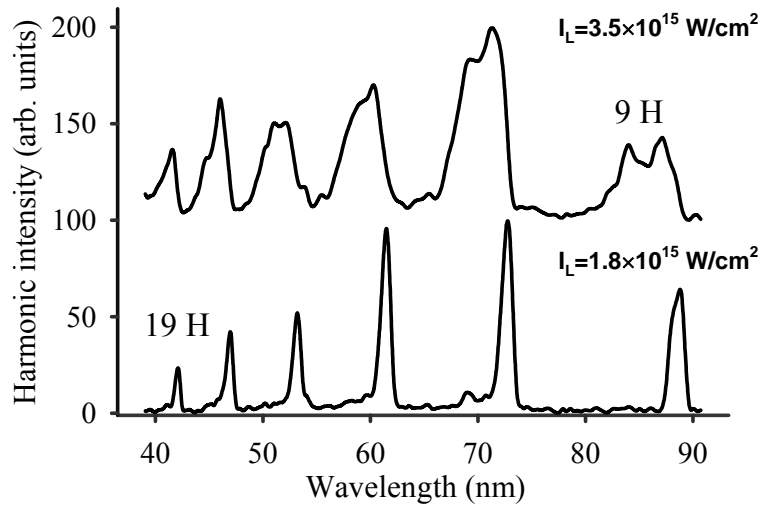


Fig. 8.3 Broadening of harmonic spectrum with increase of laser intensity. The harmonic spectrum for higher laser intensity has been shifted up for the ease of visual inspection.

was observed that the spectrum of the scattered radiation was blue broadened, which could be explained from self phase modulation of the laser pulse during its interaction with clusters at resonance phase. When an intense laser pulse interacts with a cluster / nanoparticle, the latter gets ionized and heated by the foot of the laser pulse. This heated nanoparticle behaves like a small spherical plasma of dipole moment (\vec{p})

$$\vec{p} = r^3 \frac{\epsilon - 1}{\epsilon + 2} \vec{E} = \gamma \vec{E} \quad \dots\dots\dots (8.6)$$

where r is the sphere radius, \vec{E} is the external laser field, ϵ is dielectric function of the plasma inside the nanoparticle and γ is the polarizability of the nanoparticle. In the simple Drude model [9], the dielectric function at an electromagnetic field frequency ω_L may be expressed as

$$\epsilon = 1 - \frac{\omega_p^2}{\omega_L(\omega_L + i\nu)} \quad \dots\dots\dots (8.7)$$

where ω_p is the plasma frequency ($\omega_p^2 = n_e e^2 / \epsilon_0 m$, n_e being the electron density and ν is the collision frequency). In the early stage of laser interaction with nanoparticle sphere, the electron density and temperature inside the nanoparticle increases due to heating and ionization. At this point the electron density inside the nanoparticle could be more or equal to solid density. Thereafter the electron density starts decreasing due to hydrodynamic expansion of heated nanoparticle. It must be noted here that despite high density (more than the critical density) the laser field penetrates inside the nanoparticle as evanescent field (due to its small size). The electric field inside the nanoparticle can be written as

$$E_{in} = \frac{3\epsilon}{\epsilon + 2} E_{out} \quad \dots\dots\dots (8.8)$$

From Eq. 8.7 one may note that for very high value of electron density the nanoparticle permittivity (ϵ) has a large negative value so that the laser field inside the nanoparticle is shielded. However during expansion of the heated nanoparticle, when n_e becomes equal to $3n_{cr}$ (where n_{cr} is the *plasma critical density* given by $n_{cr} = \omega_L^2 m \epsilon_0 / e^2$), $|\epsilon+2|$ goes through a minimum. At this condition of resonance, the field inside the nanoparticle is greatly enhanced with respect to the external surrounding field [10], and the polarizability of the nanoparticle undergoes a large change. This produces a rapid change in refractive index of the medium resulting in spectral broadening of the laser pulse through self phase modulation. The increase in bandwidth is given by [8]

$$\delta\omega = \frac{d\phi}{dt} = -\frac{2\pi}{\lambda} \frac{N}{2\epsilon_0} \frac{d\gamma}{dt} L \quad \dots\dots\dots (8.9)$$

where N is the number of nanoparticles per unit volume, λ is the laser wavelength, ϵ_0 is the permittivity of the free space and L is the length of the plasma medium. While the magnitude of spectral shift is governed by the rate of change of nanoparticle polarizability, its nature, *i.e.* blue or red shift, depends on whether the polarizability is

decreasing or increasing with time respectively. As explained in reference 8, $d\gamma/dt$ is negative as the nanoparticle passes through the resonance phase, so that the blue frequencies are generated. The spectral blue-broadening in the laser pulse results in spectral broadening in the generated harmonic radiation.

Next, the variation of bandwidth of harmonic radiation with the order of harmonic is shown in Fig. 8.4. It is seen that the bandwidth of harmonics decreases linearly with the harmonic order. Using the simple relation between the wavelength and frequency spread

($\Delta\omega = \frac{c}{\lambda^2} \Delta\lambda$), the wavelength spread of the harmonic radiation can be written as

$$\Delta\lambda_H = \frac{\Delta\omega_H}{\Delta\omega_L} \frac{\Delta\lambda_L}{q^2} \dots\dots\dots (8.10)$$

where the subscript L stands for laser and H stands for harmonics. If all the frequency components in the laser pulse are equally converted into their harmonics, $\Delta\omega_H$

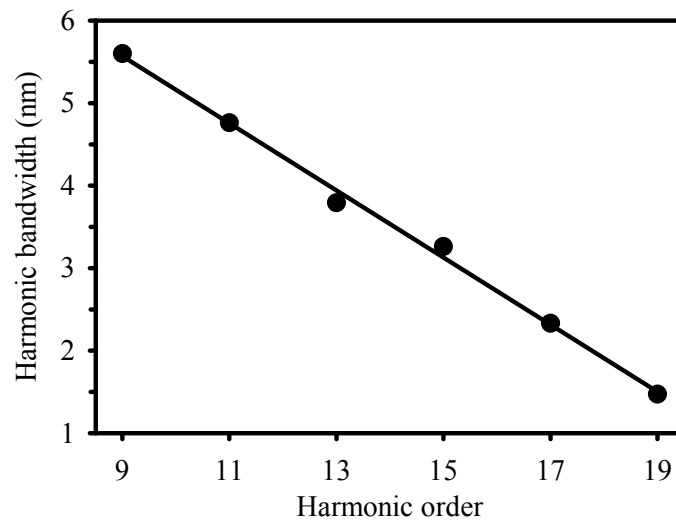


Fig. 8.4 Variation in harmonic bandwidth with harmonic order

will be q times larger than $\Delta\omega_L$. In this case, the harmonic bandwidth will decrease linearly with the harmonic order as observed experimentally. This situation is in contrast with the harmonic generation in non-linear crystals where the harmonic bandwidth is experimentally observed to decrease with the harmonic order faster than a linear decrease.

Bibliography

1. H. Singhal, R. A. Ganeev, P. A. Naik, A. K. Srivastava, A. Singh, R. Chari, R. A. Khan, J A Chakera and P D Gupta, "Study of high-order harmonic generation from nanoparticles", *J. Phys. B* **43**, 025603 (2010).
2. C. Jin, A. T. Le and C. D. Lin "Isolated attosecond pulse emission in the plateau region of high-order harmonics driven by a 7-fs 800-nm laser field", *Phys. Rev. A* **79**, 053413 (2009).
3. S. Ramakrishna, and T. Seideman, "High-order harmonic generation as a probe of rotational dynamics" *Phys. Rev. A* **77**, 53411 (2008).
4. T. Kanai, E. Takahashi, Y. Nabekawa, and K. Midorikawa, "Observing molecular structures by using high-order harmonic generation in mixed gases" *Phys. Rev. A* **77**, 41402 (2008).
5. R. A. Ganeev, M. Suzuki, M. Baba, H. Kuroda, "Generation of strong coherent extreme ultraviolet radiation from the laser plasma produced on the surface of solid targets", *Appl. Phys. B* **81**, 1081 (2005).
6. R. A. Ganeev, P. A. Naik, H. Singhal, J. A. Chakera, P. D. Gupta, and H. Kuroda, "Tuning of the high-order harmonics generated from laser plasma plumes and solid surfaces by varying the laser spectrum, chirp, and focal position," *J. Opt. Soc. Am. B* **24**, 1138 (2007).
7. R. W. Boyd, "*Nonlinear Optics 3rd edition*", Academic Press, USA, p 212 (2008).
8. H. Singhal, V. Arora, P. A. Naik, and P. D. Gupta "Spectral blue shifts in laser light scattered from argon-gas-cluster plasmas", *Phys. Rev. A* **72**, 043201 (2005).

9. W. L. Kruer, "*The physics of laser plasma interaction*", Addison-Wesley Publishing Company, UK, p 12 (1988).
10. J. Zweiback, T. Ditmire and M. D. Perry, "Resonance in scattering and absorption from large noble gas clusters", *Opt. Expr.* **6**, 236 (2000).

Chapter 9

HHG using two-colour laser pulses

In the previous chapters, we have presented an experimental study on HHG from the interaction of ultrashort fs laser pulses with low excited preformed plasma plumes of bulk materials and nanostructured targets [1-3]. Only odd harmonic orders were observed in these studies. As discussed in Chapter 1, even harmonic orders are not generated due to inversion symmetry of the HHG process. However, the inversion symmetry can be broken by simultaneous use of two or more laser pulses of different frequencies. For instance, it was observed in earlier studies that use of two-colour laser pulses for HHG resulted in the generation of even and odd harmonics of comparable intensities [4]. In these experiments, second harmonic of the driving fs laser beam was used as the second laser pulse and its intensity was about 20% of the fundamental laser pulse. In contrast to this situation, in our experiments using two-colour laser pulses, it was observed that a second harmonic beam of even 2% intensity of the fundamental laser beam was sufficient to break the inversion symmetry, resulting in generation of both even and odd harmonics. It was also observed that intensity of second harmonic pulse relative to the fundamental laser pulse affects the relative intensity of odd and even harmonics [5].

In this chapter, we present an experimental study of HHG using two-colour laser pulses comprising of fundamental Ti:sapphire laser pulse (800 nm) and its second harmonic (SH). We first present the particle trajectory analysis which demonstrates the generation of both even and odd harmonics, through the use of two-colour laser pulses in Section 9.1. Section 9.2 gives a brief description of experimental arrangement. The experimental studies are put in two categories viz. 1) weak two-colour laser irradiation in

which the second harmonic laser pulse intensity was $\sim 2\%$ of the fundamental laser intensity, and 2) strong two-colour laser irradiation where the second harmonic laser pulse intensity was $\sim 15\%$ of the fundamental laser pulse. The results of HHG using weak two-colour pulses are presented in Section 9.3. Both, even and odd harmonics with similar intensities were observed [5]. Different experimental investigations such as effect of laser polarization on HHG, resonance enhancement in both odd and even harmonic orders, HHG from nanostructured targets are presented in this section. In section 9.4, results of HHG from strong two-colour pulses are described. In this case it was observed that odd harmonics disappeared near the cut-off. Disappearance of odd harmonics has been predicted theoretically [6]. The present study [7] provides an experimental demonstration of this feature.

9.1. Even and odd harmonic generation through symmetry breaking

When one uses only a single colour laser pulse to generate high order harmonics, only odd harmonic orders are produced due to inversion symmetry of the HHG process. In Chapter 1 we have discussed the process of HHG from the three-step model [8, 9]. According to this model, when an atom interacts with a high intensity laser pulse, the atomic potential well is distorted by laser electric field and the bound electron can tunnel from the parent atom/ion. This electron then accelerates in the laser field. Depending on the laser phase at the instance of tunnelling, this electron may come back to the parent atom/ion. Its kinetic energy at the instance of collision with the parent atom/ion (e_{KE}) also depends on the tunnelling phase (ϕ). The colliding electron may undergo recombination or get scattered. Upon recombination, an XUV photon is generated of energy equal to the sum of ionization potential (I_p) of the atom and the electron energy e_{KE} . Thus, the XUV photon is phase locked with the laser pulse. It was discussed in

Section 1.2 that for a cosine laser field (wherein the field amplitude is maximum at 0 phase) the electrons which had tunnelled between phase $(0, \pi/2)$ and $(\pi, 3\pi/2)$ can return to the parent ion. It is worth noting here that during this process there are two values of ϕ_t in each half of laser field for which the kinetic energy of re-colliding electron is same. Interestingly, the electron which had tunnelled earlier would return to the parent ion later than the electron which had tunnelled later. As mentioned earlier in Chapter 1, the trajectories of these two electrons are known as *long* and *short trajectories* respectively, and are depicted as (1) and (2) in Fig. 1.1 (b). All the harmonic orders except for the cut-off harmonic order can be generated by either of the two electron trajectories. For the cut-off order, the two trajectories merge into one. One may note that an electron tunnelling out between phases $(\pi/2, \pi)$ and $(3\pi/2, 2\pi)$ will follow the trajectory (3) of the Fig. 1.1(b) and it will not return to the parent ion.

We now examine the coherent addition of harmonic photons generated in two halves of the laser pulse. Variation of e_{KE} with ϕ_t for single colour laser pulse is shown in Fig. 9.1a. Since this variation in the two halves is identical, the difference in tunnelling phase of electrons resulting in generation of same energy photons (one in each half) will be π . The corresponding phase difference in the generated XUV photons of frequency q time laser frequency will be $(q+1)\pi$ where the numeral 1 appearing in the bracket is due to initial phase difference. It follows that the XUV photons will add constructively when q is an odd integer, resulting in production of only odd harmonic orders.

The symmetry of the HHG process can be broken by introducing a very small amount of the second harmonic radiation. For instance, even 1% intensity of second harmonic pulse will alter the electric field profile of the two-colour laser pulse by 10%. Thus the phase difference between two harmonic photons of same energy generated in two halves will no longer be an exact multiple of π . Thus the even/odd orders do not

interfere completely destructively/constructively at each consecutive half of the laser field. Thus, both even and odd harmonics should be generated. Figures 9.1b and 9.1c show the variation of e_{KE} with ϕ_t for two colour laser pulses with 2% and 15% second harmonic intensity respectively. One can see that the two consecutive laser halves are significantly different. It may be noted here that unlike in the case of single-colour laser pulse (Fig. 9.1a) where the electron which tunnel out between phases $(0, \pi/2)$ and $(\pi, 3\pi/2)$ can come back to parent ion, the range of ϕ_t for which electron can come back to parent ion, is reduced in the first half and increased in the second half of the laser electric field. This effect is more pronounced in the case of strong two-colour pulses. Moreover, the peak energy of the electrons is also different in the two halves of the electric field.

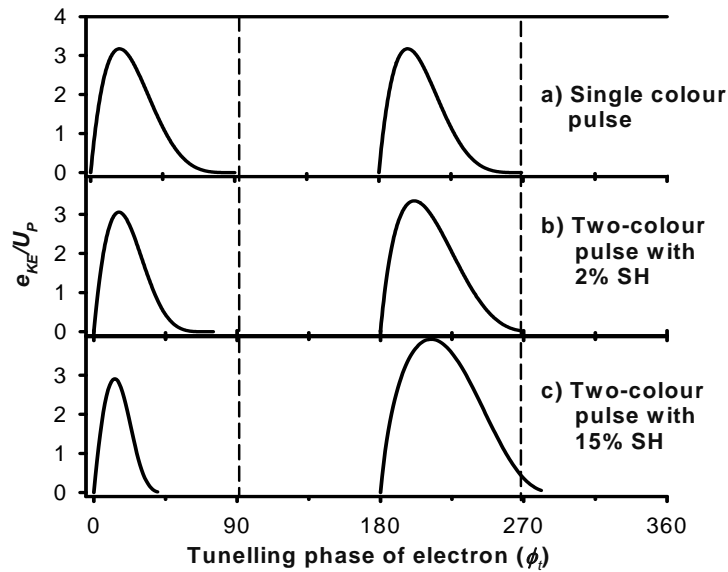


Fig. 9.1 Electron recombination energy normalized to ponderomotive energy vs. tunnelling phase of electron for (a) only fundamental laser pulse (b) two-colour laser pulse with 2% SH field and (c) two-colour laser pulse with 15% SH field.

9.2. Experimental description

A schematic of experimental setup for HHG using two-colour laser pulses is shown in Fig. 9.2. The interaction of the ps pre-pulse with the target surface creates a low excited pre-formed plasma plume. The fs laser pulse was focussed inside this plasma plume using a 500 mm focal length lens. A nonlinear crystal (Type-1 phase matched) for

the generation of SH pulse was inserted in the focussing femtosecond laser pulse to generate second harmonic radiation of the laser pulse. The nonlinear optical crystals for the generation of SH pulse used in this study are 1) 1 mm thick KDP crystal and 2) 0.3 mm thick BBO crystal, resulting in SH conversion efficiency of $\sim 2\%$ and $\sim 15\%$ respectively. The intensity of the fundamental radiation inside the SH crystal was kept $\sim 1.5 \times 10^{12} \text{ W/cm}^2$, to avoid damage to the crystal. It may be mentioned here that inside the SH crystal, the group velocity for the fundamental pulse is higher than that of SH pulse. The mismatch in the group velocity of these two pulses can result in temporal separation between the two pulses, in a thick crystal, despite the phase matching. Hence crystals of smaller thickness were used to ensure a sufficient temporal overlap of the two laser pulses.

In addition to using different intensities of the SH pulse in the two-colour laser pump, the effect of their polarizations was also studied. In the second harmonic process using Type-1 phase matching, the polarization of SH and fundamental laser pulses are orthogonal. A parallel polarization condition was obtained by inserting a zero-order half wave plate (HWP) (for 800 nm) after the crystal. A BG-39 filter could be inserted in the laser path to cut-off the fundamental radiation for experiments with SH pump only.

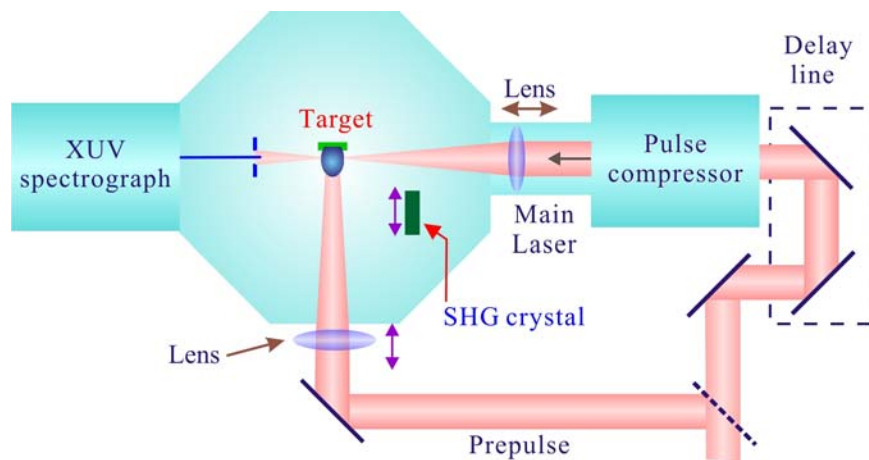


Fig. 9.2 Schematic of the experimental setup

9.3. HHG using weak two-colour pulses

9.3.1. HHG from plasma plumes of bulk materials

The HHG spectra from the interaction of single-colour (only fundamental laser pulse) and weak two-colour laser pulse with low excited plasma plume of silver are shown in Fig 9.3. Fig. 9.3a shows the harmonic spectrum from fundamental laser pulse, which comprises of only odd harmonic orders. In the case of weak two-colour laser pulse, both even and odd harmonic orders with comparable intensities were produced (Fig. 9.3b). After insertion of the HWP in the path of the laser pulse (with its optic axis 45° w.r.t. the fundamental beam polarization), the polarization of the fundamental and the second harmonic laser pulses become parallel. This is because, for the fundamental radiation, it acts as a HWP and rotates the polarization by $(2 \times 45^\circ) 90^\circ$, and acts as a full wave plate for the second harmonic, thereby doing nothing to its polarization. The high order harmonic spectrum from this two-colour laser pulse is shown in Fig. 9.3c. It may be seen from this figure that the cut-off order for even harmonics was smaller compared to that for the odd harmonics in the case of parallel polarized two-colour pump. During the experiments, it was observed that if the laser intensity inside the plasma plume is increased, the cut-off order for odd harmonics increases, whereas that for even harmonics decreases. These observations may be understood from the temporal separation of the two pulses due to their different group velocities inside the KDP crystal and half wave plate. As explained earlier due to dispersion there is only a partial overlap between fundamental and SH pulse. The fundamental pulse emerges ahead of the SH pulse. As one introduces the HWP these pulses get further separated due to GVD in HWP and the influence of the second harmonic pulse decreases. Same thing happens if one increases the laser intensity of the fundamental radiation inside the medium. As explained in

Chapter 4, in a high intensity laser pulse, the HHG comes predominantly from the leading edge of the laser pulse. With increase in laser intensity, HHG predominantly occurs from initial part of the leading edge of the pulse. This decreases the effective overlap of the SH pulse, which in turn reduces the intensity of even harmonics.

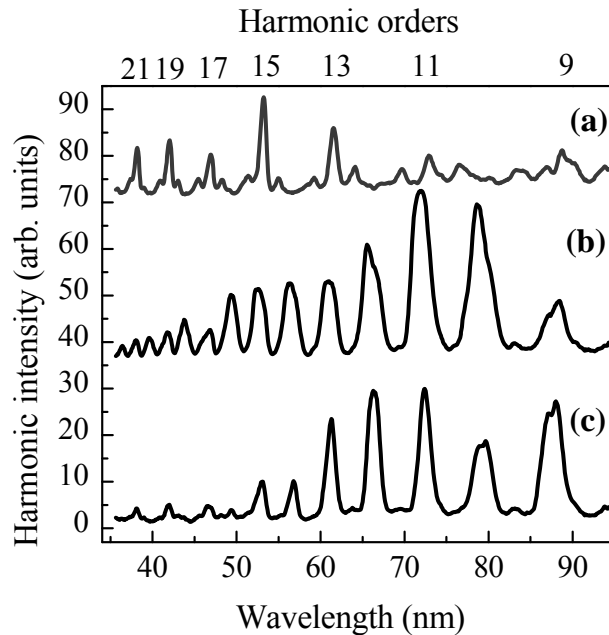


Fig. 9.3 HHG spectra from Ag plasma at : (a) single-colour (800 nm) pump, (b) orthogonally polarized two-colour pump, and (c) parallel polarized two-colour pump. Side lobes of the odd harmonics in the (a) correspond to the second-order diffraction lines of strong high-order harmonics.

The HHG from two-colour laser pulse with circularly polarized fundamental laser was also studied. It was observed earlier, in HHG studies [2] with single colour laser pulses that the harmonic emission vanishes when the laser polarization was made circular. However, with the introduction of SHG crystal after the circularly polarized laser light, both even and odd harmonics appeared (Fig. 9.4a). Since the SHG crystals are birefringent in nature the circularly polarized laser pulse gets divided into ordinary and extraordinary waves inside the crystal. These waves travel with different group velocities and hence they get separated in time when they come out of the crystal. So one now has two plane polarized laser pulses, separated temporally, with perpendicular polarizations. As these orthogonal components cannot form circularly polarized light (due to lack of

temporal overlap), the harmonic emission does not vanish. Out of these two pulses, only one pulse satisfies the phase matching condition for SHG. Hence, one of the laser pulses is a single-colour pulse (fundamental) and the other is two-colour laser pulse. The results of HHG from these pulses (Fig 9.4a) are compared with the HHG from two-colour pulses generated by linearly polarized fundamental laser light (Fig. 9.4b). One can see that the maximum even harmonic order visible in the first case (Fig 9.4a) is 30th order, whereas in the latter case it is 38th H order (Fig 9.4b). The vanishing of even harmonic orders near cut-off generated from circularly polarized fundamental laser pulses can be understood from reduced intensity of SH pulse as only one pulse is satisfying the phase matching conditions.

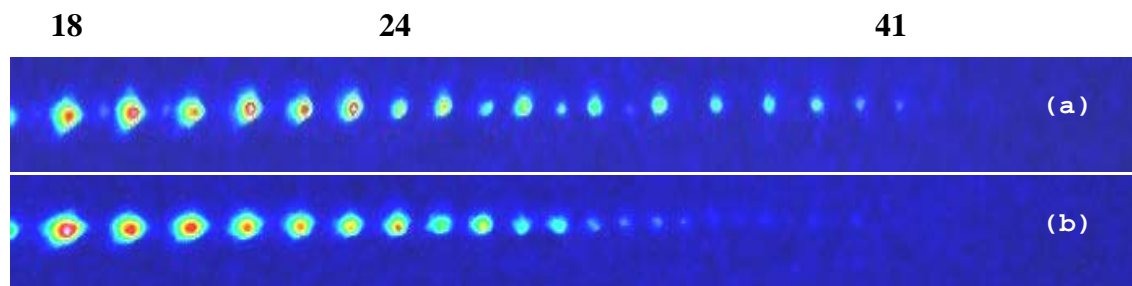


Fig. 9.4 CCD images of the harmonic spectra obtained from the silver plasma using : (a) two-colour laser pulses from circularly polarized fundamental radiation and (b) two-colour pump from linearly polarized fundamental radiation

The variation in HHG with the change in laser chirp was also studied. It was explained in Chapter 4 that the use of positively (negatively) chirped pulses results in shifting of harmonic peaks towards red (blue) wavelengths. In the case of two-colour pump also, the change of chirp of fundamental radiation resulted in wavelength shifting of both odd and even harmonics. The HHG from negatively and positively chirped pulses are shown in Fig. 9.5. It may be noted that while the intensity of odd harmonics (11th and 13th) is comparable the intensity of even orders (12th) was higher in the case of negatively chirped pulses compared to that with positively chirped radiation. The reason behind such observation is not fully understood.

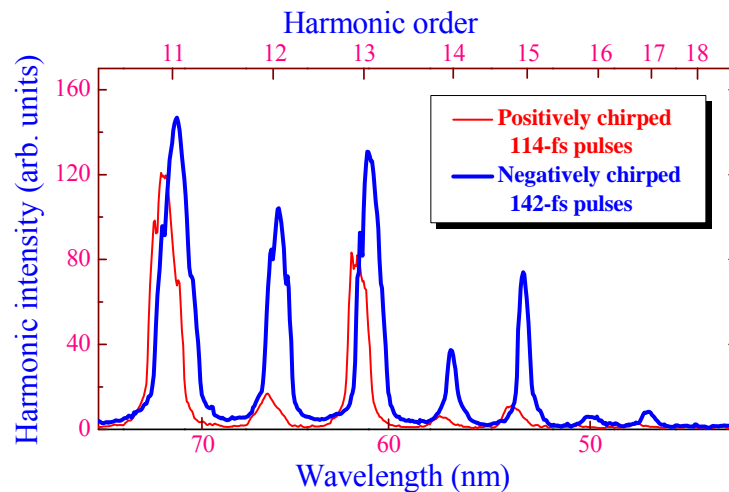


Fig. 9.5 Harmonic spectra obtained from carbon plasma plume using the two-colour pump scheme in the case of negatively chirped (thick line) and positively chirped (thin line) pulses of fundamental radiation.

9.3.2. Occurrence of new resonances

Resonant intensity enhancement in plasma plumes was observed in studies discussed in Chapter 4. For example the intensity of the 13th H of indium was ~200 times more compared to neighbouring harmonics (Fig 4.1). Since the use of fundamental radiation generates only odd harmonics, one will neither observe even harmonic orders nor any resonance enhancement in them. However, a two-colour pump results in generation of both even and odd harmonics. Hence, use of two-colour laser pulses will be helpful in searching resonance enhancement in even harmonic orders as well. Harmonic generation from indium plasma plume was studied with two-colour laser pulses. As shown in Fig. 9.6, it was found in the case of HHG from In plasma plume that a very intense 12th harmonic appears alongside the strong 13th harmonic (Fig. 9.6). Thus the use of two-colour laser pulses is also useful in increasing the HHG conversion efficiency through resonance enhancement.

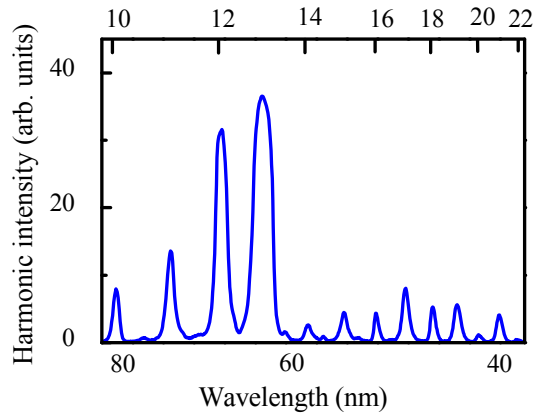


Fig. 9.6 Harmonic spectrum from indium plasma using the two-colour pump

9.3.3. Harmonic intensity enhancement in plasma plumes of nanostructured targets

Efficient HHG using fullerene (C_{60}) targets was observed in our studies described in Section 7.2. It was observed that the harmonic intensity in the range of 9th to 19th order was higher by a factor of ~ 25 in comparison to harmonics from plasma plumes of bulk silver. In this Section, we present results of HHG through the interaction of two-colour laser pulses with plasma plumes containing fullerenes. It was observed that under the same experimental conditions, using two-colour laser pulses, the intensity of the HHG radiation could be further increased by a factor of 4-8 depending on the harmonic order [10]. The harmonic spectrum, generated from plasma plumes containing fullerenes, using single-colour and weak two-colour laser pulses are shown in Fig. 9.7a and 9.7b

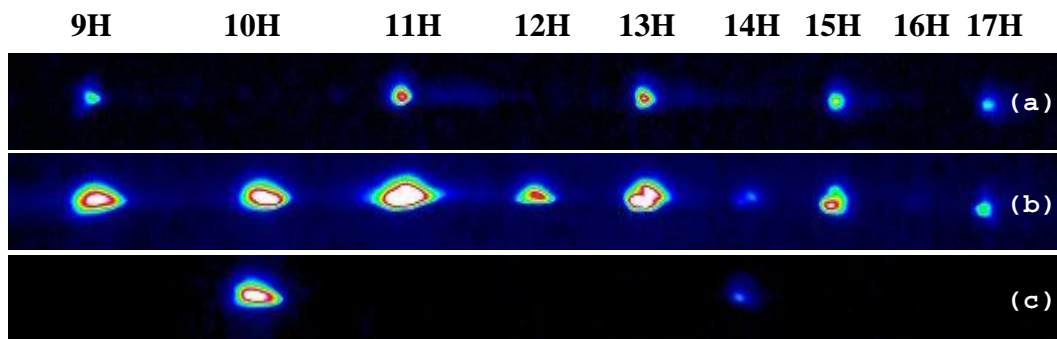


Fig. 9.7 CCD images of the harmonic spectra generated in C_{60} plasma using: (a) single-colour fundamental pump (800 nm), (b) two-colour pump (800 nm + 400 nm), and (c) single-colour SH pump (400 nm). The data were collected under similar experimental conditions.

respectively. We have also compared these two HHG spectra with the HHG spectrum generated from only SH laser pulse (Fig. 9.7c). One can see that in the case of Fig. 9.7c only the odd harmonics of the SH laser pulses are generated (*i.e.* 5th and 7th H of the SH pulse), but in the case of two-colour laser pulse both even and odd harmonic orders could be seen. One may note that when only fundamental or SH laser pulse is used, 12th H of the fundamental laser (which is also 6th H of the SH pulse) is not produced. This comparison demonstrates that the HHG from two-colour laser pulse is indeed a symmetry breaking phenomena and not the sum of HHG from individual laser pulses. Although the mechanism of HHG enhancement in fullerene targets through the use of two-colour laser pulse is not well understood, the method would be useful in increasing the conversion efficiency of HHG process.

9.4. HHG using strong two-colour pulses

HHG using strong two-colour laser pulses generated from plasma plumes of bulk silver is shown in Fig 9.8a. Both, even and odd harmonics are generated by the strong two-colour laser pulses. The harmonic emission from single colour laser pulse (Fig 9.8 b) is shown for comparison with that from strong two-colour pulses. It is seen that these two spectra reveal the suppression of odd harmonic orders near the cut-off [7]. The situation is contrary to the case of HHG from weak two-colour laser pulses where even harmonics disappeared near the cut-off. The suppression of the odd harmonics in the cut-off may be due to larger intensity of SH pulse. In order to check on this point, we decreased the intensity of SH pulse to ~5% by tilting the BBO crystal vertically by ~5°. The HHG spectrum for this situation is shown in Fig 9.8c. It is observed from Fig 9.8c that with the reduction of SH intensity all the even and odd harmonics reappeared. The

same results were also observed when the duration of the laser pulse was increased to ~ 150 fs to reduce the laser intensity and hence the intensity of SH pulse.

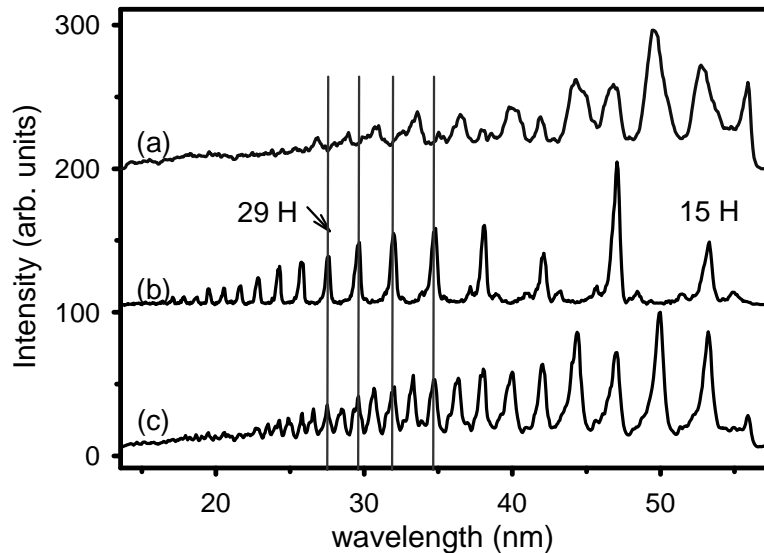


Fig. 9.8 HHG spectra from excitation with a) strong two-colour pump (b) single-colour fundamental pump (800 nm), and (c) two-colour pump with reduced efficiency through tilting the SH crystal. One may see that odd harmonics reappear with the reduction in SH intensity. The spectra are normalized and shifted vertically to facilitate visual comparison

Bibliography

1. R. A. Ganeev, H. Singhal, P. A. Naik, U. Chakravarty, V. Arora, J. A. Chakera, R. A. Khan, M. Raghuramaiah, S. R. Kumbhare, R. P. Kushwaha, and P. D. Gupta, "Optimization of the high-order harmonics generated from silver plasma", *Appl. Phys. B* **87**, 243 (2007).
2. R. A. Ganeev, H. Singhal, P. A. Naik, V. Arora, U. Chakravarty, J. A. Chakera, R. A. Khan, I. A. Kulagin, P. V. Redkin, M. Raghuramaiah, and P. D. Gupta, "Harmonic generation from indium-rich plasmas", *Phys. Rev. A* **74**, 063824 (2006).
3. H. Singhal, R. A. Ganeev, P. A. Naik, A. K. Srivastava, A. Singh, R. Chari, R. A. Khan, J. A. Chakera and P. D. Gupta, "Study of high-order harmonic generation from nanoparticles", *J. Phys. B* **43**, 025603 (2010).

4. I.J. Kim, H.T. Kim, C.M. Kim, J.J. Park, Y.S. Lee, K.-H. Hong and C.H. Nam, “Efficient high-order harmonic generation in a two-color laser field”, *Appl. Phys. B* **78**, 869 (2004).
5. R. A. Ganeev, H. Singhal, P. A. Naik, I. A. Kulagin, P. V. Redkin, J. A. Chakera, M. Tayyab, R. A. Khan, and P. D. Gupta, “Enhancement of high-order harmonic generation using a two-colour pump in plasma plumes”, *Phys. Rev. A* **80**, 033845 (2009).
6. M. Dahlström, “Strong field approximation for high order harmonic generation in $w/2w$ laser fields”, *Lund Reports on Atomic Physics* 381 (2007).
7. R. A. Ganeev, P. A. Naik, H. Singhal, J. A. Chakera, M. Kumar, M. P. Joshi, A. K. Srivastava, and P. D. Gupta, “High-order harmonic generation in carbon-nanotube-containing plasma plumes”, *Phys. Rev. A* **83**, 013820 (2011).
8. P. B. Corkum, “Plasma perspective on strong field multiphoton ionization”, *Phys. Rev. Lett.* **71**, 1994 (1993).
9. M. Lewenstein, Ph. Balcou, M. Yu. Ivanov, Anne L’Huillier, and P. B. Corkum, “Theory of high-harmonic generation by low-frequency laser fields”, *Phys. Rev. A* **49**, 2117 (1994).
10. R. A. Ganeev, H. Singhal, P. A. Naik, J. A. Chakera, A. K. Srivastava, T. S. Dhami, M. P. Joshi and P. D. Gupta, “Enhanced harmonic generation in C_{60} containing plasma plumes”, *Appl. Phys. B* **100**, 581 (2010).

Chapter 10

Conclusion

10.1. Summary of the important results

This thesis has investigated the generation of high order harmonics through the interaction of ultrashort femtosecond laser pulses with low excited preformed plasma plumes. The high order harmonics being coherent, ultrashort, and in the XUV region, this radiation has potential of applications in a variety of fields such as microlithography, spectroscopy, attosecond pulse generation etc. Increasing the intensity of high order harmonic generation (HHG) remains a major area of research in order to enhance their practical applicability. The conversion efficiency of the HHG process depends greatly on the properties of the nonlinear medium used. Conventionally, high order harmonics are generated by the interaction of ultrashort pulses with noble gases and hence the choice of nonlinear medium was very limited. To overcome the problem of small number of nonlinear media, we have generated high order harmonics using low excited under-dense plasma plumes of solids and nanoparticles, thereby expanding the range of HHG explorations to a large variety of elements / compounds.

The subject research area of the thesis *i.e.* high order harmonic generation from preformed plasma plumes has been extensively reviewed in Chapter 1. The characterization of laser parameters and the experimental arrangement of HHG from low excited plasma plumes has been presented in Chapter 2. High order harmonics has a typical spectrum in which the intensity of the first few orders falls rapidly with the harmonic order, thereafter the intensity of harmonics remains nearly constant over a range of high order harmonics (the intensity plateau) followed by a well-defined cut-off. The experimental results on HHG from plasma plumes of solids in the plateau region

have been presented in Chapter 3. The tunability in harmonic radiation is required for various spectroscopic studies in order to overlap harmonic wavelengths with atomic / ionic transitions. In this regard, the results on the spectral tuning of harmonics through the introduction of chirp in the laser pulses were presented in this chapter.

Low-excited plasma plumes are useful towards the generation of resonantly enhanced harmonics through the matching of harmonic wavelengths with atomic / ionic transitions. Observation of resonantly enhanced high order harmonics from the interaction of ultrashort laser pulses with plasma plumes of different materials was described in Chapter 4. The effect of laser intensity and medium length on the intensity of harmonics was discussed in Chapter 5. Since the high order harmonics are coherent radiation, they are affected by their phase mismatch with respect to the laser pulse. A study of the harmonic intensity variation with respect to the laser focal position in the plasma plume was performed and inference were drawn on the role of plasma free electrons in producing phase mismatch between laser pulse and harmonic radiation. Further, the HHG from an elongated plasma medium helped in understanding the role of various phase mismatch factors on HHG process.

Next, any improvement in the stability and cut-off of the HHG is important for their use as coherent x-ray sources in practical applications. The effect of various laser and plasma parameters on the stability of the harmonics has been discussed in Chapter 6. A theoretical analysis of the high order harmonic cut-off on ionization potential was also presented in this chapter. Further, a second plateau of the harmonics was observed in Mn plasma plumes. It was experimentally observed that through optimization of the laser and plasma conditions, one can increase the cut-off of this second plateau to $\sim 73^{\text{rd}}$ H order.

In order to increase the harmonic intensity, we have investigated HHG from plasma plumes containing metal nanoparticles/fullerenes and results of the same have

been presented in Chapter 7. It was observed that intensity of the harmonics in the range of 9th to 19th H was increased by a factor of ~25. We have also demonstrated the generation of high order harmonics from nanoparticles produced *in situ* during the interaction of laser pre-pulse with metal surfaces.

Overlapping of the harmonic wavelengths with atomic / ionic transitions is required for their applications in spectroscopy. In this regard, the generation of the harmonics of a large bandwidth would facilitate their easier overlap. A study on the generation of spectrally broadened harmonics was carried out and presented in Chapter 8. These harmonics were generated by using either spectrally broadened fs laser pulses or plasma plumes containing nanoparticles. In the latter case, the bandwidth of 11th harmonic was observed to increase from ~1.4 nm to ~5 nm. This broadening was towards blue side only, and it has been explained from the interaction of the intense laser pulses with expanding nanoparticles at resonance phase.

The interaction of femtosecond laser pulses with plasma plumes resulted in the generation of only odd harmonic orders. Two-colour laser excitation was used to break the inversion symmetry of the HHG process. In this case, both even and odd harmonics were produced. The results of these studies have been presented in Chapter 9.

10.2. Suggestions for further research work

Although the present thesis describes an extensive experimental study of different aspects of HHG from the interaction of ultrashort laser pulses with low excited plasma plumes of various materials, there is a good scope of further explorations. The increase in conversion efficiency and cut-off order is desirable for practical applications. Hence harmonic generation using plasma plumes created from novel materials could be helpful in this regard. Next, measurements of spatial and temporal coherence, pulse duration of

the harmonic radiation are major areas in which further research could be carried out. High order harmonics are a route towards the generation of attosecond pulses and hence characterization and optimization of these pulses is a very important research area. Moreover, state-of-the-art detectors are required for measurements of attosecond pulses. Development of such detectors (not available commercially) is also a very challenging task. Further, single attosecond burst is required for the measurement of electron dynamics inside an atom. Single attosecond bursts can be generated by few-cycle parent laser pulses. Generation of high energy few-cycle laser pulses is an area of extensive research involving many technological challenges.